AEDC-TDR-63-49

cy!

MEASUREMENT OF PRESSURE IN AN ULTRA-HIGH VACUUM

By

R. L. Heimburg, A. B. Huang, E. A. Jackson
T.J. Mueller, and S.L. Soo
Department of Mechanical and Industrial Engineering
University of Illinois
Urbana, Illinois

TECHNICAL DOCUMENTARY REPORT NO. AEDC-TDR-63-49

March 1963

AFSC Program Area 850E, Project 7778, Task 777801

(Prepared under Contract No. AF 40(600)-909 by the University of Illinois, Urbana, Illinois)

ARNOLD ENGINEERING DEVELOPMENT CENTER
AIR FORCE SYSTEMS COMMAND
UNITED STATES AIR FORCE

MEASUREMENT OF PRESSURE IN AN ULTRA-HIGH VACUUM

By

R. L. Heimburg, A. B. Huang, E. A. Jackson,

T. J. Mueller, and S. L. Soo

Department of Mechanical and Industrial Engineering

University of Illinois

Urbana, Illinois

(The reproducibles used in the reproduction of this report were supplied by the authors.)

March 1963

CONTENTS

TABLES

ILLUSTRATIONS

NOMENCLATURE

(List of Terms)

A	inside surface area of gauge, cm^2
A_o	total boundary of all areas of outer surface, cm.
A_s	total surface area of the system, cm^2
A_1	constant, $r_t/\pi C$, cm^2/sec.
a	constant, defined in Eq. [2.8.20]
a_1	lattice parameter of solid, cm.
a_o	Bohr radius, cm.
B_1	constant, $2\alpha\sqrt{\pi}/r_t$, mm Hg/$\sqrt{sec}$.
b_1	constant, defined by Eq. [3.6. 1], mm Hg.
C	constant, $\frac{3}{4}\left(\frac{1}{(2\pi RT)^{1/2}}\right)$, sec/cm.
$\bar{C}$	mean speed of molecules, cm/sec.
C_1	constant, defined by Eq. [3.6. 1], mm Hg.
C_o'	function defined after Eq. [3.6. 2].
c	velocity of light, $2.99.7929 \times 10^8$ cm/sec.
D	closest distance between gas and solid atom, cm.
D'	diffusion coefficient, cm^2/sec.
D_o, D_1	constants in environment pressure equation for linear pressure with time, defined in Eq. [3.4. 1], mm Hg.
d	parameter defined by Eq. [2.8.20], cm.
E	energy, erg.
E_o	activation energy, cal/g-mole.
e	charge of an electron, esu.
G	grand partition function of the system.
G^o	grand partition function for an ideal gas in volume V_a.
G^*	grand partition function for the adsorbed phase.
H	Hamiltonian function of the system.
h	Planck's constant, 6.6237×10^{-27} erg sec.
I	total influx of gas to a system.
i_+	ion current, ma.
i_-	electron current, ma.
K	constant, defined by Eq. [2.3.35].

K'	sensitivity of an ultra-high vacuum gauge, $(\text{mm Hg})^{-1}$.
k	Boltzmann constant, 1.38×10^{-16} erg/°K.
L	length of tube, cm.
L^{-1}	symbol of inversed transform.
M_o, M_1	constants in environment pressure equation for sinusoidial pressure variation with time, defined in Eq. [3.5. 1], mm Hg.
m	mass of a molecule, g.
m_e	mass of an electron, g.
N	total number of gas molecules.
N'	total activated gas atoms.
N_a	number of adsorbed molecules.
N_c	number of atoms per cc. of the solid.
N_o	total number of gas molecules which would be held in the adsorption container if there is no gas-surface interaction.
N_s	total number of solid atoms on the surface area A_s.
n	number of electrons.
n_o	initial density of molecules.
P_o	parameter defined by Eq. [2.3.27].
P_L	Laplace transform of p.
P_N	configuration integral.
P_{S_N}	function defined by Eq. [2.3.17].
p	pressure, mm Hg.
p_e	equilibrium pressure, mm Hg.
p_i	initial pressure in gauge, mm Hg.
p_o	pressure in system, mm Hg.
p_{x_i}, p_{y_i}, p_{z_i}	generalized momentum coordinates.
p_2	pressure constant defined by Eq. [3.6. 1], mm Hg.
p^*	p/p_o, dimensionless.
$p^{*'}$	p/M_o, dimensionless.
p_i^*	p_i/p_o, dimensionless.
Q	mass rate of flow, mass/sec.
Q'	canonical ensemble partition function.
q	surface outgassing rate, mass $(\text{sec cm}^2)^{-1}$.
q'	RTq, μcm/sec.

R	gas constant, 8.31436×10^{10} erg $(\text{mol}^{\circ}\text{K})^{-1}$.
r_i	generalized configuration coordinates.
r_o	orifice radius, cm.
r_t	tube radius, cm.
S	complex variables of Laplace transform.
S'	function defined by Eq. [2.7. 1].
S_p	effective pump speed, ℓ/sec.
T	absolute temperature, $^{\circ}$K.
t	time, sec.
t_L	time constant defined in Ref. (3), part 3.
t^*	$A_1 t/L^2$, dimensionless.
U_N	interaction potential, defined by Eq. [2.3. 3].
U_{gg}	interaction potential between two gas molecules.
U_{gs}	interaction potential of gas and solid molecules.
V	volume of the system, cm^3.
V_a	volume of ideal gases, cm^3.
V_g	volume of an ultra-high vacuum gauge, cm^3.
V_s	volume of adsorbed gases, cm^3.
v_o	average velocity of the activated atoms, cm/sec.
$\bar{v}$	average lateral velocity of the activated atoms, cm/sec.
x_1	diamagnetic susceptibility of a gas atom, cm^3.
x_2	diamagnetic susceptibility of a solid atom, cm^3.
x^*	x/L, dimensionless.
x, y, z	coordinates of the space.
Z	function defined by Eq. [2.3. 9].
ρ	density, g/cm^3.
ρ_o	gas density in the adsorption volume V, in the absence of gas-surface interaction.
$\rho^{(1)}(r_1)$	probability that a molecule will be found at r_1, irrespective of the positions of the other molecules.
α	parameter, $q'\sqrt{t}$, defined in Eq. [3.2. 1], (mm Hg cm)$(\text{sec})^{-1/2}$.
α_o	atomic polarizability, cm^3.
α_1	polarizability of a gas atom, cm^3.
α_2	polarizability of a solid atom, cm^3.

β parameter defined by Eq. [2.3.28].

β_o $\frac{a\sqrt{C}}{\sqrt{r_t}}$, mm Hg. β'_o $\frac{aC}{\sqrt{t}}$, mm Hg.

β_1 $\frac{a\sqrt{C}}{p_o\sqrt{r_t}}$, dimensionless β'_1 $\frac{a\sqrt{C}}{M_o\sqrt{r_t}}$, dimensionless

β_2 V_g/r_t^3, dimensionless β_3 v_g/r_o^3, dimensionless

β_4 A/r_t^2, dimensionless β_5 A/r_o^2, dimensionless

β_6 L/r_t, dimensionless β_7 L/r_o, dimensionless

β_8 r_t/r_o, dimensionless β_9 $\frac{D_1 r_t^{3/2} C^{1/2}}{a}$, dimensionless

β_{10} $D_1 L/a\ (\text{sec})^{-1/2}$ β'_{10} $\frac{a\sqrt{C}}{M_1\sqrt{r_t}}$, dimensionless

β_{11} $\pi CL^2/r_t$, sec β'_{11} ωCL, dimensionless

θ N_a/N_s, coverage of adsorption, dimensionless.

θ_1 $2\beta_2 - \beta_4 = (2V_g - A r_t)/r_t^3$, dimensionless.

θ_2 $4(\beta_5/\beta_6 - 2\beta_3/\beta_7)/3\sqrt{\pi} = 4(A r_t/L r_o^2 - 2 V_g/L r_o^2)/3\sqrt{\pi}$, dimensionless.

θ_3 $\beta_2/\pi^{3/2}\beta_6\beta_1 = p_o V_g/\pi^{3/2} r_t^{3/2} L\, a\, C^{1/2}$, dimensionless.

θ'_3 $\beta_2/\pi^{3/2}\beta'_1\beta_6 = M_o V_g/\pi^{3/2} r_t^{3/2} L\, a\, C^{1/2}$, dimensionless.

θ_4 $\beta_2\beta_6\beta_9 = C^{1/2} D_1 V_g L/a\, r_t^{5/2}$, dimensionless.

θ'_4 $\beta_2\beta_6\beta'_9 = C^{1/2} M_1 V_g L/a\, r^{5/2}$, dimensionless.

ω circular frequency, $(\text{sec})^{-1}$.

μ chemical potential of the adsorbed gas, erg.

Λ function defined by Eq. [2.3. 5].

ε^* $\frac{\pi N_c K}{6 D^3}$, gas-solid interaction potential at the hard-sphere distance D, erg/mole.

τ^* interval of time between two successive activations of the same gas atom.

τ_o period of vibration of an adsorbed atom normal to the surface, ~ 10^{-13} sec.

INTRODUCTION

This study concerns the measurement of pressure in simulation chambers and in the upper atmosphere. Factors affecting gauge calibration, measurement (and response) and interpretation of data were analyzed theoretically and experimentally. Significant factors affecting measurements are adsorption, outgassing, streaming and radiation, which are usually different when measurements are made in simulation chambers and in the upper atmosphere. In simulation chambers, when several gauges are used, the interaction among the gauges is important. Present studies are aimed at determining the magnitudes of these effects and generalizing the procedures.

Little needs to be said about the importance of pertinent gauge interpretation and design for measurements in the upper atmosphere and in space simulation. For these measurements, available means are: ionization gauges, magnetron gauges, omegatron gauges for molecular species, and determination from satellite drag. The simplest and the lightest device is probably the ionization gauge. Our aim is to deduce logical methods of interpretation of gauge readings in various environments as well as to understand and to determine the desirable design features. The contribution of the environments to its reading include streaming, such as occur in measurements with rockets and artificial satellites, the effect of solar and space radiation and the effect of its mounting and container wall. The latter is significant when dealing with space simulation.

The variables to be encountered by an ionization gauge in upper atmosphere measurements include primarily the altitude. Due to solar effect, these physical parameters may vary from day to night, and from latitude to latitude--the variation is to the order of a factor of 2. Present experimental error of results of densities at different altitudes may vary from 2.5 to 9.7 (1). In space simulation, it is not uncommon for similarly calibrated ionization gauges to read differently when one is mounted at the top of a simulation chamber while another is mounted on the test body (2). This shows the significance of knowledge concerning the interaction of a gauge with its environment and the proper interpretation of its reading.

Measurement at high altitudes is believed to be strongly influenced by thermal and solar wind effects. The solar coronal gas is believed to consist mainly of hydrogen up to a particle density of 10^{11} per m^3. In the vicinity of the earth, the known ionizing solar flux and recombination rates lead to 10^8 to 10^9 protons per m^3. At several earth radii from the earth, kinetic temperature of particles reaches 2×10^5 °K and the corresponding particle energy is 28 ev. Solar flares consist of a 500 to 2000 km/sec wind, with corresponding proton energy and density to the order of 1 to 20 kev and 10^8 to 10^{11} protons per m^3. This and the influx of hydrogen from distant clouds accounts

for the diurnal and annual variations. (3).

This report consists of the following parts:

1. Elementary gauge theory. The basis of using the Bayard-Alpert gauge, its sensitivity as related to geometry and operating parameters, and the influences of environment were studied.

2. Adsorption phenomena. The problems studied include production of ultra-high vacuum and generalization of the results on physical and chemical adsorption.

3. Gauge response. Effect of adsorption on gauge response in various environments, and behavior of standard gauges and nude gauges were studied.

4. Experimental system and procedure. Presentation includes our experimental system, the 1' × 1' vacuum chamber, instrumentation and methods.

5. Experimental results. Results obtained from flash filament, multi-gauge operations, bake-out and molecular species are presented. Interpretation of results and correlations with theoretical results were made.

6. General discussion.

7. Conclusions and recommendations.

In this investigation much time and effort was expended in the designing and assembling of apparatus. Also, since much of the information on adsorption was scattered and lacking generalization, a fundamental study on the adsorption phenomena had to be made. From this study, one only begins to understand what is the real meaning of a gauge reading when a gauge is installed in a certain way in a given environment. Therefore, in spite of the extent of this study, the result can be considered only as a preliminary toward a broader understanding and more thorough study of measurements of this type.

REFERENCES

(Introduction)

(1). H. K. Kallman, "A preliminary model of atmosphere based on rocket and satellite data," Rand Report R-339, Aerodynamics of the Upper Atmosphere, June (1959), pp. 3-1 to 3-27.

(2). R. A. Hindle, "Space simulation," ASME paper #62-AB-34, presented at Aviation Conference of ASME, Washington, D. C., June 26-28 (1962).

(3). M. Bader, "The problem of obtaining thermal proton background and solar wind measurements in space," Rand Report R-339 (1959), pp. 20-1 to 20-30.

1.0 ELEMENTARY THEORY OF THE BAYARD-ALPERT GAUGE

In this part, the Bayard-Alpert gauge is studied analytically to determine and to understand the relation between its sensitivity and its geometry and operating parameters, as well as the effect of its environment in space or in a simulation chamber. The Bayard-Alpert gauge is believed to be the most desirable device for pressure or density measurement in these applications because of its small x-ray current.

Earlier studies of gauge theory are those by Morgulis (1) and Ramey (2). Further details are considered in the present paper. The Bayard-Alpert gauge is taken as our example in discussing the nature of the gauge and its interaction with its environment. The method, of course, can be extended to other types of ionization gauges.

The Bayard-Alpert gauge has three basic elements: the filament (cathode) is outside the cylindrical grid and the ion collector (anode) is suspended within the grid. The ion collector is made of .006" dia. (.15 mm) tungsten wire. The grid structure is helically wound .005" dia. (.125 mm) molybdenum wire and supporting members. The filaments are made from .006" (.15 mm) dia. tungsten wire (3). For this elementary study, the gauge may be treated as a two-dimensional system as shown in Fig. 1.1. The potentials of the elements as indicated in Fig. 1.1 are typical and subject to further elaboration. We shall consider the contribution of these aspects:

(1) Electron path outside the grid and electron capture by the grid.
(2) Electron path inside the grid and the effect of space charge.
(3) Electron capture by the grid.
(4) Theoretical sensitivity of the gauge.
(5) Distribution of potential.
(6) Influence of streaming and charge.
(7) Influence of radiation.

1.1 PATH OF ELECTRONS OUTSIDE THE GRID

Due to the predominance of electrons in an ionization gauge system, much of its behavior is due to the space charge.

1.1.1 Spread of Electrons from the Filament

Take the simple system as shown in Fig. 1.1. We first consider a sheet of thermal electrons from the filament drawn toward the grid without space charge effects. The thermionic current density J at the filament is given by:

$$J = AT_f^2 \exp(-\varphi e/kT_f) \quad , \qquad [1.1]$$

where

$$A = 2\pi m_e ek^2/h^3 \sim 60.2 \times 10^4 \text{ amp/m}^2 (^\circ\text{K})^2 \quad ,$$

T_f is the temperature of the filament, φ is the thermionic potential ($\phi \sim 4.5$ v for tungsten), e is the electronic charge, k is the Boltzmann constant, m_e is the electronic mass, h is the Planck constant.

Neglecting electrostatic repulsion among electrons at this point, thermionic emission from the filament consists of a geometric line source. The emitted electrons are then accelerated by the grid potential. The thermionic emission occurs diffusely according to:

$$\frac{1}{2} m_e v_e^2 \sim \frac{1}{2} kT_f \quad , \qquad [1.2]$$

where v_e is the mean radial velocity of electrons, for $T_f \sim 2000^\circ$ K, $kT_v \sim .2$ ev. The emitted electrons are subject to a field such that over the distance d between the filament and the nearest point of the grid, each electron is accelerated by the field to an energy eV_g where V_g is the grid potential, or

$$\frac{1}{2} m_e v_g^2 = eV_g \quad , \qquad [1.3]$$

where v_g is the velocity of an electron entering the grid. Since

$$v_g^2 \sim 2ad \quad , \qquad [1.4]$$

where a is the average acceleration, and

$$d \sim \frac{1}{2} a\tau^2 \quad , \qquad [1.5]$$

where τ is the time of flight over distance d,

$$\tau \sim \sqrt{2 m_e d^2/eV_g} \quad . \qquad [1.6]$$

The width of the beam is thus

$$\delta = 2\tau v_e = 2d\sqrt{2kT_f/eV_g} \quad . \qquad [1.7]$$

Therefore, for $kT_f \sim .2$ ev, $eV_g \sim 150$ ev, for $d = 2$ mm , $\delta \sim .2$ mm. Hence, for a filament of .15 mm , this result would indicate that the width of the electron sheet averages only .3 mm , and the density decreases toward the grid. In reality, the electrons leaving the filament repel each other due to electrostatic forces. Using the approximation of an electron interacting with an infinite plane of charge density given by 2 eny, where n and y are electron concentration and the width of the electron sheet. The electric field is given by:

$$E = 2 \text{ eny}/\varepsilon \quad , \qquad [1.8]$$

where ε is the permittivity. For total electronic current i when the width of the beam spreads to y at location x as shown in Fig. 1.2, the average number density is given by:

$$n = i/2y\ell\sqrt{2eV_g/m_e} \quad , \qquad [1.9]$$

where ℓ is the length of the filament. Using the Lagrangian frame of reference, (4) and taking the coordinate systems such that y is normal to the direction of mass motion of electrons, v_y and v_x being the velocities, the equation of motion is:

$$v_y \frac{dv_y}{dy} = \frac{i}{\ell\varepsilon}\sqrt{\frac{e}{2m_e V_g}} \qquad [1.10]$$

for an electron at the surface of the sheet of electrons. Integration once gives

$$v_y^2 = \frac{i}{\ell\varepsilon}\sqrt{\frac{2e}{m_e V_g}}\,(y - \delta) \qquad [1.11]$$

further

$$v_y = \frac{dy}{dt} = v_x \frac{dy}{dx} = \sqrt{\frac{2eV_g}{m_e}}\,\frac{dy}{dx} = \left(\frac{i}{\varepsilon\ell}\sqrt{\frac{2e}{m_e V_g}}\right)^{\frac{1}{2}}\sqrt{y - \delta}$$

and

$$y - \delta = 2\sqrt{z}\,\frac{i}{\ell\varepsilon}\sqrt{\frac{m_e}{eV_g^{3/2}}}\,x^2 \qquad [1.12]$$

for electrons spreading from an initial thickness δ of the beam. We get for $V_g \sim 150$ v, $i/\ell \sim 1.5$ amp/m , for filament diameter of 0.15 mm , $T_f \sim 2000\ ^oK$, x = 3 mm , y ~ 0.4 m. Hence, due to electrostatic repulsion or space charge effect the electrons actually enter into the periphery of the grid almost uniformly instead of entering as a sheet or beam of electrons.

1.1.2 Spread of Electrons Outside the Grid

Since the above shows that electrons tend to spread around the grid uniformly, now we want to determine the range of spreading of electrons outside the grid; that is, to determine the range of electron motion. We take for our simple approximation the voltage distribution outside the grid as

$$V = V_g\, \ell n(r/r_f)/\ell n(r_g/r_f) \qquad [1.13]$$

where r_f is the radius at which the filament is situated, r_g the radius

of the grid, assuming for the present that the grid is floating (zero voltage). Since the electric field due to space charge is

$$E = \frac{e \int_{r_g}^{r} n\, 2\pi r dr}{4\pi r \varepsilon} = \frac{e\, n_o\, r_o (r - r_g)}{2r\varepsilon} \qquad [1.14]$$

assuming $n = n_o\, r_o/r$, r_o is the radius of the filament wire; the voltage distribution due to space charge is therefore:

$$V_s = \frac{e n_o r_o}{2} \int_{r_g}^{r} \left(1 - \frac{r_g}{r}\right) dr = \frac{e n_o r_o}{2} (r - r_g) - r_g \ln\left(\frac{r}{r_g}\right) \qquad [1.15]$$

Now we want to determine the range at which the kinetic energy of electrons is zero. The energy equation gives:

$$m v_r \frac{dv_r}{dr} = - eV_g \frac{\ln (r/r_f)}{\ln (r_f/r_g)} + \frac{e n_o r_o}{2} \left[(r - r_g) - r_g \ln \left(\frac{r}{r_g}\right)\right] = 0 \qquad [1.16]$$

denoting

$$B = \ln(r_f/r_g) \quad , \qquad [1.17]$$

$$A = \frac{n_o r_o r_g}{2V_g \varepsilon} \quad , \qquad [1.18]$$

hence, the outer range of electrons is given by radius r according to the following relationship:

$$\ln\left(\frac{r}{r_g}\right) - B = AB \left[\frac{r}{r_g} - 1 - \ln\left(\frac{r}{r_g}\right) \right] \quad . \qquad [1.19]$$

For the following numerical data:

$$n_o = 10^{17}/m^3, \quad r_o = .075 \text{ mm.}, \quad r_g = 15 \text{ mm.}, \quad r_f = 16 \text{ mm.},$$

it can be shown that the spread tends to the order of $\frac{r}{r_g} \sim 1.1$.

1.2 MAXIMUM EFFECT OF SPACE CHARGE INSIDE THE GRID

At this point, we still consider the grid an equipotential surface, in the form of an infinitely long cylinder, and the ion collector is concentric with the grid. Without the space charge effect, the distribution of potential inside the grid follows:

$$V = V_c + \frac{V_g - V_c}{\ell n(r_g/r_c)} \ell n\,(r/r_c) \quad , \qquad [1.2.1]$$

where V_c is the collector voltage and r_c is the radius of the ion collector (Figure 1.1). Space charge effect modifies the distribution represented by the above relation to ℓ as shown in Fig. 1.4, where r_1 is the furthest point an electron can reach inside the grid. Let i be the total current coming into the grid. The time an electron stays within the grid is less than $2\,r_g/v_g$ where

$$v_g = \sqrt{\frac{2eV_g}{m_e}}$$

as before, so the net charge due to electrons inside the grid is less than $-(2r_g/v_g)\,i$. Assume all electrons get reflected at some point r_1, where the potential is zero, and that otherwise they have a constant velocity. Lump all electrons into a cylinder of radius r_1, then the resulting potential represents the greatest effect of space charge.

On the cylinder of radius of r_1 the charge per unit area is less than

$$\sigma = -\frac{2r_g}{v_g}\, i\, \frac{1}{2\pi r_1 \ell} \qquad [1.2.2]$$

then the potential, including space charge effect, is given by

$$\begin{aligned} V &= V_c + V_2\, \ell n(r/r_c) \quad , \quad \text{for } r < r_1 \quad ; \\ V &= V_g + V_1\, \ell n(r/r_g) \quad , \quad \text{for } r > r_1 \quad ; \end{aligned} \qquad [1.2.3]$$

and

$$\begin{aligned} V_c + V_2\, \ell n(r_1/r_c) &= V_g + V_1\, \ell n(r_1/r_g) = 0 \quad , \\ (-V_1 + V_2)/r_1 &= \frac{\sigma}{\varepsilon_o} \quad , \end{aligned} \qquad [1.2.4]$$

(jump in E across cylinder) which determines r_1, where ε_o (8.854×10^{-12} Farad/m) is the permittivity. This yields

$$(V_g - V_c)\, \ell n(r_1/r_c) + V_c\, \ell n(r_g/r_c) = \frac{r_1 \sigma}{\varepsilon_o}\, \ell n(r_1/r_c)\, \ell n(r_1/r_g) \quad , \qquad [1.2.5]$$

and

$$\frac{r_1 \sigma}{\varepsilon_o} = -\frac{r_g i}{\pi \ell \varepsilon_o \sqrt{2eV_g/m}} \quad . \qquad [1.2.6]$$

For the following numerical data, $i \sim 10^{-3}$ amp., $r_g = 10$ mm., $\ell \sim 20$ mm., $V_g \sim 150$ v, $v_g \sim 7.3 \times 10^6$ m/sec.,

$$\frac{r_1 \sigma}{\varepsilon_o} \approx - \frac{10^{-5} \times 36 \times 10^9}{2 \times 10^{-2} \times 7.3 \times 10^6} \sim - 2.47 \text{ joule coulomb},$$

for $eV_c \sim - 20$ ev, we get $r_1/r_c < 1.82$.

Thus we see that the volume from which the electrons are excluded is negligible, even when the space charge is taken into account.

1.3 ELECTRON CAPTURE BY THE GRID

Some of the electrons in their motion toward the grid are captured. Treating the problem as two-dimensional as in Fig. 1.5, and approximating the grid wires as infinite cylinders, capture and scattering of electrons can be visualized as indicated by the following relationship:

$$1 - \gamma = \frac{2 b_c}{\text{pitch of coil}} = \frac{2 b_c}{h} \qquad [1.3.1]$$

where γ is the fraction passing through the grid, b_c is the range within which electrons will be captured. b_c and h are represented in Fig. 1.5.

If all the electrons are accelerated from infinity, their motion will not be significantly affected by the close range distribution of potential around the wire. Then b_c is nearly equal to the radius of the wire of the grid, or

$$1 - \alpha \qquad \frac{2 r_{og}}{h} \qquad [1.3.2]$$

is the minimum fraction captured. This is when the filament is located far away from the grid. At close range, the local potential distribution becomes more significant. If the grid wire is treated as a stationary scatterer, all crude approximations of local potential distribution as a logarithmic function gives $b_c/r_{og} \sim \sqrt{2}$. The variation of fraction captured, therefore, in conformity with Nottingham's result (5), is, for

$$\sqrt{2} \sim b_c/r_{og} > 1 \qquad [1.3.3]$$

depending on the value of r_f, and greater for larger r_f.

For $h/r_{og} \sim 10$, we have:

b_c/r_{og}	γ	Average no. of passes to capture $\gamma/(1-\gamma^2)$
1	.8	2.22
2	.7172	1.473

Hence, the closer the filament, the smaller the electron concentration inside the grid.

Since not all the electrons are captured after one pass through the grid, but after several passes, the electron concentration inside the grid is, in general, greater than by calculation based on emission current from the filament alone.

The above potential distribution inside the grid shows that the region in which the kinetic energy of the electrons is less than, say, 30 ev, where the probability of ionization is small, is about four to five times the collector radius. Hence, nearly all the region inside the grid contains electrons energetic enough to ionize. The effective electron path is nearly twice the radius of the grid for each pass. More specifically, the fraction sensitive volume is defined by: (2)

$$V_s^* = \frac{Q}{\pi \ell r_g^2} = \frac{\pi \ell (r_g^2 - r_{oe}^2)}{\pi \ell r_g^2} = 1 - \left(\frac{r_g}{r_c}\right)^2 \left\{ [(V_i - V_c)/(V_g - V_c)] - 1 \right\} \qquad [1.3.4]$$

where Q is the volume where electrons actually exist, r_{oe} is the radius within which there are no electrons, r_c is the radius of the ion collector, V_i is the ionization potential of the gas. Hence, depending on the species of gas present, the sensitive volume of a gauge varies.

It should be noted, however, that the less energetic electrons could form negative ions with the gas atoms present. In particular, atomic oxygen and hydrogen, molecular oxygen, the halogens and large organic molecules readily form negative ions, although nitrogen and the rare gases do not. The probability of attachment is greatest for electrons of low energy (nearly 1 ev), which spend an appreciable time within the influence of the atomic field (6). From the above considerations, however, the fraction of negative ions formed is very small compared to the large sensitive volume usually available.

1.4 THEORETICAL SENSITIVITY

With the above knowledge of the Bayard-Alpert gauge, the method due to Morgulis and Reynolds (1) can be extended to the present case.

In the Bayard-Alpert gauge the electron energy is nearly constant inside the grid. The probability of ionization, W(V), of each collision is the same at all radii, and

$$W(V_g) = \alpha (V_g - V_i) \exp [- (V_g - V_i)/\beta] \qquad [1.4.1]$$

where V_i is the ionization potential of the gas atom, and α and β are constants.

The number of ions produced per second for one pass of all electrons is nearly:

$$N/\text{pass} \sim n Z P W(V_g) 2(r_g - r_{oe}) V_s^* \qquad [1.4.2]$$

for n electrons passing through the same volume per second, Z is the number of molecular collisions made by each electron per cm path at a gass pressure of 1 mm Hg at 25° C. Since $r_g >> r_{oe}$, and each excursion of the electron offers two chances of capture,

$$N \sim P Z \frac{2n\gamma}{1 - \gamma^2} r_g W(V_g) V_s^* \quad , \qquad [1.4.3]$$

and the sensitivity,

$$\frac{N}{nP} = \frac{I_+}{I_e P} \sim 2 Z \frac{\gamma}{1 - \gamma^2} r_g W(V_g) V_s^* \qquad [1.4.4]$$

in amp /amp mm Hg. I_+ is the ion current, I_e is the electron current.

For a design with h = 0.125", $2r_{og}$ = .006", $\gamma/(1 - \gamma^2) \sim 2$. For the case of nitrogen (V_i = 15.6 v) with V_g = 150 v, v_c = - 20 v, 9.9 ions (= WZ) are formed per electron per cm path at 1 mm pressure (7). For r_g = 10 mm , r_c = .075 mm , giving $V_s^* = 1 - 4.37 \times 10^{-4}$,

$$\frac{N}{nP} = 2 \times 2 \times 1 \times 9.9 \sim 40$$

For other gases the relative sensitivities are: (3)

Gas	W Z	Computed	Experimental (3)
He	1.6	.1618	.16 - . .21
H_2	3.6	.364	.42 - .47
Ne	2.8	.283	.24 - .33
A	10.3	1.04	1.19 - 1.5
N_2	9.9	1.	1.
Hg	19.4	1.96	3.4

1.5 FURTHER ON POTENTIAL DISTRIBUTION

In the simple geometry we have so far considered, the filament was assumed to be floating (zero voltage). This is not the actual situation. The filament usually carries a voltage of the order of 20 volts. This modifies the potential distribution, especially when there is an outside wire screen (Bayard-Alpert MIT gauge) or a metallized surface (Bayard-Alpert NRC gauge). This, together with the space charge effects (8, 9), gives rise to the situation of an equivalent cylindrical filament at greater radius than r_f.

Here we shall consider two basic aspects of potential distribution: one is the distribution due to the non-floating filament (Fig. 1.7); the other is distribution due to finite grid and filament dimensions (Fig. 1.8).

Nottingham found that the sensitivity of his ionization gauge was roughly proportional to the distance between the filament and the grid. The possibility arises that this phenomenon may be due to a variation in the number of electrons which enter the ionization region inside the grid. To examine this possibility it is necessary to estimate the fraction of the electrons emitted from the filament which is collected by the grid. When the grid and filament are well separated the electrons are subjected to essentially only a radial electric field over most of the region of acceleration. Therefore, if d is the distance between the concentric rings of the grid, and r_{og} is the radius of the grid wires, the fraction collected should be $(2r_{og}/d)$. As the distance between the grid and filament is decreased the z-component of the electric field should have more effect on the electrons' paths, causing them to converge on the grid wires. It thus appears that the number of electrons in the ionization region, and hence the sensitivity, should decrease as the grid-to-filament distance decreases, in agreement with Nottingham's observation. To see whether this qualitative agreement can be extended to a quantitative agreement, it is necessary to obtain an approximate expression for the electric field in the ionization gauge.

Referring to Fig. 1.8, the electrostatic potential has an angular dependence, arising from the fact that the filament produces an asymmetry. As was discussed before, the space charge effects of the electrons will greatly reduce the angular effect. Hence, the first approximation will be to treat the filament as a cylinder, and therefore neglect all angular dependence. Making use of the periodicity in the z-direction, the solution of Poisson's equation is then:

$$\phi = A + B \ln r + \sum_{n=1}^{\infty} \cos \frac{2\pi n}{d} z \left[D_n I_o\left(\frac{2\pi n}{d} r\right) + E_n K_o\left(\frac{2\pi n}{d} r\right)\right]$$

where I_o, K_o are respectively the modified Bessel functions of the

first and second kind. Using the boundary conditions $\phi(r=r_c, z) = \phi_c$, $\phi(r=r_f, z) = \phi_f$, one obtains, for $r_c \leq r \leq r_g - r_{og}$:

$$\phi'(r, z) = \phi_c + B' \ell n \frac{r}{r_c} + \sum_{n=1}^{\infty} C'_n \cos \frac{2\pi n}{d} z \left[K_o\left(\frac{2\pi n}{d} r_c\right) I_o\left(\frac{2\pi n}{d} r\right) - I_o\left(\frac{2\pi n}{d} r_c\right) K_o\left(\frac{2\pi r}{d}\right)\right] \quad [1.5.1]$$

and, for $r_g + r_{og} \leq r \leq r_c$:

$$\phi(r, z) = \phi_f + B \ell n \frac{r}{r_f} + \sum_{n=1}^{\infty} C_n \cos \frac{2\pi n}{d} z \left[K_o\left(\frac{2\pi n}{d} r_f\right) I_o\left(\frac{2\pi n}{d} r\right) - I_o\left(\frac{2\pi n}{d} r_f\right) K_o\left(\frac{2\pi n}{d} r\right)\right] \quad [1.5.2]$$

where r_g is the radius of the grid. These potentials can be extended into the region $r_g - r_{og} \leq r \leq r_g + r_{og}$ if they satisfy the boundary conditions

$$\phi'(r_g - \sqrt{r_{og}^2 + z^2}, z) = \phi_g = \phi(r_g + \sqrt{r_{og}^2 + z^2}, z) \quad [1.5.3]$$

for $0 \leq z \leq r_{og}$; which insures that the grid wires are equipotentials, and for $r_{og} \leq z \leq d - r_{og}$

$$\phi'(r_g, z) = \phi(r_g, z) \quad , \quad \left(\frac{\partial \phi'}{\partial r}\right)_{r_g} = \left(\frac{\partial \phi}{\partial r}\right)_{r_g} \quad [1.5.4]$$

Just as the space charge reduces the angular dependence of the electrostatic potential, it will also help to reduce the variation in z. In any case a reasonable first approximation to ϕ is probably obtained by retaining only the term n=1 in Eqs. [1.5.1] and [1.5.2].* Within this approximation the four boundary conditions (Eqs. [1.5.3] and [1.5.4]) can each be satisfied at only one point, yielding the conditions necessary to determine B, B', C_1 and C_1'. Because of the periodic behavior of $\phi(z)$, the obvious selection of z = 0, d/2 may not be the optimum one, but rather $z = r_{og}/\sqrt{2}$ and d/4. By using the latter points the boundary conditions are actually satisfied at four, rather than two points.

Since r_g/d is between 3 and 10, $\phi(r,z)$ can be further simplified by using the asymptotic form of the Bessel functions; and one obtains:

* This is probably the case only if $(r_f - r_g)/d > 1$.

$$\phi(r,z) \simeq \phi_f + B\ell n \frac{r}{r_f} + C \cos\left(\frac{2\pi}{d} z\right) \frac{d}{2\pi\sqrt{r-r_f}} \sin h \left[\frac{2\pi}{d}(r-r_f)\right] \qquad [1.5.5]$$

Using this potential, one can in principle determine the fraction of electrons collected by the grid. However, since the equations of motion for the electrons cannot be solved analytically, further approximations must be devised and examined before a quantitative comparison can be made with Nottingham's results.

1.6 STREAMING

In space probing with the nude gauge, streaming of molecules through the gauge modifies the gauge sensitivity. For an artificial satellite orbiting at 10^4 m/sec., different atoms will have different kinetic energy due to mass motion:

Atom	ΔV
N	7.3 ev
O	8.33 ev
He	2.08 ev
H	0.52 ev

Atoms ionized (with very small transfer of kinetic energy from electrons) at ΔV less than the above from the grid tend to stream through the grid and never reach the ion collector. The effect shows up as represented in Fig. 1.6. For inlet at distance b from the center of the nearest approach as given by:

$$\left[1 - \frac{V(R_o)}{\Delta V}\right] R_o^2 = b^2$$

giving R_o the nearest approach. For R_o greater than where V from the grid is of the magnitude of ΔV, the ion formed will stream through. The net result is a reduction of sensitive volume in the grid and the gauge shows up as having a lower sensitivity.

$$V(R_o) = V_g - \left[V_c - \frac{V_c - V_g}{\ell n \frac{r_g}{r_c}} \ell n \frac{R_o}{r_o}\right]$$

for $\Delta V = 10$ ev, $V_c = -20$ v, $V_g = 150$ v, $\ell n\left(\frac{r_g}{r_c}\right) \sim 5.3$, $\ell n\left(\frac{R_o}{r_g}\right) = -.312$,

where $R_o/r_g = \frac{1}{1.366} = .731$,

thus excluding quite a large portion of the sensitive volume. The sensitivity is reduced by more than 50%.

Ions streaming toward a grid will be repelled by the grid even if the minimum potentials through the spacing between successive coils is

down to 10 volts. Therefore, in space probing in general, a gauge calibrated on the ground shows up as having a lower sensitivity. When streaming is involved, different species of gases have different sensitive volumes.

1.7 EFFECTS OF RADIATION

X-ray current in a gauge itself was studied by Schuetze and Ehlbeck (10). The photo-electron constant k_x was shown to be:

$$k_x = \left(\frac{I_+ - I_+^o}{I_e} \right)_{p=o} = 6 \times 10^{-12} \, Z \, U^{1.5} \eta \qquad [1.7.\ 1]$$

where I_+ is the ion current, I_+^o is the ion current at $I_e = 0$, I_e is the electron current, Z is the atomic number, U is the grid voltage, η is the ratio of the diameter of the ion collector to the circumference of the grid:

$$\eta = r_c / \pi r_d \qquad [1.7.\ 2]$$

for the Bayard-Alpert gauge, The lower limit of pressure measurement with an error of 10% is

$$P_{min} = 10 \frac{k_x}{k_y} \qquad [1.7.\ 3]$$

where

$$k_y = \frac{1}{p} \frac{I_+}{I_e} \quad . \qquad [1.7.\ 4]$$

Radiation on the ion collector of a gauge in space probing contributes in a similar way. It raises the electron current in addition to the above x-ray effect. In this case the photo-current is given by:

$$I_x = e \int_{\theta,\phi,\nu} \frac{B_\nu}{h\nu} D_\nu \, (\theta,\phi) \, Y(\nu) \, d\nu \, g(\theta,\phi) \, d\sigma \, d\omega \quad , \qquad [1.7.\ 5]$$

where B_ν is the radiation intensity, ν is the frequency, θ, ϕ are spherical coordinators, σ is the area collecting radiation, ω is the solid angle, $Y(\nu)$ is the quantum yield, $g(\theta,\phi)$ is the space pattern, D_ν is the transmittance of the ion collector and is nearly a constant. $g(\theta,\phi)$ may be assumed as 1.

$$\int \frac{d\sigma \, d\omega}{2\pi} \sim 2 r_c \ell \qquad [1.7.\ 6]$$

where ℓ is the length of the ion collector. In a material of work function eU_1, $h\nu_1 = eU_1$, and

$$Y(\nu) = \frac{\Lambda}{2}\left(\Lambda - \frac{\Lambda}{\sqrt{\Lambda + \frac{\nu - \nu_o}{\nu_1}}}\right) \qquad [1.7.7]$$

where ν_o is the threshold frequency. Hence, the additional electron current due to radiation is

$$I_x = 2r_c\ell \int_\nu \frac{B_\nu}{h\nu} D_\nu Y(\nu)\, d\nu = 2\pi r_c \ell J_x \quad ; \qquad [1.7.8]$$

J_x is the average current density of the ion collector. Thus, radiation onto the ion collector tends to have the net effect of increasing the gauge sensitivity.

1.8 DISCUSSION

When dealing with standard gauges, conductance of gas through gauge tabulation does not follow the Knudsen formula if $\ell > d$, where ℓ and d are the length and diameter of the conducting tube. As ℓ/d goes from zero to ∞, the conductance drops by a factor of 2 (11).

The electric field of the ion collector (Z) is nearly 2×10^6 v/m (3), suggesting the possibility of Schottky emission of electrons, which could give rise to a constant background current. However, this appears to be negligible for pressures above 10^{-12} mm Hg. The modification of current density is given by (7):

$$J = AT^2 \exp\left[-\frac{(\phi - eZ)e}{kT}\right]$$

Secondary emission by ions hitting the collector at 100 to 150 ev: from 1 to 10 electrons might be ejected from the collector depending upon the energy of the ion (8). For two electrons per ion, the collector current is three times what it would be if the electrons were not ejected. The net effect is an apparent increase of ion current. Actual data shows that I_s/I_p (secondary current over primary current) for tungsten is between .1 and .25 for a dirty surface and a clean surface respectively. This means that the sensitivity differs by 10 to 25% from what it should. Thus, it is not entirely negligible.

REFERENCES
(Section 1.0)

(1) J. H. Leck, "Pressure measurement in vacuum systems," Inst. of Phys., London (1957), pp. 70-73.

(2) R. L. Ramey, "Vacuum Technology Transactions," proceedings of the 6th National Symposium, Pergamon Press (1959), pp. 85-88.

(3) D. Alpert, "Production and measurement of ultra-high vacuum," Westinghouse Research Laboratories, Scientific Paper No. 6-94436-4-T-6, April (1957).

(4) S. L. Soo, "Effect of electrification on the dynamics of a particulate system," Project SQUID Report to ONR No. Ill-5-P, March (1962).

(5) W. B. Nottingham, "Design parameters' influence on MIT Bayard-Alpert gauge sensitivity," paper presented at meeting of The Vacuum Society (1961).

(6) E. H. Kennard, "Kinetic Theory of Gases," McGraw-Hill Book Co., Inc., (1938), pp. 116-120.

(7) K. T. Compton and C. C. Van Voorhis, "Probability of ionization of gas molecules by electron impacts," Phys. Rev., 26, (1925), p. 436.

(8) J. D. Cobine, "Gaseous Conductors," Dover Publications (1958), pp. 118, 126, 156.

(9) I. Langmuir and K. B. Blodgett, "Currents limited by space charge between co-axial cylinders," Phys. Rev., 22, (1923), pp. 347-356.

(10) H. J. Schuetze and H. W. Ehlbeck, "The x-ray limit in ionization gauges," paper presented at meeting of The Vacuum Society, (1961).

(11) C. Kittel, "Elementary Statistical Physics," John Wiley, p. 213.

2.0 ADSORPTION PHENOMENA

For calculation of pressures and the entropies of gas molecules which are adsorbed on solid surfaces, the thermodynamics of adsorption and experimental data in this region has acquired great significance. For vacuum techniques, measurements of the adsorption of gases at low pressures have practical usage.

Measurements of ultra-high vacua have been made so far without the above considerations, and a vacuum of 10^{-12} mm Hg has not been produced conclusively. However, several investigators have reported achieving 10^{-12} mm Hg in very small volumes - usually the inside of an ionization gauge tube or a mass spectrometer tube. Early in 1953, Alpert (1) reported reaching 3×10^{-11} mm Hg, using an ionization gauge as a pump. In 1956, Reynolds (2) reached a pressure of 5×10^{-11} mm Hg in the spectrometer envelope while analyzing several noble gases. Both Hobson and Redhead (3) and Venema (4) reported reaching 10^{-12} mm Hg in 1958; Hobson and Redhead used a magnetron gauge with a liquid helium trap, and Venema used a diffusion pump. At an undetermined date (estimated between 1959 and 1960), Power (5) reported that pressures of 10^{-13} mm Hg are now regularly attainable with a system which is pumped by two oil diffusion pumps and has both a water-cooled chevron baffle and a liquid gas-cooled chevron baffle after the last diffusion pump. Very recently Davis and Vanderslice (6) indicated that a partial pressure of 10^{-13} mm Hg has been measured by their mass spectrometer.

In this part, our study of the processes of physical and chemical adsorption of molecular gases on surfaces and their effect on the attainment and measurement of ultra-high vacua is presented.

2.1 THE PROBLEM OF ACHIEVING ULTRA-HIGH VACUUM AND ITS MEASUREMENT

The general pumping equation for any system of volume V, being evacuated by a pump of effective speed S_p, is:

$$V \frac{dp}{dt} = - pS_p + I \qquad [2.1.\ 1]$$

where I is the total influx of gas and p is the pressure of the system. In general, S_p and I are both functions of p and t. If it is assumed that they are constants, in the steady state, Eq. [2.1. 1] gives the equilibrium pressure:

$$pe = \frac{I}{S_p} \qquad [2.1.\ 2]$$

Thus, it is clear that in order to achieve ultra-high vacuum (the region of pressures below 10^{-8} mm Hg (8)), the ratio of total influx I divided by the pumping speed S_p must be made comparable to the

required ultimate pressure (below 10^{-8} mm Hg). The pumping speed S_p of a vacuum pump is a characteristic property of the pump. The main problem is what are the sources of I. The influx of gas into this system is caused by leaks, back streaming and back diffusion from pumps, and gas desorption from walls (7). Clearly, the first two kinds of influx are problems of technical development. The gas physically adsorbed at the surfaces of an evacuated system constitutes a major source of influx into a well designed vacuum system. In addition, gas diffusion into the envelope walls and the interactions at the surface may add to the influx. In order to understand these latter contributions to the influx, a further study of the physical and chemical interactions of gas molecules or atoms on surfaces is required.

The sorption processes have a critical role in the measurement of pressure, since each atom adsorbed within the measuring device causes the device to act as a pump, while each atom desorbed or released from a gauge surface causes it to act as a source of gas. In measuring ultra-high vacua, ionization gauges give the volume density within the gauge. However, if the conductance to the volume of the system is small, the pressure within the gauge may not be identical to that in the system. Hence, the processes which may take place in such gauges and the errors which they may introduce to measurements has been an objective of this study.

It is, therefore, important to evaluate the various mechanisms for the influx of gas into an evacuated system. Among the most important processes are the evolution of gas from surfaces by desorption, and the diffusion of gases through solid surfaces.

2.2 INTERACTIONS OF GAS ATOMS WITH SOLID SURFACES

The surface of a solid exposed to a gas is always covered with a thin molecular film of the gas. In the ultra-high vacuum range it is assumed that a monomolecular layer of the gas is formed. The gas-solid interactions in this film govern to a large extent the properties of such a monolayer, and become very pronounced at low pressures.

The interaction of gas atoms with solid surfaces has been studied by numerous authors (9 - 14). A few experimental data have been interpreted in the theoretical calculations by Barrer (15), Orr (16) and Young (17, 18). However, the data have in general been taken below the critical temperature of the adsorbate, usually in the region of the boiling point. In this region lateral interaction, multilayer formation and possible capillary condensation (19) are important; and their theories are analogous to the theory of liquids. In the case of ultra-high vacuum, interaction between the gas atoms can be ignored. Thus, the interaction of a single atom with the solid surfaces - the mechanism of the monolayer adsorption - must be considered.

The adsorption of gases on solids may be divided into two classifications - physical adsorption and chemical adsorption (10, 20). The model adopted here was proposed by Lennard-Jones (10), accepted by Trapnell (21), and recently adopted by Becker (22) in his studies of nitrogen adsorption on tungsten. In Fig. 2.1, the curves (1) and (2) show the potential energy of a molecule AB (respectively adsorbed and chemisorbed) as a function of its distance from the surface. An adsorbed molecule approaching the metal with an energy E, insufficient to reach P might, according to quantum mechanics, penetrate the barrier and be chemisorbed; but the probability is small unless E is very nearly of the same height as the point of intersection P. Therefore, a molecule reaching the surface will have to possess an energy higher than E (the activation energy) in order to be chemisorbed. The activation energies for gases and various metals are compiled in Ref. (36).

Physically speaking, Fig. 2.1 is an approximation to account for: (a) different proportion of chemisorption and physical adsorption at different temperatures while retaining the generality of potentials being independent of temperature, (b) activation energy to chemisorption, and (c) heat of reaction for different molecular species as a result of the two mechanisms.

2.3 MONOLAYER PHYSICAL ADSORPTION ON SOLID SURFACES

Various aspects of the physical adsorption problem have already been discussed by Wheeler (23), Ono (24), Freeman and Halsey (25), Hill (26, 27 - 32), and Steele (33 - 35).

Here it is assumed that the adsorbed atoms move in a potential field in the vicinity of the surface of the solid adsorbent, and that this potential field is not perturbed by the presence of adsorbed atoms. In general, the potential energy of an atom near the surface of a solid depends on all three position coordinates of the interacting atom. One may expect that the potential function will show a simple minimum as the perpendicular distance to the surface is varied, but that the position and magnitude of the minimum will show a periodic variation as the adsorbed atom is moved parallel to the surface. It is also assumed that monolayer adsorption occurs at temperatures and pressures such that there is a negligible probability of finding an adsorbed atom anywhere other than at (or very near to) the distances from the surface which correspond to the positions of the minima of the potential energy with respect to variations in the coordinate perpendicular to the surface. Thus, adsorbed atoms are restricted to move along the surface which is the locus of these potential minima. Localized adsorption will occur if the amplitude of the periodic variations in potential energy with motion parallel to the surface is large compared to kT, and mobile adsorption if it is small.

Since adsorption systems are generally at known T and μ (the

chemical potential of the adsorbed gas is obtained from the adsorption pressure), it is clear that it is most convenient to use the grand canonical ensemble in computing the properties of the system.

If the total number of gas atoms and the total volume of the system are N and V respectively, the canonical ensemble partition function for our problem is (37):

$$Q' = \frac{1}{h^{3N}\, N!} \int \cdots \int e^{-H/kT}\, dp'_1 \cdots dp'_N\, dr_1 \cdots dr_N \qquad [2.3.\ 1]$$

where $dp'_i = dp'_{x_i}\, dp'_{y_i}\, dp'_{z_i}$, $dr_i = dx_i\, dy_i\, dz_i$

and the Hamiltonian function of the system is:

$$H = \sum_{i=1}^{N} \frac{1}{2m} \left(P'^2_{x_i} + P'^2_{y_i} + P'^2_{z_i}\right) + U_N\,(r_1, \ldots, r_N) \qquad [2.3.\ 2]$$

$$U_N\,(r_1, \ldots, r_N) = \sum_{i=1}^{N} u_{gs}\,(r_i) + \sum_{1 \leqslant i < j \leqslant N} u_{gg}\,(r_{ij}) \qquad [2.3.\ 3]$$

We substitute Eq. [2.3. 2] into Eq. [2.3. 1] and carry out the momentum integrations. The result is:

$$Q' = \frac{P_N}{N!\, \Lambda^{3N}} \qquad [2.3.\ 4]$$

where

$$\Lambda = \frac{h}{(2\pi mkT)^{1/2}} \qquad [2.3.\ 5]$$

and

$$P_N = \int_V \cdots \int e^{-U_N/kT}\, dr_1 \cdots dr_N \qquad [2.3.\ 6]$$

where P_N is the "configuration integral".

Several definitions of physical adsorption are possible (38). However, from the viewpoint of statistical mechanics calculation, (39) the Gibbs definition is the most convenient and correct definition of the number of adsorbed atoms N_a (38);

$$N_a = \int_V \left[\rho^{(1)}(r_1) - \rho_o\right] dr_1 \qquad [2.3.\ 7]$$

where ρ_o is the gas density in the adsorption volume V in the absence of gas-surface interactions, and $\rho^{(1)}(r_1)$ is, of course, a function of the position of atom 1 (denoted by r_1) and is expected to be large

compared to ρ_o when atom 1 is in the vicinity of the surface, and to decrease rapidly to ρ_o as the distance from the surface increases. In general, $\rho^{(1)}(r_1)$ is defined as the probability that a molecule will be found at r_1, irrespective of the positions of the other molecules. The expression of $\rho^{(1)}(r_1)$ in a canonical ensemble of N particles is given by a Boltzmann factor which includes the interaction energies of all N atoms with the surface and with each other, integrated over all possible positions of all atoms except atom 1; and divided by the proper normalizing factor. In the grand canonical ensemble, N is unrestricted and therefore one has a sum of Boltzmann factors, one for each possible value of N. The number density $\rho^{(1)}(r_1)$ may be written as (37 - 40):

$$\rho^{(1)}(r_1) = \frac{1}{G} \sum_{N\geq 1} \frac{Z^N}{(N-1)!} \int_V \cdots \int \exp\left[- U_N(r_1, \ldots, r_N)/kT\right] dr_2 \cdots dr_N \qquad [2.3.\ 8]$$

where

$$Z = \exp(\mu/kT)/\Lambda^3 \quad , \quad \Lambda = h/(2\pi mkT)^{1/2} \qquad [2.3.\ 9]$$

The grand partition function of the system is defined as:

$$G = \sum_{N\geq 0} \frac{Z^N}{N!} P_N \qquad [2.3.10]$$

When Eq. [2.3. 8] is substituted in Eq. [2.3. 7], we have

$$N_a = \int_V \left\{ \frac{1}{G} \sum_{N\geq 1} \frac{Z^N}{(N-1)!} \int_V \cdots \int \exp\left[- U_N(r_1, \ldots, r_N)/kT\right] \times dr_2 \cdots dr_N - \rho_o \right\} dr_1$$

$$= \frac{1}{G} \sum_{N\geq 1} \frac{Z^N}{(N-1)!} \int_V \cdots \int \exp\left[- U_N(r_1, \ldots, r_N)/kT\right] dr_1\, dr_2 \cdots dr_N - \int_V \rho_o\, dr_1$$

$$= \frac{1}{G} \sum_{N\geq 1} \frac{Z^N}{(N-1)!} P_N - \int_V \rho_o\, dr_1 \qquad [2.3.11]$$

Now, if we define $N_o = \int_V \rho_o \, dr_1$ as the total number of atoms which would be held in the adsorption container if there were no gas-surface interactions, then we have

$$N_a = \frac{1}{G} \sum_{N \geq 1} \frac{Z^N}{(N-1)!} P_N - N_o \qquad [2.3.12]$$

It is known from statistical mechanics (41) that the total number of gas atoms in the container equals

$$N = N_a + N_o = kT \left(\frac{\partial \ell n \, G}{\partial \mu}\right)_{V.T.} \qquad [2.3.13]$$

but,

$$Z = \exp(\mu/kT)/\Lambda^3$$

$$\frac{dZ}{d\mu} = \frac{1}{kT\Lambda^3} \exp(\mu/kT) = \frac{Z}{kT} \qquad [2.3.14]$$

Thus,

$$N = kT \left(\frac{\partial \ell n \, G}{\partial Z} \cdot \frac{\partial Z}{\partial \mu}\right)_{V.T}$$

$$= kT \left(\frac{Z}{kT}\right) \left(\frac{\partial \ell n \, G}{\partial Z}\right)_{V.T}$$

$$= \frac{Z}{G} \left(\frac{\partial G}{\partial Z}\right)_{T.V} \qquad [2.3.15]$$

In order to express the grand partition function in a better form, we will divide the volume of integration into two parts; a relatively small volume in the immediate vicinity of the solid surface (denoted by V_s), and the remainder of the gas space volume (denoted by V_a). The dividing line is chosen to be at the point where the gas-surface interactions become negligibly small. If the surface of division between solid and gas is defined as passing through the centers of the atoms that make up the surface of the solid, and if the area of the surface and the closest distance between the gas atoms and the solid atoms are A_s and D respectively, then we may take $V_s \cong 2DA_s$ (observed from the shape of interaction potential between the gas atom and entire solid (26)). We notice that a portion of V equal to A_sD is unavailable to the centers of the gas atoms.

Here, we assume the gas in the volume V_a is perfect, i.e., the pair interaction potential of gases in V_a is zero. Thus, we have

$$P_N = \int_V \cdots \int e^{-U_N/kT} \, dr_1, \ldots, dr_N$$

$$= \left[\int_V e^{-U_N/kT} \, dr_1 \right]^N$$

$$= \left[\int_{V_s} e^{-U_N/kT} \, dr_1 + \int_{V_a} e^{-U_N/kT} \, dr_1 \right]^N$$

$$= \left[\int_{V_s} e^{-U_N/kT} \, dr_1 + V_a \right]^N$$

$$= P_{s_N} + N V_a P_{s_{N-1}} + \frac{N(N-1)}{2} V_a^2 P_{s_{N-2}} + \cdots + V_a^N \qquad [2.3.16]$$

where

$$P_{s_N} = \int_{V_s} \cdots \int \exp \left[-U_N/kT \right] dr_1, \ldots, dr_N \qquad [2.3.17]$$

By substituting Eq. [2.3.16] into Eq. [2.3.10], we get

$$G = \sum_{N \geq 0} \frac{Z^N}{N!} P_{s_N} \sum_{N \geq 0} \frac{Z^N}{N!} V_a^N \qquad [2.3.18]$$

where Z is defined as the activity of the adsorption system. Under equilibrium, Z is equal to that of the perfect gas system. Thus, from the perfect-gas las (37), we have

$$Z = \rho = \frac{p}{kT} \qquad [2.3.19]$$

where ρ is the density of gas.

Here, we notice that the second sum in Eq. [2.3.18] is exactly the grand partition function for an ideal gas in volume V_a, while the first sum is the grand partition function for the adsorbed phase.

We define

$$G^o = \sum_{N \geq 0} \frac{Z^N}{N!} V_a^N \qquad [2.3.20]$$

and

$$G^* = \sum_{N\geq 0} \frac{Z^N}{N!} P_{sN} \qquad [2.3.21]$$

then

$$\ell n\, G = \ell n\, G^* + \ell n\, G^o \qquad [2.3.22]$$

By assuming $V_a \cong V$, we have

$$N_a = kT \left(\frac{\partial\, \ell n\, G}{\partial \mu}\right)_{V.T} - N_o = kT \left[\frac{\partial\, \ell n\, G^*}{\partial \mu} + \frac{\partial\, \ell n\, G^o}{\partial \mu}\right]_{V.T.} - N_o$$

$$= kT \left[\frac{\partial\, \ell n\, G^*}{\partial Z}\right]_{V.T} \left(\frac{\partial Z}{\partial \mu}\right) + N_o - N_o = Z \left[\frac{\partial\, \ell n\, G^*}{\partial Z}\right]_{V.T.} \qquad [2.3.23]$$

Noting that Eq. [2.3.21], the partition function for the adsorbed phase, is in the form of the grand partition function for an imperfect gas, we can obtain the adsorption isotherm by the usual methods of imperfect gas theory:

$$\ell n \sum_{N\geq 0} \frac{Z^N}{N!} P_{s_N} = \sum_{j\geq} V_s\, b_j\, Z^j \qquad [2.3.24]$$

But the right side of the above equation can be expanded to give a power series in Z. Denote the coefficient of Z^j in this series by $V_s b_j$. Then

$$N_a = \sum_{j\geq 1} V_s\, b_j\, j!\, Z^j \qquad [2.3.25]$$

where

$$\begin{aligned} 1!\, V_s\, b_1 &= P_{s_1} \\ 2!\, V_s\, b_2 &= P_{s_2} - P_{s_1}{}^2 \\ 3!\, V_s\, b_3 &= P_{s_3} - 3 P_{s_1} P_{s_2} + 2 P_{s_1}{}^3 \\ &\cdots\cdots \end{aligned} \qquad [2.3.26]$$

Thus,

$$N_a = P_{s_1}(Z) + (P_{s_2} - P_{s_1}{}^2)(Z)^2 + \cdots\cdots = P_{s_1}(p/kT) + (P_{s_2} - P_{s_1}{}^2)(p/kT)^2 + \cdots\cdots$$

Here, we assume the surface is homogeneous, i.e., it is made of N_s elements of area A_s, all of which are identical. We introduce parameters P_o and β such that

$$kT/P_o = P_{s_1}/N_s = \frac{1}{N_s} \int_D \int_{A_s} \left[\exp\left(-U_{gs}[r_1]/kT\right) \right] dr_1 \qquad [2.3.27]$$

and

$$\beta = 1 - P_{s_2}/P_{s_1}^2$$

$$= \left[\int_D \int_{A_s} \int_D \int_{A_s} \exp\left\{ - [U_{gs}(r_1) + U_{gs}(r_2)]/kT \right\} dr_1\, dr_2 \right.$$

$$\left. - \int_D \int_{A_s} \exp\left[U_2(r_1 r_2)/kT\right] dr_1\, dr_2 \right]$$

$$\div \left[\int_D \int_{A_s} \int_D \int_{A_s} \exp\left\{ - [U_{gs}(r_1) + U_{gs}(r_2)]/kT \right\} dr_1\, dr_2 \right] \qquad [2.3.28]$$

But

$$U_2(r_1 r_2) = \sum_{i=1}^{2} U_{gs}(r_i) + \sum_{1 \leq i < j \leq 2} U_{gg}(r_{ij}) \qquad [2.3.29]$$

and

$$\exp\left[- \sum_{1}^{2} U_{gg}(r_{12})/kT \right] = \Pi \exp\left[- U_{gg}(r_{12})/kT \right]$$

$$= \prod_{1 \leq i < j \leq 2} (1 + f_{ij}) \qquad [2.3.30]$$

where

$$f_{ij} = \exp\left[- U_{gg}(r_{ij})/kT \right] - 1 \qquad [2.3.31]$$

Thus

$$\beta = \frac{ - \int_D \int_{A_s} \int_D \int_{A_s} f_{12} \exp\left\{ - [U_{gs}(r_1) + U_{gs}(r_2)]/kT \right\} dr_1\, dr_2 }{ \int_D \int_{A_s} \int_D \int_{A_s} \exp\left\{ - [U_{gs}(r_1) + U_{gs}(r_2)]/kT \right\} dr_1\, dr_2 } \qquad [2.3.32]$$

The isotherm equation (42) is:

$$\theta = \frac{N_a}{N_s} = \frac{1}{N_s}\left[P_{s_1}(p/kT) + (P_{s_2} - P_{s_1}{}^2)(p/kT) + \ldots .\right]$$

$$= \frac{p}{P_o}\left[1 - (\frac{p}{P_o})(N_s - \frac{N_s P_{s_2}}{P_{s_1}{}^2}) + \ldots .\right]$$

$$= (\frac{p}{P_o})\left[1 - (\frac{p}{P_o})\beta + \ldots .\right] \qquad [2.3.33]$$

For small (p/P_o) or a system of very low pressure, higher terms can be neglected and Eq. [2.3.33] becomes:

$$\theta = \frac{N_a}{N_s} = \frac{(p/P_o)}{[1 + \beta(p/P_o)]} \qquad [2.3.34]$$

Further, in the ultra-high vacuum case, the mean free path of gas molecules inside the chamber is much larger than the characteristic length of the chamber, and so it is reasonable to neglect the collisions between the gas atoms (molecules) inside the chamber. Hence, $f_{ij} = 0$, i.e., $\beta = 0$.

Equation [2.3.34] becomes

$$\frac{N_a}{N_s} = \frac{p}{P_o} \qquad [2.3.35]$$

where

$$\frac{1}{P_o} = \frac{1}{kT\,N_s}\int_{V_s}[\exp(-U_{gs}(r_1)/kT)]\,dr_1 \qquad [2.3.36]$$

2.4 THE INTERACTION POTENTIAL

In order to calculate the parameter P_o in Eq. [2.3.35], it is necessary to investigate the interaction potential of the gas atom and the entire solid atoms extensively. Here we consider a simple square lattice of solid atoms with parameter a_1 lying in the plane $z = 0$ and extending from $z=0$ to $-\infty$. Metallic interaction theory has been studied by Lennard-Jones (10)(see Fig. 2.1) and modified by Bardeen (43) by taking into account the interaction of the electrons in the metal. Margeneau and Pollard (44) showed that a metal could not be considered ideally polarizable when interacting with a system whose resonant frequency was in the far-ultraviolet. Non-metallic

interaction theory has been studied by Palanyi (45), and extended by Slater and Kirkwood (46), and Kirkwood and Muller (7, 48). Pierotti (49) showed that the Kirkwood-Muller equation is the most suitable of the theories considered and that it yields semi-quantitative agreement with experiment for both metallic and non-metallic adsorbents in his thesis dissertation.

The general form of the interaction potential of an adsorbed atom with a solid lattice has been computed by summing the pair interactions between an adsorbed atom and the atoms in the solid (35). The sum is taken over the entire solid, and the pair interaction is assumed to have the form of the Lennard-Jones potential function.
Hill (26) assumed that the distances between the atoms of the adsorbent (the lattice parameter of the solid, a_1) are small compared with the distances between the gas atoms and the solid atoms. Thus, the summation over the solid atoms can be replaced by an integration. This leads to an $r^{-3} - r^{-9}$ gas-solid potential function (26, 47) and an $r^{-6} - r^{-12}$ gas-gas potential function. Freeman (50) showed that there is a considerable disagreement between experimental values of the third virial coefficient, and the third virial coefficient computed for an $r^{-3} - r^{-9}$ gas-solid potential function, and an $r^{-6} - r^{-12}$ gas-gas potential curve.

Palanyi (45) showed that the Kirkwood-Muller interaction potential of a gas atom with a solid surface is:

$$U_{gs} = -\frac{\Pi N_c K}{6} \times \frac{1}{z^3} \qquad [2.4.1]$$

where N_c is the number of atoms per cm^3 of the solid. K is a constant and z is the perpendicular distance of the gas atom from the surface of the solid. The constant K has been approximated theoretically by several workers (46, 47). Kirkwood and Muller (47) modified the Slater-Kirkwood expression. They used the atomic property of diamagnetic susceptibility and obtained

$$K = 6 m_e c^2 \frac{\alpha_1 \alpha_2}{\frac{\alpha_1}{x_1} + \frac{\alpha_2}{x_2}} \qquad [2.4.2]$$

where m_e is the mass of an electron, c is the velocity of light, α_1 and α_2 are the polarizabilities and x_1, x_2 the diamagnetic susceptibilities of the gas atoms and the solid atoms respectively. Notice here that negative interaction potential denotes attraction.

2.5 CALCULATION OF PARAMETER (P_o)

From Eq. [2.3.36] we have

$$\frac{1}{P_o} = \frac{1}{kT\,N_s}\left\{\int_V [\exp(-U_{gs}/kT)]\,dV - V_a\right\}$$

$$= \frac{1}{kT\,N_s}\left\{\int_V [\exp(-U_{gs}/kT) - 1]\,dV\right\} \qquad [2.5.1]$$

where we make an approximation $V \cong V_a$.

Now, the limit of integration can be removed as in the usual virial coefficient integral because the interaction potential, U_{gs} is effective only in the small range V_s. Thus,

$$\frac{1}{P_o} = \frac{1}{kT\,N_s}\left\{\int_o^\infty [\exp(-U_{gs}/kT) - 1]\,dV\right\} \qquad [2.5.2]$$

The integral in the parenthesis corresponds to the negative quantity of twice the second virial coefficient for a pair of atoms (39).

Here, as shown in Eq. [2.4.1], we have

$$U_{gs}(z) = -\frac{\Pi N_c K}{6} \times \frac{1}{z^3} \qquad [2.5.3]$$

where z is the perpendicular distance of the gas atom from the surface of the solid. Recalling that D is the distance of closest approach of the centers of the gas atoms, we can put the interaction potential in the following form:

$$U_{gs} = +\infty \qquad z < D$$

$$U_{gs} = -\varepsilon^*(D/z)^3 \qquad z > D \qquad [2.5.4]$$

Here,

$$\varepsilon^* = \frac{\Pi N_c K}{6 D^3} \qquad [2.5.5]$$

is the value of interaction potential at the hard-sphere distance D.

When this interaction potential, Eq. [2.5.3], is put into Eq. [2.5.2], it becomes:

$$\frac{1}{P_o} = \frac{1}{kT\,N_s}\left\{A_s D \sum_{m=1}^{\infty} [1/m!\,(3m-1)]\,(\frac{\varepsilon^*}{kT})^m - A_s D\right\}$$

$$= \frac{A_s D}{kT\,N_s}\left\{\sum_{m=1}^{\infty} [1/m!\,(3m-1)]\,(\frac{\varepsilon^*}{kT})^m - 1\right\} \qquad [2.5.\ 6]$$

Formula [2.5. 6] is analogous to Keesom's expression (51) for the second virial coefficient (39). Thus, Eq. [2.3.35] becomes

$$\frac{N_a}{A_s} = \frac{DP}{kT}\left\{\sum_{m=1}^{\infty} [1/m!\,(3m-1)]\,(\frac{\varepsilon^*}{kT})^m - 1\right\} \qquad [2.5.\ 7]$$

where N_a is the number of adsorbed atoms or molecules, A_s is the adsorbing surface area in m^2, D is the closest distance of the centers of the gas atoms with the surface in m. P is the measured pressure above adsorbed layer in newtons per m^2, k is the Boltzmann's gas constant = 1.38×10^{-23} joule/°K, and T is the absolute temperature in °K.

By substituting the Kirkwood and Muller's constant, K into Eq. [2.5. 5] we get

$$\varepsilon^* = \frac{\pi\, N_c\, m_e\, c^2\, \alpha_1\, \alpha_2}{D^3\,(\frac{\alpha_1}{x_1} + \frac{\alpha_2}{x_2})} \qquad [2.5.\ 8]$$

where N_c is the number of atoms per cubic centimeter of solid, m_e is the mass of an electron, c is the velocity of light. D is the distance of closest approach of the centers of the gas atoms, α_1 and α_2 are the polarizabilities, and x_1 and x_2 the diamagnetic susceptibilities of the gas atoms and the solid atoms respectively.

2.6 PHYSICAL PROPERTIES OF SUBSTANCES

For the numerical calculations of the parameter, it is necessary to compile a list of the appropriate physical properties of the substances to be considered. In certain cases where no experimentally determined values were available, estimations based on either observed related properties or theoretically calculated properties were made.

While the diamagnetic susceptibilities are not available, the indexes of refraction or the polarizabilities are available. From the Kirkwood formula (47):

$$x = \frac{e^2 N_c a_o}{4 m_e c^2} (n \alpha_o)^{1/2} \qquad [2.6.\ 1]$$

where x is the diamagnetic susceptibility, e and m_e are the charge and mass of an electron. N_c is the number of atoms per cm^3 of the solid, c is the velocity of light, a_o is the Bohr radius, n is the number of electrons and α_o is the atomic polarizability. Compiled data on densities, atomic polarizabilities, atomic susceptibilities and ionization potentials for various substances are given in Table 2.1.

The values of D can be obtained by the true numerical calculation of the shape of Palanyi interaction potential (Eq. [2.4. 1]), since D is assumed to be the distance of the minimum attractive potential from the solid surface.

2.7 A TEST OF THE PRESENT THEORY

It is desirable to compare the predictions of the theory presented here with experimental results obtained on some systems. To do this, it is necessary to evaluate P_o from Eq. [2.5. 6]. For convenience, we put

$$S' = \sum_{m=1}^{\infty} [1/m!\ (3m - 1)] \left(\frac{\varepsilon^*}{RT}\right)^m \qquad [2.7.\ 1]$$

The values of S' were computed by the ILLIAC computer and are shown in Fig. 2.2.

For large m (low temperature):

$$S' \sim \sum_{m=1}^{\infty} \frac{1}{3(m+1)!} \left(\frac{\varepsilon^*}{RT}\right)^m$$

$$\sim \frac{1}{3} \left(\frac{\varepsilon^*}{RT}\right)^{-1} \sum_{m=1}^{\infty} \frac{1}{(m+1)!} \left(\frac{\varepsilon^*}{RT}\right)^{m+1}$$

$$\sim \frac{1}{3} \left(\frac{\varepsilon^*}{RT}\right)^{-1} \left[e^{\left(\frac{\varepsilon^*}{RT}\right)} - 1 - \left(\frac{\varepsilon^*}{RT}\right) \right]$$

$$\sim \frac{1}{3} \left[\left(\frac{\varepsilon^*}{RT}\right)^{-1} e^{\left(\frac{\varepsilon^*}{RT}\right)} - \left(\frac{\varepsilon^*}{RT}\right)^{-1} - 1 \right] \qquad [2.7.\ 2]$$

For the first numerical calculation, we want to compare our

analytical results with the helium adsorption isotherm on pyrex at 4.2°K, measured by Hobson (63). Aston, Mastrangelo and Tykodi (64) in 1955 found ε^* to be 700 - 200 cal/mole. We have arbitrarily taken $\varepsilon^* = 296$ cal/gmole, and D = 1.87°A (19) for calculation. (The calculated value from Eq. [2.5. 8] is about 300 cal/gmole, if we take

$N_c \cong 10^{22}$ atom/cm^3, $m_e = 9.1 \times 10^{-28}$ g and $C = 3 \times 10^{10}$ cm/sec.)

Here $\varepsilon^*/RT = 35.2$, $\log_{10} S' = 13.37$, $S' = 10^{13.37} = 2.34 \times 10^{13}$. The results of calculations from Eq. [2.5. 7] are shown in Fig. 2.3, which shows us that the present theory is adequate in the region of ultra-high vacuum ($p \leq 5 \times 10^{-10}$), and that the first adsorbed layer is complete at a pressure $\leq 10^{-9}$ mm Hg. From Fig. 2.3 we also observe that the limiting pressure, 1.5×10^{-12} mm Hg, represents an instrumental limit of the apparatus.

For the second numerical example, we want to calculate the adsorption isotherms of nitrogen on Pyrex glass from Eq. [2.5. 7] over ranges of temperature and pressure of $63.3 \leq T \leq 90.2$°K, and $10^{-15} \leq p \leq 10^{-9}$ mm Hg respectively. Steele and Halsey (19) have found ε^* and D for N_2 on Pyrex glass to be 4000-5000 cal/mole., and 1.99° A respectively. Here we have assumed $\varepsilon^* = 4800$ cal/mole. for calculation. Numerical calculations for $p = 10^{-12}$ mm Hg are tabulated in Table 2.2 for various temperatures. The results of calculations are shown in Fig. 2.4 by solid lines.

The adsorption isotherms of nitrogen on Pyrex glass over the same range of temperature but higher range of pressure, $5 \times 10^{-10} \leq p \leq 10^{-3}$ mm Hg, were measured by Hobson (65); and it was found useful to plot the data in the coordinates of an adsorption isotherm equation proposed by Duhinin and Radushkevich (66). This equation is $\log \sigma = \log \sigma_m - D [\log (p/P_o)]^2$, where σ is the amount adsorbed (molecules/cm^2), p/P_o is the relative pressure, σ_m is a constant which Kaganer (69) has identified with the number of molecules/cm^2 in a monolayer; and $D = AT^2$, where A is a constant. Values of $\sigma_m = 6.4 \times 10^{-14}$ and $A = 3.28 \times 10^{-6}$, which gave a good fit to the experimental data, were found by trial and error.

Figure 2.4 shows that the physical adsorption of nitrogen on Pyrex at 77.4°K was found to follow the Dubinin-Radushkevich equation for p from 10^{-3} to 10^{-9} mm Hg. However, it is a particular equation within the theory of condensation and might not be expected to apply to physical adsorption at very low coverage. Furthermore, most of the adsorbents to which the Dubinin-Radushkevich equation have been applied (69) have been porous, whereas Hobson (65) concluded that Pyrex glass is nonporous for nitrogen from his measurements of the adsorption isotherm. Thus, unless and until a basic derivation for this equation is provided, it can only be considered as a useful empirical equation for p from 10^{-3} to 10^{-9} mm Hg.

2.8 CHEMISORPTION THROUGH SOLID SURFACES

Physical adsorption is a necessary prerequisite to chemisorption. It is the rate of collision of physically adsorbed molecules with the substrate rather than the direct impingement of gas upon the surface.

An adsorbed atom will normally vibrate about the positions of minimum potential energy. If it receives from the solid enough energy to reach the continuous equipotential line, it may travel along the surface until it loses energy by colliding with another adsorbed atom, or by interaction with the solid. Thus, there are two states of adsorbed atoms, a vibrating state and a mobile state. Only those adsorbed atoms in mobile or activated state (possessing the energy which is higher than the activation energy, E_o (36)) can diffuse from the outer to the inner area.

Suppose that each atom is activated to the mobile state δ times per second, so that δ n dx dy is the number of atoms which leave an area dx dy (Fig. 2.5(a)) in a unit time, n being the concentration of adsorbed atoms on the outer surface. These atoms will travel an average distance ℓ before deactivation (analogous to the free path of atoms in a gas). The probability that an atom will travel a distance equal to or greater than r is then $e^{-r/\ell}$.

Let dx dy be an element at distance r from dσ, and situated in a direction making an angle θ with its normal. Then the number of the atoms which are activated in dx dy in a unit time and across d is given by:

$$\delta \, n \, e^{-r/\ell} \quad \left(\frac{\cos \theta \, d \, \sigma}{2 \pi r}\right) dx \, dy \qquad [2.8.\ 1]$$

since dσ cos $\theta/2\pi r$ is the fraction of atoms which travel in the direction of dσ. If the gradient in the concentration in direction perpendicular to dσ is uniform, then

$$n = n_o + r \cos \theta \frac{\partial n}{\partial x} \qquad [2.8.\ 2]$$

where n_o is the concentration at the boundary dσ. The excess of those crossing from the side of greatest concentration over those coming from the other side is

$$\int_o^{\infty} \int_o^{2\pi} \delta \left(n_o + r \cos \theta \frac{\partial n}{\partial x}\right) e^{-r/\ell} \frac{\cos \theta \, d\sigma}{2\pi r} \, r \, d \, \theta \, dr. \qquad [2.8.\ 3]$$

This leads to the result that the net flow across unit length of the boundary is

$$(1/2) \delta \, \ell^2 \frac{\partial n}{\partial x} \qquad [2.8.\ 5]$$

Let the average lateral velocity of atoms to be $\bar{v}$ and the time during

which they remain mobile, τ, then $\ell = \bar{v}\tau$. δ, being the number of times a single atom is activated per second, is equal to the reciprocal of the interval of time between two successive activations of the same atom. Defining this time as τ^*, we have a net flow:

$$F = -\frac{\bar{v}^2 \tau^2}{2\tau^*} \frac{\partial n}{\partial x} \qquad [2.8.\ 5]$$

the negative sign indicating flow in a direction opposite to that of increasing concentration.

Consideration of the numbers entering and leaving an area included between two parallel boundaries distant dx apart [Fig. 2.5(b)] gives:

$$\frac{\partial n}{\partial t} = -\frac{\partial F}{\partial x} = D' \frac{\partial^2 n}{\partial x^2} \qquad [2.8.\ 6]$$

where

$$D' = \frac{\bar{v}^2 \tau^2}{2\tau^*} \qquad [2.8.\ 7]$$

Equations [2.8. 6] and [2.8. 7], which are ordinary diffusion equations, determine the flow from the outer surfaces along the cracks to the inner surface. The concentration of adsorbed atoms at the outer surface will be kept at a constant value by the bombarding gas, provided the amount of the latter is large compared with the amount adsorbed.

The solution of the equation is:

$$n = n_o \left\{ 1 - \frac{2}{\sqrt{\pi}} \int_0^{\xi} e^{-\xi^2} d\xi \right\} \qquad [2.8.\ 8]$$

where

$$\xi = \frac{x}{2} \frac{1}{\sqrt{D't}} \qquad [2.8.\ 9]$$

The net number flowing at any time from the outer patch of surface to the inner surface per unit length of its perimeter is

$$F\Big]_{x=o} = -D'\left(\frac{\partial n}{\partial x}\right)_{x=o} = n_o \sqrt{\frac{D'}{\pi t}} \qquad [2.8.10]$$

Hence, the total amount in the interior of the solid per unit length of boundary of an outer patch of surface is

$$N_o = \int_o^t F\Big|_{x=o} dt = 2 n_o \sqrt{\frac{D't}{\pi}}$$

$$= 2 n_o \frac{\bar{v}\tau}{\sqrt{2\tau^*}} \sqrt{\frac{t}{\pi}} = n_o \bar{v}\tau \sqrt{\frac{2t}{\pi\tau^*}} \qquad [2.8.11]$$

It can easily be shown that the fraction of atoms with an energy E_o or higher, which are traveling toward the wall normally, is $e^{-E_o/kT}$. It follows that the ratio of the time during which any one atom is activated to the time during which it is not activated, is $e^{-E_o/kT}$. Hence, we may substitute for τ and τ^* the values

$$\tau = \tau_o; \qquad \tau^* = \tau_o e^{E_o/kT} \qquad [2.8.12]$$

where τ_o is the period of vibration of an adsorbed atom normal to the surface.

Finally, if A_o is the total perimeter of all the patches of surface which are exposed to the bombardment of the gas, we have, for the total amount of gas "inside" the solid after time t,

$$N' = A_o n_o \bar{v} e^{-E_o/2kT} \sqrt{\frac{2\tau_o t}{\pi}} \qquad [2.8.13]$$

Assuming a Maxwellian distribution of velocities

$$f(u,v) = \left(\frac{m}{2\pi kT}\right) e^{-m(u^2 + v^2)/2kT} \qquad [2.8.14]$$

The fraction of atoms with an energy greater than $E_o = 1/2\ m\ v_o^2$ is then

$$\int_{v_o}^{\infty} f(u,v)\ 2\pi v dv = e^{-mv_o^2/2kT} = e^{-E_o/kT} \qquad [2.8.15]$$

The average velocity is

$$\bar{v} = \frac{\int_v^{\infty} f(u,v)\ v^2\ dv}{\int_v^{\infty} f(u,v)\ v\ dv}$$

$$= v_o + \left(\frac{\pi kT}{2m}\right)^{1/2} e^{mv_o^2/2kT} \left[1 - \mathrm{erf}\left(v_o \sqrt{\frac{m}{2kT}}\right) \right] \qquad [2.8.16]$$

When E_o is large compared with kT, the second part in Equation [2.8.16] for $\bar{v}$ is vanishingly small, and we have approximately

$$\bar{v} = v_o \qquad \left(= \sqrt{\frac{2E_o}{m}}\right) \qquad [2.8.17]$$

Therefore, we may have the total amount of gas adsorbed.

$$N' = A_o n_o v_o e^{-E_o/2kT} \sqrt{\frac{2\tau_o t}{\pi}} \qquad [2.8.18]$$

where A_o is the total boundary of all the areas of outer surface, n_o is the total concentration of adsorbed atoms on the outer surface, which can be calculated from the physical adsorption equation, Eq. [2.5. 7], E_o is the energy required for an atom to become mobile, and equals $1/2\ m\ v_o^2$, τ_o is the period of vibration of an adsorbed atom normal to the surface, and t is the time at which N' is measured, assuming N' = 0 when t = 0.

Here it is assumed that each patch of the outer surface is a square of side d. The number of patches will be A_s/d^2, where A_s is the total area of the outer surface. The total perimeter,

$$A_o = 4d \cdot \frac{A_s}{d^2} = 4\frac{A_s}{d} \qquad [2.8.19]$$

where the side of each patch was given by Ward (70), i.e.,

$$d = \left[\frac{32 V_o^2 \tau_o}{\pi 10^a} \right]^{1/2} \qquad [2.8.20]$$

The value of "a", from Ward's figures (70), is approximately 8.3. However, Ward measured time in minutes, so that the value of "a" to be used here is $8.3/\log_{10} 60$.

2.9 THE NATURE OF THE CHEMISORPTION PROCESS THROUGH SILICA GLASS

Various observers (71 - 73) have found that silica glass is permeable to gases. Dunn (74), Wilkins and Rideal (75), and Ward (70) have shown that gases can diffuse along inter-crystalline boundaries or at higher temperature through a crystal lattice; and that the diffusion process can be regarded as possessing a definite energy of activation E_o. Lennard-Jones (10) observed that different energies

of activation would be anticipated for gases which are held to the surface by Van der Waals forces, or by chemical forces, an electron switch having occurred in the latter case. Barrer (76) found that the gases hydrogen, helium and neon with small energies of activation for the migration passed easily through the crystal lattice of crystalline silica or the less symmetrically arranged micelles of "amorphous" silica glass.

For application, a list of activation energies for different gases on various natures of glass is compiled in Table 2.3. It is important to note in Table 2.3, first, that the activation energy for hydrogen in a whole series of silica glasses is remarkably constant, and, second, that there is close agreement for the energy for helium between Barrer's data (76) and that of T'Sai and Hogness (71).

2.10 THE NATURE OF THE CHEMISORPTION PROCESS THROUGH METALS

The chemisorption processes of gases through metals have been studied for over a decade by Sieverts and his co-workers, and by many others. Reference 82 gives a full list of references to the work of Sieverts and his co-workers up to 1930. Summaries of findings on gas-metal equilibria are referred to in the books of McBain (82) and of Smithells (83); and it is intended to give a resume of the data here.

The metals which absorb common gases are summarized in Ref. (84).

A list of activation energies for different gases on various metals is compiled in Table 2.4. For other values for alloys the reader is referred to Ref. (36).

REFERENCES
(Section 2.0)

1. D. Alpert, "New developments in the production and measurement of ultra-high vacuum," J. Appl. Phys. 24, p. 860 (1953).

2. J. H. Reynolds, "High sensitivity mass spectrometer for noble gas analysis," Rev. Sci. Inst. 27, p. 928 (1956).

3. J. P. Hobson and P. A. Redhead, "Factors limiting ultimate pressure in ultra-high vacuum systems," Advances in Vacuum Science and Technology, Pergamon Press, Vol. 1, p. 384 (1960).

4. A. Venema, "The production of ultra-high vacua by means of a diffusion pump," Advances in Vacuum Science and Technology, Pergamon Press, Vol. 1 (1960).

5. B. D. Power, "Ultra-high vacuum by means of diffusion pumps," Edwards High Vacuum, Inc., Niagara Falls, New York (unpublished lecture), (1961).

6. W. D. Davis and T. A. Vanderslice, "A small, sensitive, bakeable mass spectrometer," General Elect. Res. Lab., Rept. No. 60-RL-2501G, Sept. (1960).

7. D. Alpert, "Recent advances in ultra-high vacuum technology," Advances in Vacuum Science and Technology, Pergamon Press, Vol. 1, p. 31, (1960).

8. D. Alpert, "Recent advances in ultra-high vacuum technology," Handbuch der Physik, Encyclopedia of Physics, Vol. XII, Springer-Verlag, p. 609 (1958).

9. R. H. Fowler, Statistical Mechanics, Cambridge Univ. Press, Cambridge, (1939).

10. J. E. Lennard-Jones, "Processes of adsorption and diffusion on solid surfaces," Trans. Faraday Soc., 28, p. 333 (1932).

11. J. E. Lennard-Jones and A. F. Devonshire, "The interaction of atoms and molecules with solid surfaces, III," Proc. Roy. Soc. (London), A156, p. 6, (1936).

12. J. E. Lennard-Jones and A. F. Devonshire, "The interaction of atoms and molecules with solid surfaces, VI," Proc. Roy. Soc. (London), A158, p. 242, (1937).

13. W. J. C. Orr, "Calculations of the adsorption behavior of argon on alkali halide crystals," Trans. Faraday Soc., 35, p. 1247 (1939).

14. D. M. Young, "Calculation of the adsorption behavior of argon on octahedral potassium chloride," Trans. Faraday Soc., 47, p. 1228 (1951).

15. R. M. Barrer, "An analysis by adsorption of the surface structure of graphite," Proc. Roy. Soc. (London), A161, p. 476 (1937).

16. W. J. C. Orr, "The adsorption of non-polar gases on alkali halide crystals," Proc. Roy. Soc., (London), A173, p. 349 (1939).

17. D. M. Young, "The adsorption of gases on caesium iodide," Trans. Faraday Soc., 47, p. 77 (1951).

18. D. M. Young, "The adsorption of argon on octahedral potassium chloride," Trans. Faraday Soc., 48, p. 548 (1952).

19. W. A. Steele and G. D. Halsey, Jr., "The interaction of gas molecules with capillary and crystal lattice surfaces," J. Phys. Chem., 59, p. 57 (1955). (Ph. D. thesis of Steele).

20. A. Wheeler, "Chemisorption on solid surfaces," Structure and Properties of Solid Surfaces, Ch. 13, Univ. of Chicago Press, Chicago (1953).

21. B. M. W. Trapnell, Chemisorption, Academic Press, New York (1955).

22. J. A. Becker, "Adsorption on metal surfaces and its bearing on catalysis," Advances in Catalysis, 7, p. 135 (1955).

23. A. Wheeler, "A new approach to a general theory of adsorption," American Chemical Society Meeting, Atlantic City, N. J. (1949).

24. S. Ono, "Statistical mechanics of adsorption from multicomponent systems, I," J. Phys. Soc. Japan, 6, p. 10 (1951).

25. M. P. Freeman and G. D. Halsey, "The interaction of pairs of gas atoms with surfaces," J. Phys. Chem., 59, p. 181, (1955). (Ph. D. thesis of Freeman).

26. T. L. Hill, "Statistical mechanics of multimolecular adsorption, IV, ...," J. Chem. Phys., 16, 3, p. 181 (1948).

27. T. L. Hill, "Statistical mechanics of multimolecular adsorption, I," J. Chem. Phys. 14, 4, p. 263 (1946).

28. T. L. Hill, "Statistical mechanics of multimolecular adsorption, II, ...," J. Chem Phys., 14, 7, p. 441 (1946).

29. T. L. Hill, "Statistical mechanics of multimolecular adsorption, III, ...," J. Chem Phys., 15, 11, p. 767 (1947).

30. T. L. Hill, "Statistical mechanics of multimolecular adsorption, V, ...," J. Chem. Phys., 17, 6, p. 520 (1949).

31. T. L. Hill, "Statistical mechanics of multimolecular adsorption, VI, ...," J. Chem. Phys., 17, 9, p. 762 (1949).

32. T. L. Hill and S. Greenschlag, "Statistical mechanics of monatomic systems in an external periodic potential field, I," J. Chem. Phys., 34, p. 1538 (1961).

33. W. A. Steele, "An approximate site distribution function from adsorption data; application to adsorbed helium," J. Phys. Chem., 61, p. 1551 (1957).

34. W. A. Steele, "A general theory of monolayer physical adsorption," Advances in Chemistry Series, p. 269 (1961).

35. W. A. Steele and M. Ross, "General theory of monolayer physical adsorption on solids," J. Chem. Phys., 35, p. 850 (1961).

36. A. B. Huang, "Energies of interaction between gases and various surfaces," TR No. 2, Ultra-High Vacuum Proj., Univ. of Ill., Contract No. AF 40(600)-909, AEDC, USAF, (1961).

37. T. L. Hill, Statistical Mechanics: Principles and Selected Applications, McGraw-Hill, New York, Ch. 5, 6, (1956).

38. T. L. Hill, "Relations between different definitions of physical adsorption," J. Phys. Chem., 63, p. 456 (1959).

39. R. H. Fowler and E. A. Guggenheim, Statistical Thermodynamics: A Version of Statistical Mechanics for Students of Physics and Chemistry, Cambridge Univ. Press, Cambridge, p. 444, (1939).

40. W. A. Steele and M. Ross, "Distribution function of a fluid in an external potential field: application to physical adsorption," J. Chem. Phys., 33, 2, p. 464 (1960).

41. T. L. Hill, An Introduction to Statistical Thermodynamics, Addison-Wesley Pub. Co., Inc., (1960).

42. A. R. Miller, "The adsorption of gases on solids," Cambridge Univ. Press, Cambridge (1949).

43. J. Bardeen, "The image and van der Waals forces at a metallic surface," Phys. Rev., 58, p. 727 (1940).

44. H. Margeneau and W. G. Pollard, "The forces between neutral molecules and metallic surfaces," Phys. Rev., 60, p. 128 (1941).

45. M. Polanyi, "Theories of the adsorption of gases: a general survey and some additional remarks," (Introductory paper to Sect. III), Trans. Faraday Soc., 28, p. 316, (1932).

46. H. Margeneau, "Van der Waal's forces," Rev. Modern Phys., 11, pp. 1-34, (1939).

47. J. G. Kirkwood, "Polarisierharkeiten, Suszeptibilitalen und von der wallssche Kräfte der Atome mit mehreren Elektron," Physik. Z., 33, p. 57 (1932).

48. A. Muller, "The van der Waal's potential and the lattice energy of a N-CH_2 chain molecule in a paraffin crystal," Proc. Roy. Soc. (London), A154, p. 624 (1936).

49. R. A. Pierotti and G. D. Halsey, Jr., "The interaction of krypton with metals: an appraisal of several interaction theories," J. Phys. Chem., 63, p. 680 (1959). (Ph. D. thesis of Pieratti).

50. M. P. Freeman, "The nautre of the van der Waal's interaction of gases and solids, II, third order interaction," J. Phys. Chem., 62, p. 729 (1958).

51. W. H. Keesom, Translation from: "Verslagen van de Afdeeling natur-kunde der Kon. Akad. van Wetenschappen te Amsterdam," pp. 1406-1422, 26 Apr. (1912); Comm. Phys. Lab., Leiden, Holland, Suppl. 24B, 32, (1912).

52. J. R. Partington, "An advanced treatise in physical chemistry," Longman's, Green and Co., New York, (1952). (Vol. III, p. 149.)

53. International Critical Tables, Vols. I and IV, McGraw-Hill, New York, pp. 102-174, (1926-28).

54. Handbook of Chemistry, 6th Ed., Handbook Publishers, Inc., Sandusky, Ohio, (1949).

55. American Institute of Physics Handbook, McGraw-Hill, (1957).

56. Handbook of Chemistry and Physics, Chemical Rubber Pub. Co., Cleveland, Ohio, (1949).

57. H. Margeneau, "Quadrupole contributions to London's dispersion forces," J. Chem. Phys., 6, p. 896, (1938).

58. J. W. Mellar, "A comprehensive treatise on inorganic and theoretical chemistry," Longman's, Green and Co., New York, (1939). (Vol. XI.)

59. K. E. Mann, "Suszeptibilitatsmessungen an Sauerstoff un Edelgasen" Z. Physik, 98, p. 548 (1936).

60. J. H. Van Vleck, The Theory of Electric and Magnetic Susceptibilities, Oxford Univ. Press, London, (1932), p. 225.

61. E. C. Stoner, Magnetism, Methuen and Co., Ltd., London (1948) p. 38.

62. C. E. Moore, "Atomic energy levels as derived from the analyses of optical spectra," Washington, US Dept. Commerce, Nat. Bureau of Stds. Circ. 1, p. 46.7, (1947).

63. J. P. Hobson, "First adsorbed layer of helium at 4.2°K," Can. J. Phys. 37, p. 300 (1959).

64. J. G. Aston, S. V. R. Mastrangelo and R. J. Tykodi, "Adsorption of helium on titanium dioxide," J. Chem. Phys., 23, p. 1633 (1955).

65. J. P. Hobson, "Physical adsorption of nitrogen on Pyrex at very low pressures," J. Chem. Phys., 34, p. 1850 (1961).

66. M. M. Dubinin and L. V. Radushkevich, Proc. Acad. Sci., USSR, (Doklad, Akad. Nauk., CCCP,) 55, p. 331, (1947).

67. H. Wüstner, "Uber Diffusion und Absorption von Wasserstoff in Quarzglass," Gekürzte Leipzigen Dissertation, Ann. Phys. Lpz., 46, p. 1095 (1915).

68. J. P. Hobson, "First adsorbed layer of nitrogen on Pyrex at 77.4°K," Can. J. Phys., 37, p. 1105 (1959).

69. M. G. Koganer, "A method for the determination of specific surfaces from the adsorption of gases in the monomolecular region," (English translation), Proc. Acad. Sci., USSR, 116, p. 603 (1957).

70. A.F.H. Ward, "The sorption of hydrogen on copper, I and II," Proc. Roy. Soc., (London), A133, pp. 506-535 (1931).

71. L. S. T'sai and T. R. Hogness, "The diffusion of gases through fused quartz," J. Phys. Chem., 36, p. 2595 (1932).

72. C. C. van Voorhis, "The diffusion of helium through several widely different glasses," Phys. Rev., 23, p. 557 (1924).

73. G. A. Williams and J. B. Ferguson, "The diffusion of hydrogen and helium through silica glass and other glasses," J. Amer. Chem. Soc., 44, p. 2160 (1922).

74. J. S. Dunn, "The low temperature oxidation of copper," Proc. Roy. Soc. (London), 111, p. 210, (1926).

75. F. J. Wilkins and E. K. Rideal, "The kinetics of the oxidation of copper, I and II," Proc. Roy. Soc. (London), A128, p. 394 (1930).

76. R. M. Barrer, "The mechanism of activated diffusion through silica glass," J. Chem. Soc., p. 378 (1934).

77. E. O. Braaten and G. Clark, "The diffusion of helium through fused silica," J. Amer. Chem. Soc., 57, p. 2714 (1935).

78. A. Piutti and E. Poggiolera, R. C. Accad. Lincei, (5), 14, (1923); R. C. Accad. Sci. Napoli, (3), 29, p. 111 (1923).

79. W. D. Urry, "Further studies in the rare gases, II," J. Amer. Chem. Soc., 55, p. 3242 (1933).

80. E. C. Mayer, "Leakage of gases through quartz tubes," Phys. Rev., 6, p. 283 (1915).

81. J. B. Johnson and R. C. Burt, "The passage of hydrogen through quartz," J. Opt. Soc. Amer., 6, p. 734 (1922).

82. J. W. McBain, "Sorption of gases by solids," Routledge (1932).

83. C. Smithells, Gases and Metals, Chapman and Hall (1937).

84. R. M. Barrer, "Diffusion in and through solids," Cambridge Univ. Press, Cambridge, p. 12 (1951).

85. C. B. Post and W. J. Ham, "The diffusion of hydrogen through nickel," J. Chem. Phys., 6, p. 598 (1938).

86. M. V. Lombard, "Sur la perméabilité du nickel à l'hydrogène," C. R. Acad. Sci. Paris, 177, p. 116 (1923).

87. H. Deming and B. Hendricks, "The diffusion of hydrogen through metals," J. Amer. Chem. Soc., 45, p. 2857 (1923).

88. W. R. Ham, "Diffusion of hydrogen through platinum and nickel and through double layers of these metals," J. Chem. Phys., 1, p. 476 (1933).

89. C. Smithells and C. E. Ransley, "The diffusion of gases through metals," Proc. Roy. Soc. (London), A150, p. 172 (1935).

90. O. W. Richardson, J. Nicol and T. Parnell, "The diffusion of hydrogen through hot platinum," Phil. Mag. (6), 8, p. 1 (1904).

91. R. Jovan, "Etude comparative des vitesses de diffusion de l'hydrogène et du deuterium a travers le platine chauffé," J. Phys. Radium, 7, p. 101 (1936).

92. H. W. Melville and E. K. Rideal, "The sorption of hydrogen and deuterium by copper and palladium, II, the sorption by palladium and diffusion through copper," Proc. Roy. Soc. (London), A153, p. 89 (1936).

93. M. V. Lombard, C. Eichner, and M. Albert, "Perméabilité du palladium à l'hydrogène," Bull. Soc. Chem. Paris, 4, p. 1276 (1937).

94. R. M. Barrer, "Stationary and non-stationary states of flow of hydrogen in palladium and iron," Trans. Faraday Soc., 36, p. 1235 (1940).

95. E. O. Braaten and G. Clark, "The diffusion of hydrogen through copper," Proc. Roy. Soc. (London), A153, p. 504 (1936).

96. C. B. Post and W. R. Ham, "The diffusion of hydrogen through carbonyl iron at temperatures from 800°C to 1100°C," J. Chem. Phys., 5, p. 913 (1937).

97. C. Smithells and C. E. Ransley, "The diffusion of gases through metals, II," Proc. Roy. Soc. (London) A152, p. 706 (1935).

98. L. Spencer, "The diffusion of oxygen through silver," J. Chem. Soc., 123, p. 2124 (1923).

99. H. M. Ryder, Elect. (Cl.) J., 17, p. 161 (1920).

3.0 EFFECT OF ADSORPTION ON LOW PRESSURE MEASUREMENT

3.1 FORMULATION OF THE PROBLEM

When the characteristic dimension of the tube (see Fig. 3.1) is many times smaller than the molecular mean free path in free space for similar number density of molecules, the flow becomes free-molecule diffusion or Knudson flow (1). The flow of the gas is determined almost entirely by the collisions with the wall and is practically unaffected by intermolecular collisions. The flow rate at any point in a tube depends on the pressure and temperature distribution along the entire tube. For steady isothermal flow in a long tube with a constant pressure gradient, the flow rate is proportional to the overall pressure gradient. We assume that the instantaneous flow rate is proportional to the instantaneous local pressure gradient. The axial mass rate of flow is thus (2):

$$Q = \left(-\frac{r_t^3}{CRT}\right)\left(\frac{dp}{dx}\right) \qquad [3.1.1]$$

The radial mass rate of flow from the sides due to surface outgassing is, for a ring of width dx (Fig. 3.2):

$$dQ = 2\pi r_t q\, dx \qquad [3.1.2]$$

A mass balance on the element of the length dx gives:

$$\frac{dm}{dt}\left(\frac{\pi r_t^2}{v}\right) dx = 2\pi r_t q\, dx + \frac{r_t^3}{CRT}\left[\left(\frac{\partial p}{\partial x}\right)_{x+dx} - \left(\frac{\partial p}{\partial x}\right)_x\right] \qquad [3.1.3]$$

The gas law $p = \rho RT$ gives:

$$\frac{dm}{dt} = \frac{V}{RT}\frac{\partial p}{\partial t} \qquad [3.1.4]$$

Equating [3.1.3] and [3.1.4], we have

$$\frac{\partial p}{\partial t} = \left(\frac{r_t}{\pi C}\right)\left(\frac{\partial^2 p}{\partial x^2}\right) + \frac{2q'}{r_t} \qquad [3.1.5]$$

where $q' = RTq$, and q' is given by Eq.[2.8.18] as: $q' = \alpha/\sqrt{t}$, where $\alpha = A_o k T n_o v_o \sqrt{2\tau_o}\,\{\exp(-E_o/2kT)\}/2A\sqrt{\pi}$, until equilibrium is established at the surface, q' can be + (desorption) or - (adsorption).

At the boundary condition $x = 0$. A mass balance on the element as shown in Fig. 3.3 gives:

$$\frac{\partial m}{\partial t} = \frac{V_g}{RT} \left.\frac{\partial p}{\partial t}\right|_{x=0} = Aq + \frac{r_t^3}{CRT} \left.\frac{\partial p}{\partial x}\right|_{x=0}$$

Hence

$$\left.\frac{\partial p}{\partial t}\right|_{x=0} = \frac{Aq'}{V_g} + \left(\frac{r_t^3}{V_g C}\right) \left(\frac{\partial p}{\partial x}\right)_{x=0} \qquad [3.1.\ 6]$$

At the boundary condition x = L, the net molecular flow is given by (2):

$$\frac{dm}{dt} = \left(\frac{4\pi C r_o^2}{3}\right) (p - p_o) \qquad [3.1.\ 7]$$

A mass balance on the element as shown in Fig. 3.4 gives

$$-\frac{r_t^3}{CRT} \left.\frac{\partial p}{\partial x}\right|_{L-dx} - \frac{4\pi C\, r_o^2}{3} (p - p_o) + 2\pi r_t\, q\, dx = \frac{dm}{dt} \left(\frac{\pi r_t^2}{V}\right) dx \qquad [3.1.\ 8]$$

as $dx \to 0$. At x = L,

$$-\frac{r_t^3}{CRT} \left(\frac{\partial p}{\partial x}\right)_L = \frac{4\pi C\, r_o^2}{3} (p - p_o)$$

or,

$$\left(\frac{\partial p}{\partial x}\right)_L = \frac{3 r_o^2}{8 r_t^3} (p_o - p) \qquad [3.1.\ 9]$$

3.2 CALCULATION OF THE CONSTANT a

From the above section, we have the constant,

$$a = \frac{n_o A_o V_o kT \sqrt{2\tau_o} \left[\exp\left(-E_o/2kT\right)\right]}{2A\sqrt{\Pi}} \qquad [3.2.\ 1]$$

which depends upon the nature of the gas and the surfaces. In Eq. [3.2. 1], a has the dimension of $\frac{(\text{Pressure})\ (\text{Length})}{(\text{Time}^{1/2})}$, n_o is the total concentration of adsorbed atoms on the outer surface which can be calculated from the physical adsorption equation, Eq. [2.5. 7], and has the dimension of (molecule/cm^2), A_o is the total boundary of all the areas of outer surface (cm), V_o is the average velocity of the activated

atoms and equals $\sqrt{\frac{2E_o}{m}}$(cm/sec), k is the Boltzmann constant ($= 1.38 \times 10^{-16}$ erg/°K), T is the absolute temperature (°K), τ_o is the period of vibration of an adsorbed atom normal to the surface and is usually assumed to be 10^{-13} sec, A is the inside surface area of the gauge (cm^2) and E_o is the activation energy.

From Section 2.8, we have

$$A_o = 4 \frac{A_s}{d} \qquad [3.2.\ 2]$$

and

$$d = \left[\frac{32\ V_o^{\,2}\ \tau_o}{\pi 10^a}\right]^{1/2} \qquad [3.2.\ 3]$$

where

$$a \cong \frac{8.3}{\log_{10} 60} = 4.67.$$

For a numerical example, let us take the conditions from the case used by Schaaf (3). The surface is Pyrex glass and the dimensions of the gauge are L = 25.4 cm, r_t = 0.11 cm. The initial pressure in the gauge is $P_i = 10^{-3}$ mm Hg, T = 293°K. We take $\varepsilon^* = 4.8$ Kcal/mole (N_2 on Pyrex glass), $\varepsilon^*/RT = 8.23$, Log S = 2×10^2 (from Fig. 3.5). By using Eq. [2.5. 7] we get $n_o = N_a/A_s = 1.31 \times 10^8$ molecules/cm^2. From table 2.3, $E_o = 14 \times 10^3$ cal/g-mole (air on fused silica glass), $E_o/2RT \cong 12$, $e^{-12} = 6.1 \times 10^{-6}$, $V_o \cong 10^6$ cm/sec. By Eq. [3.2. 3] we estimate $d \cong 2 \times 10^{-4}$ cm and $\frac{A_o}{A} = 2 \times 10^4$. Thus:

$$\alpha = \left[1.3 \times 10^8 \times 2 \times 10^4 \times 10^6 \times 1.38 \times 10^{-16} \times 293 \times 4.5 \times 10^{-7} \times 6.1 \times 10^{-6}\right] + \left[2 \times 1.77\right]$$
$$\cong 10^{-7} \text{ dyne/cm} \sqrt{\text{sec}}$$

3.3 GAUGE RESPONSE TO STEP-WISE CHANGE IN PRESSURE OF ENVIRONMENT AS A FURTHER REFINEMENT OF THE STUDY BY SCHAAF (3)

Solution of Eq. [3.1. 5] subjecting to Eqs. [3.1. 6] and [3.1. 9] at the case, $\tau \leq 0$, $p = p_i$; $\tau > 0$, $p = p_o$, gives the following results. The method of solution includes Laplace transformation and inversion with asymptotic expansions from $\tau = 0$ and $\tau = \infty$. The procedures are well known.

Results are:

For step-wise change of environment pressure from asymptotic expansion from t=0, that is, for the initial variation of envelope pressure:

$$P^*(x^*,t^*) = \frac{3}{4\sqrt{\pi}} \frac{\beta_7}{\beta_8} \sqrt{t^*}\,(1-P_i^*) \exp\left[-\frac{1}{4}\left(\frac{1}{t^*} - 2\frac{x^*}{t^*} + \frac{x^{*2}}{t^*}\right)\right]$$

$$- \frac{3}{8} \frac{\beta_7}{\beta_8} (1-P_i^*)(1-x^*) \operatorname{erfc}\left[\frac{1}{2}(1-x^*)/\sqrt{t^*}\right]$$

$$+ P_i^* + 4\sqrt{\pi}\,\beta_1 \frac{\beta_7}{\beta_8} \sqrt{t^*} \qquad [3.3.1]$$

at $t^* \to 0$.

From asymptotic expansion from $t \to \infty$, that is, the long time behavior of response:

$$P^*(x^*,t^*) = \beta\frac{1}{2}\left\{\left[\theta_1 \operatorname{erfc}\left(\frac{1}{2}\sqrt{t^*}\right) + [\beta_4 + 2\pi\beta_6 x^* + (1-P_i^*)/\beta_1\right]\operatorname{erfc}(x^*/2\sqrt{t^*}\right]$$

$$+ \left[(2\theta_2/\sqrt{t^*}) + (\theta_1 x^*/\sqrt{\pi t^*}) + \left(\theta_2 + \frac{\theta_1 x^*}{4\sqrt{\pi}}\right)\frac{x^*}{t^{*3/2}}\right]\exp\left(-\frac{1}{4}t^*\right)$$

$$+ \left[\left(-\frac{\theta_1}{\sqrt{\pi}} + 2\theta_2 + \theta_3 P_i^* - \theta_3\right)\frac{1}{\sqrt{t^*}} + \left(\theta_2 - \frac{\theta_1}{4\sqrt{\pi}}\right)\frac{x^*}{t^{*3/2}}\right.$$

$$\left. - 4\sqrt{\pi}\,\beta_6 \sqrt{t^*}\right] \exp\left(-x^{*2}/4t^*\right)$$

$$+ \left[\frac{1}{\beta_1}(1+P_i^*) - 2\beta_2 - 2\pi\beta_6 x^* + 4\sqrt{\pi}\,\beta_6 \sqrt{t^*}\right]$$

$$\left. - \left[\theta_3 (P_i^* - 1) + \frac{2}{\sqrt{\pi}}\beta_2 x^* + \frac{x^*}{\sqrt{\pi}\,\beta_1}(P_i^* - 1) + \sqrt{\pi}\,\beta_6 x^{*2}\right]\frac{1}{\sqrt{t^*}}\right\}$$

[3.3.2]

as $t^* \to \infty$.

In the above constants β_i's and θ_i's are related to the geometry of the envelope, and

$$\beta_1 = \frac{\alpha\sqrt{C}}{p_o\, r_t^{1/2}} \qquad \beta_5 = \frac{A}{r_o^2} \qquad P^* = p/p_o$$

$$\beta_2 = \frac{V_g}{r_t^3} \qquad \beta_6 = \frac{L}{r_t} \qquad x^* = x/L$$

$$\beta_3 = \frac{V_g}{r_o^3} \qquad \beta_7 = \frac{L}{r_o} \qquad t^* = \frac{t\, r_t}{\pi C L^2}$$

$$\beta_4 = \frac{A}{r_t^2} \qquad \beta_8 = \frac{r_t}{r_o} \qquad A = \pi r_t^2$$

$$C = \tfrac{3}{4}/\sqrt{2\pi RT}$$

$$\theta_1 = 2\beta_2 - \beta_4 = (2V_g - Ar_t)/r_t^3$$

$$\theta_2 = \frac{4}{3\sqrt{\pi}}\left(\frac{\beta_5}{\beta_6} - 2\frac{\beta_3}{\beta_7}\right) = -4\,(2V_g - Ar_t)/3\sqrt{\pi}L\, r_o^2$$

$$\theta_3 = \beta_2/\pi^{3/2}\,\beta_6\,\beta_1 = p_o\, V_g/\pi^{3/2}\, r_t^{3/2}\, L\alpha\sqrt{C}$$

Computations were made first with the data from the case calculated by Schaaf (3) as a test of the present method. The basic data for that case are as follows:

$\alpha = \pm 2.36 \times 10^{-6}$ * $\beta_1 = \pm 25$ * $V_g = 164\ cm^3$

$L = 25.4$ cm $r_t = 0.11$ cm $r_o = 0.02$ cm

$t_L = 41$ sec $p_i = 10^{-3}$ mm Hg, and $p_o = 10^{-9}$ mm Hg

The results of the computations are shown in Fig. 3.6, which shows us the improvement in accuracy and pertinency of our assumption. It is seen that when $\alpha/\sqrt{t}$ is taken as a constant, we get the results of Schaaf (3).

Another set of computations was made for the gauge envelope as shown in Fig. 3.7. The numerical data are:

$$C \simeq 1.225 \times 10^{-5}\ \text{sec/cm (for } T = 20^{\circ}C)$$

* This is an estimation for a Pyrex glass surface, positive for desorption and negative for adsorption.

$\alpha = \pm 5.22 \times 10^{-6}$ (for copper) $\quad \beta_3 = 0 \quad V_g = 0$

$A_1 = 2.599 \times 10^4 \quad \beta_4 = 3.14 \quad A = \pi$

$t^* = 1.04 \times 10^3 \, t \quad \beta_5 = 12.56 \quad \beta_6 = 5$

$\beta_1 = \pm 18.445 \quad \beta_7 = 10 \quad \beta_8 = 2$

$\beta_2 = 0 \quad P_i = 10^6$

Results of calculations are shown in Table 3.1, and in Fig. 3.8.

3.4 GAUGE RESPONSE TO A LINEARLY DECREASING PRESSURE OF ENVIRONMENT TO APPROXIMATE THE ASCENT OF A SOUNDING ROCKET

In this case we consider a linear variation of pressure with time, such as during the ascent of a rocket. Here, we are only interested in the long time behavior, or $t^* \to \infty$. Solution for asymptotic expansion from infinity for

$$p_o = D_o + D_1 \, t \qquad [3.4.1]$$

is straight-forward. The result is as follows:

$$P^* = \frac{\beta_1}{2}\Bigg\{\theta_1 \operatorname{erfc}\left(\frac{1}{2\sqrt{t^*}}\right) + \left[\beta_4 + 2\pi\beta_6 x^* + \frac{1}{\beta_1}(D_o^* - P_i^*) + \theta_4\right] \operatorname{erfc}\left(\frac{x^*}{2\sqrt{t^*}}\right)$$

$$+ \left[2\theta_2 \frac{1}{\sqrt{t^*}} + \frac{1}{\sqrt{\pi}}\theta_1 \frac{x^*}{\sqrt{t^*}} + \left(\theta_2 + \frac{1}{4\sqrt{\pi}}\theta_1 x^*\right)\frac{x^*}{t^{*3/2}}\right] \exp\left(-\frac{1}{4t^*}\right)$$

$$+ \left[\left(-\frac{1}{\sqrt{\pi}}\theta_1 + 2\theta_2 + \theta_3 (P_i^* - D_o^*)\right)\frac{1}{\sqrt{t^*}} + \left(-\frac{1}{4\sqrt{\pi}}\theta_1 + \theta_2\right)\frac{x^*}{t^{*3/2}}\right.$$

$$\left. - 4\sqrt{\pi}\,\beta_6\sqrt{t^*} - \frac{2}{\sqrt{\pi}}\theta_4\right] \exp\left(-\frac{x^{*2}}{4t^*}\right)$$

$$+ \frac{1}{2}\beta_{10} x^* \int_o^{\beta_{11} t^*} \frac{1}{\tau^{3/2}} \exp\left(-\frac{\beta_{11}}{4} x^{*2} \frac{1}{\tau}\right)(\beta_{11} t^* - \tau)\, d\tau$$

$$+\left[\left(\frac{1}{\beta_1}\left(D_o^* + P_i^*\right) - 2\beta_2 - 2\pi\,\beta_6\,x^* + \theta_4\right) + \left(4\sqrt{\pi}\,\beta_6 + \frac{2}{\sqrt{\pi}}\,\theta_4\right.\right.$$

$$\left. + 2\sqrt{\pi}\,\beta_6^2\,\beta_9\,x^*\right)\sqrt{t^*}\Big] - \Big[\theta_3\left(P_i^* - D_o^*\right) + \frac{2}{\sqrt{\pi}}\,2x^* + \frac{1}{\sqrt{\pi}}\,\frac{1}{\beta_1}\left(P_i^* - D_o^*\right)x^*$$

$$\left. + \sqrt{\pi}\,\beta_6\,x^{*2} + \frac{1}{2\sqrt{\pi}}\,\theta_4\,x^{*2}\right]\frac{1}{\sqrt{t^*}} + \pi\,\beta_6^2\,\beta_9\,t^*\Big\} \qquad [3.4.\ 2]$$

where $P^* = p/D_o$, and $\beta_1, \ldots, \beta_8$ are the same as in section 3.3. In addition,

$$\beta_9 = \frac{C^{1/2}\,D_1\,r_t^{3/2}}{\alpha} \qquad \beta_{10} = \frac{D_1\,L}{\alpha} \qquad \beta_{11} = \frac{\pi C L^2}{r_t}$$

$$\theta_1 = 2\beta_2 - \beta_4 \qquad \theta_2 = \frac{4}{3\sqrt{\pi}}\left(\frac{\beta_5}{\beta_6} - 2\,\frac{\beta_3}{\beta_7}\right)$$

$$\theta_3 = \frac{1}{\pi^{3/2}}\,\frac{\beta_2}{\beta_6\,\beta_1} \qquad \theta_4 = \beta_2\,\beta_6\,\beta_9$$

For a numerical example, we take

$$p_o = D_o + D_1 t = 10^{-3} - \tfrac{1}{3} \times 10^{-5}\,t$$

$$p_{of} = 10^{-9} \text{ mm Hg}$$

and the geometry as given in Fig. 3.7,

$$\frac{p_o}{p_{of}} - P_o^* = 10^6 - 3.205\,t^*$$

$$t^* = 1.04 \times 10^3\,t \qquad \beta_1 = \pm 18.445 \qquad \beta_9 = 8.97 \times 10^{-4}$$

$$\beta_{10} = -.3.16 \qquad \beta_{11} = 9.6 \times 10^{-4}$$

The results of our computations are shown in Figure 3.9, and in Table 3.2.

3.5 GAUGE RESPONSE TO A PERIODICALLY VARYING PRESSURE OF ENVIRONMENT TO APPROXIMATE THE ORBITAL MOTION OF A SATELLITE

For the long time periodic behavior of an orbiting satellite, we approximate the environment pressure variation as:

$$p = M_o + M_1 \sin \omega t \qquad [3.5.1]$$

where $M_o + M_1$ is the pressure at the perigee and $M_o - M_1$ is the pressure at the apogee, ω is the circular frequency of the orbit. The method of solution includes Laplace transformation and inversion with the asymptotic expansion from time infinity. The procedures are straight-forward, and the result is as follows:

$$P^{*\prime} = \frac{\beta'_1}{2}\left\{\theta_1 \operatorname{erfc}\left(\frac{1}{2\sqrt{t^*}}\right) + \left[\beta_4 + 2\pi\beta_6 x^* + \frac{1}{\beta'_1}\left(1 - \frac{p_i}{M_o}\right)\right] \operatorname{erfc}\left(\frac{x^*}{2\sqrt{t^*}}\right)\right.$$

$$+ \left[2\theta_2 \frac{1}{\sqrt{t^*}} + \frac{1}{\sqrt{\pi}}\theta_1 \frac{x^*}{\sqrt{t^*}} + \left(\theta_2 - \frac{1}{4\sqrt{\pi}}\theta_1 x^*\right)\frac{x^*}{t^{*3/2}}\right] \exp\left(-\frac{1}{4t^*}\right)$$

$$+ \left[-\frac{1}{\sqrt{\pi}}\theta_1 + 2\theta_2 + \theta_3\left(\frac{p_i}{M_o} - 1\right)\frac{1}{\sqrt{t^*}} - \left(\frac{1}{4\sqrt{\pi}}\theta_1 - \theta_2\right)\frac{x^*}{t^{*3/2}}\right.$$

$$\left. - 4\sqrt{\pi}\beta_6\sqrt{t^*}\right] \exp\left(-\frac{x^{*2}}{4t^*}\right)$$

$$- \frac{1}{\pi}\frac{M_1 V_g}{r_t^2 \alpha}\int_0^{\frac{\pi CL^2}{r_t}t^*} \frac{1}{\sqrt{\tau}} \exp\left(\frac{\pi}{4}\frac{CL^2}{r_t}\frac{x^{*2}}{\tau}\cos\omega\left(\pi\frac{CL^2}{r_t}t^* - \tau\right)\right) d\tau$$

$$+ \frac{1}{2}\frac{M_1 L}{\alpha} x^* \int_0^{\frac{\pi CL^2}{r_t}t^*} \frac{1}{\tau^{3/2}} \exp\left(-\frac{\pi}{4}\frac{CL^2}{r_t}\frac{x^{*2}}{\tau}\right) \sin\omega\left(\pi\frac{CL^2}{r_t}t^* - \tau\right) d\tau$$

$$+ \left[\frac{1}{\beta'_1}\left(1 + \frac{p_i}{M_o}\right) - 2\beta_2 - 2\pi\beta_6 x^* + 4\sqrt{\pi}\beta_6\sqrt{t^*}\right] - \left[\theta_3\left(\frac{p_i}{M_o} - 1\right)\right.$$

$$\left. + \frac{2}{\sqrt{\pi}}\beta_2 x^* + \frac{1}{\sqrt{\pi}}\frac{1}{\beta'_1}\left(\frac{p_i}{M_o} - 1\right)x^* + \sqrt{\pi}\beta_6 x^{*2}\right]\frac{1}{\sqrt{t^*}} + \frac{1}{\beta'_{10}}\sin\pi\beta'_{11}\beta_6$$

$$+ \frac{1}{\beta'_{10}} (\beta_2 \beta'_{11} x^* + \frac{\pi}{2} \beta_6 \beta'_{11} x^{*2}) \cos \pi \beta'_{11} \beta_6 t^*$$

$$+ (\frac{M_1 \omega L}{a} x^* + \frac{M_1 \omega V_g}{\pi r_t^2 a}) \int_o^{\frac{\pi CL^2}{r_t} t^*} \frac{1}{\sqrt{\tau}} \cos \omega (\pi \frac{L^2}{r_t} t^* - \tau) \, d\tau \Big\} \quad [3.5.\ 2]$$

where $\beta'_1 = \frac{a\sqrt{C}}{M_o \sqrt{r_t}}$ and $\beta_2, \ldots, \beta_8, \theta_1, \theta_2$ are as before. In addition

$$\beta'_{10} = \frac{a\sqrt{C}}{M_1 \sqrt{r_t}} \qquad \beta'_{11} = \omega CL \qquad P^* = \frac{p}{M_o}$$

$$\theta_3 = \beta_2 / \pi^{3/2} \beta'_1 \beta_6 = \frac{M_o V_g}{\pi^{3/2} r_t^{3/2} La\sqrt{C}} \qquad \theta'_4 = \beta_2 \beta_6 \beta'_9$$

Further, for large values of t^*,

$$\frac{1}{t^{*n}} \to o, \exp (m/_t n) \to 1, \operatorname{erfc} (m/_t n) \to 1, \text{ for } n > o$$

Eq. [3.5. 2] is simplified to:

$$P^* = 1 - \frac{\beta'_1}{2} (\frac{\theta_1}{\sqrt{\pi}} - 2\theta) + \frac{\beta'_1}{2\beta_{10}} \Big[\sin \omega t$$

$$+ (\beta_2 \beta_{11} x^* + \frac{\pi}{2} \beta_6 \beta_{11} x^{*2}) \cos \omega t \Big] \quad [3.5.\ 3]$$

from which the change in median pressure, the phase lag θ and the amplitude can be calculated. Writing the gauge pressure as

$$p = M'_o + M'_1 \sin (\omega t + \theta) \quad [3.5.\ 4]$$

we have

$$M'_o = M_o - \frac{a\sqrt{C} (2V_g - Ar_t)}{2\sqrt{\pi r_t}} (\frac{8}{3 L r_o^2} + \frac{1}{\sqrt{\pi} r_t^3}) \quad [3.5.\ 5]$$

$$M'_1 = \frac{M_1}{2}\sqrt{1 + \tan^2\theta} \qquad [3.5.\ 6]$$

$$\tan\theta = \omega CL\left[\frac{V_g}{r_t^3}x^* + \frac{\pi}{2}\frac{L}{r_t}x^{*2}\right] \qquad [3.5.\ 7]$$

Hence, whenever a gauge envelope is used, the pressure variation in its interior has an amplitude of half of that of the environment. Its median pressure depends on the relation as given by Eq. [3.5. 3]. The phase lag varies from zero at the inlet to $\omega CL(V_g + \pi Lr_t^2)/r_t$ at the bottom of the gauge.

For a numerical example, we take the condition (4) of

$$p = 4.18 \times 10^{-4} \text{ mm Hg at 100 Km}$$

$$p = 3.48 \times 10^{-9} \text{ mm Hg at 500 Km}$$

$$p = 1.24 \times 10^{-8} \text{ mm Hg at 300 Km}$$

$$2\pi/\omega = 90 \text{ min} \qquad [3.5.\ 8]$$

Although the variation of ambient pressure is not simple harmonic, we take the approximation:

$$M_o = 2.0900174 \times 10^{-4}$$

$$M_1 = 2.0899826 \times 10^{-4}$$

$$\omega = 0.00116 \text{ rad/sec}$$

and

$$p_o = 2.0900174 \times 10^{-4} + 2.0899826 \times 10^{-4} \sin 0.00116t \qquad [3.5.\ 9]$$

for an illustration of response of periodically varying pressures. For the more accurate case, we can superpose various harmonics of pressure variation.

For the gauge envelope in Fig. 3.7, we now have

$$\beta'_1 = \pm 8.825 \times 10^{-5}$$

$$\beta'_{10} = 8.8254 \times 10^{-5}$$

$$\beta'_{11} = 7.105 \times 10^{-8}$$

The result as calculated is shown in Fig. 3.10.

3.6 GAUGE RESPONSE TO AN EXPONENTIAL VARYING PRESSURE OF ENVIRONMENT

In this case we consider an exponential variation of pressure with time, such as

$$p_o = p_2 + C_1 e^{-b_1 t} \qquad [3.6.\ 1]$$

Solutions of Eq. [3.1. 5], subjecting to Eqs. [3.1. 6] and [3.1. 9] can be obtained. The method of solution which includes Laplace transformation and inversion with asymptotic expansions from $t = 0$ and $t = \infty$ is straight-forward. Here we are especially interested in the long time behavior, or $t \to \infty$. Asymptotic expansion from infinity for Eq. [3.6. 1] gives:

$$p_{x=o} = C_1 e^{-b_1 t} + p_2 - 2\beta_o \beta_2 - \frac{1}{2}\beta_o \theta_1 \operatorname{erf}\left(1/2\sqrt{t^*}\right)$$

$$+ \frac{4}{3}\beta'_o \left(\beta_5 - 2\beta_2 \beta_8{}^2\right)\left[1 + \exp\left(-\frac{1}{4t^*}\right)\right] + \frac{1}{\pi}\beta_2 C_o'$$

$$- \frac{2}{\pi}\beta_2 \sqrt{r_t C}\left[C_1\sqrt{b_1}\, e^{-b_1 t}\int_o^{\sqrt{b_1 t}} e^{\tau^2}\, d\tau\right] \qquad [3.6.\ 2]$$

where $\beta_2, \ldots, \beta_8$ and θ_1 are the same as before; in addition,

$$\beta_o = \frac{a\sqrt{C}}{\sqrt{r_t}}, \qquad \beta'_o = \frac{aC}{\sqrt{t}}, \qquad C_o' = C_1\sqrt{\frac{r_t C}{t}}, \qquad C_o'' = C_2\sqrt{\frac{r_t C}{t}}.$$

3.7 NUDE GAUGE

When a nude gauge is installed over a given surface, it is still under the influence of the outgassing when the environment pressure changes.

To see the order of magnitude of events, we consider the variation of number density of molecules, near an outgassing surface when the pressure at infinity changes suddenly from n_o (initial number density in the semi-infinite medium) to n_∞. We take $n_o >> n_\infty$.

The distribution in number density is given by:

$$\frac{\partial n}{\partial t} = \bar{C} \bigwedge \frac{\partial^2 n}{\partial x^2} \qquad [3.7.\ 1]$$

where $\bar{C}$ is the mean speed of molecules

$$\bar{C} = \sqrt{\frac{8kT}{\pi m}} = \sqrt{\frac{8RT}{\pi}} \qquad [3.7.\ 2]$$

Λ is the mean free path

$$\Lambda = \frac{1}{\sqrt{2}\, n \sigma}$$

where σ is the collision cross-section. In order to keep the problem linear, we take the diffusivity,

$$\bar{C} \Lambda \sim \text{constant}.$$

The boundary conditions of Eq. [3.7. 1] are:

$$t = 0, \qquad n = n_\infty . \qquad [3.7.\ 3]$$

that is, the pressure is changed suddenly in the half-plane with the outgassing rate given by:

$$t > 0, \qquad \frac{\partial(N/A)}{\partial t} = \frac{\alpha}{kT\sqrt{t}} = \frac{1}{4} n \bar{C} \qquad [3.7.\ 4]$$

The solution to Eq. [3.7. 1] by Laplace transformation gives

$$n = n_\infty + \frac{4\alpha}{\bar{C}kT} \frac{\exp\left(-x^2/4Dt\right)}{\sqrt{t}} \qquad [3.7.\ 5]$$

The time for the number density to increase to n at x = 0 is given by:

$$\sqrt{t} = \frac{4\alpha}{\bar{C}kT\,(n - n_\infty)} \qquad [3.7.\ 6]$$

For the surface given in the above example,

$$\sqrt{t} = \frac{4 \times 5.27 \times 10^{-6}}{3 \times 10^{4} \times 1.38 \times 10^{-16} \times 300\,(n - n_\infty)}$$

$$= \frac{5.27 \times 10^{4}}{9 \times 1.38\,(n - n_\infty)} \sim \frac{10^{4}}{2\,(n - n_\infty)} \qquad [3.7.\ 7]$$

Thus, for the ordinary range of n_∞, it takes a very short time for n to increase to correspond to a maximum outgassing rate. It takes a short time for n to reach values to the same order of n_∞, which is what a gauge reads. Therefore, for a nude gauge in a regime of varying pressure, it will read the environment closely before outgassing proceeds sufficiently. Even where outgassing rate is high,

the gauge proper will reduce quickly to the same as the environment. This may also be visualized as a very thin boundary layer due to outgassing. The nude gauge will measure effectively the pressure of the medium.

The above study was made under the simplifying assumptions of an isothermal system and a semi-empirical model of adsorption and desorption. However, the usefulness of the method is tested by experimental results of transient response. (Fig. 3.6)

It is seen that a gauge in an envelope will always experience great time lag in pressure (or number density) measurement, in a sounding rocket or an orbiting satellite. In the case of the orbiting satellite especially, effort toward extrapolating from measurement made by a gauge in an envelope will involve great errors in the low pressure side because in the gauge, the pressure will remain at the same order of magnitued of the highest pressure (Fig. 3.7). A gauge in an envelope should not be used for outer atmosphere measurement in spite of its ease of installation and the ease of shielding against radiation. Where response is important, the nude gauge should always be used. Corrections for the effects of radiation are then necessary.

In static measurement, a gauge in an envelope needs corrections for adsorption of the surfaces as well as for thermal effects.

REFERENCES
(Section 3.0)

1. R. D. Present, Kinetic Theory of Gases, McGraw-Hill, New York, p. 56 (1958).

2. L. B. Loeb, Kinetic Theory of Gases, McGraw-Hill, New York, p. 308 (1927).

3. S. A. Schaaf and R. R. Cyr, "Time constants for vacuum gauge systems," J. of Appl. Phys., 20, 9, p. 860 (1949).

4. B. S. Danilin, "The problem of measuring the pressure and density of the upper layers of the atmosphere using an artificial earth satellite," International Physical Index, Inc., New York, p. 95 (1958).

5. P. D. Porta and Z. Ricca, "Investigations on the adsorption of gases by the getters evaporated from barium alloys - adsorption of nitrogen," Advances in Vacuum Science and Technology, Pergamon Press, 1960, pp. 661-666.

4.0 EXPERIMENTAL SYSTEM AND PROCEDURE

The metal ultra-high vacuum system shown in Fig. 4.1 was designed and constructed to carry out the objectives outlined in the previous sections. Although the ultimate goal of this experimental apparatus was set at the 10^{-12} torr range, vacua up to the 10^{-8} torr range were also considered to be of value to this program. In designing a metal system capable of attaining such a degree of vacuum, it is evident that the system must be simple in order to be fabricated with a minimum amount of leakage--either real or virtual. Simplicity is also advantageous so that, as the system develops and as future needs change, modifications can be easily made. Although most of the present system was based on accepted ultra-high vacuum techniques (1 - 5), some parts of the system had to be based on untried, although logically sound, concepts, since the immediate objective is somewhat beyond the established "state of the art." (6)

The ultra-high vacuum system shown in Fig. 4.2 consists of a stainless steel chamber 12" in length and 11.5" in diameter, which is attached through a Granville Phillips bakeable UHV valve to the forepump system. A cryogenic pump, a mechanical pump and an 8 liter/sec. cold cathode ion getter pump constitute the forepump system. In addition, another 8 liter/sec. cold cathode ion getter pump is located on top of the chamber and is used for terminal pumping. The chamber has five ports, which make it possible to accommodate various combinations of ionization gauge sensing tubes and an ometatron type mass spectrometer tube. One inch tubulation is used throughout the system. The mechanical forepump and/or a helium leak detector can be attached to the system at the extra flange on the cryogenic pump.

Details of the chamber construction are shown in Fig. 4.2. The entire system--excluding the glass gauges and sealing gaskets--is made of 304 stainless steel. Internal welds which might provide virtual leaks are eliminated by machining the sealing surfaces in the chamber wall. All mating surfaces, except the two end plates, are of the step type and use annealed O.F.H.C. copper gaskets for seals. The end plates as well as the ends of the chamber are machined flat, polished with jeweler's rouge and sealed by means of 0.030" dia. gold wire. In order to press directly on the gold gaskets when tightening down the end plates and to take up any thermal expansion during baking and cooling, spring rings are used.

The ultra-high vacuum system is mounted on a table which also supports an electric furnace (indicated by the dashed lines in Fig. 4.2) so that the entire portion above the table top can be conveniently baked out at as high as 450°C. This table also supports the truck which holds the omegatron magnet. This magnet truck can be rolled back so that it is outside the electric furnace during bakeout. The furnace consists of 13 identical rectangular panels. Identical panels are used so that the size of the furnace can be varied to accommodate

larger systems. The table is provided with sixteen 220 volt outlets so that the individual furnace panels can be plugged directly into the table (see Fig. 4.2).

Since the cold cathode ion getter pumps are easier to start and have a longer life when the pressure at which they are started is lower than the 10 microns obtained with the cryopump, an additional forepump can be justified. The additional forepump used is a Welch Duo-Seal mechanical pump which is connected to the cryogenic pump through a liquid nitrogen trap. The pressure in the system can now be reduced to about 10^{-5} torr since the mechanical pump removes gases which cannot be pumped by the cryogenic pump.

For experiments in which minute traces of oil vapor--which invariably back stream from the mechanical pump, even though a liquid nitrogen trap is present--are undesirable, the mechanical pump is eliminated so that the cryogenic pump is the only forepump.

In order to study the effect of low temperature on the system, a reservoir type cooling unit geometrically similar to the bakeout furnace is mounted around the UHV portion of the system. Using this unit, the chamber and attached instrumentation are exposed to a heat sink down to the liquid nitrogen temperature.

4.1 INSTRUMENTATION

The basic instrumentation for this UHV system consists of two standard Bayard-Alpert ionization gauges, a magnetron cold cathode ionization gauge, a nude Bayard-Alpert ionization gauge, an omegatron mass spectrometer and four thermocouples mounted at different depths in the chamber wall in order to determine the inside wall temperature of the chamber.

Although the Bayard-Alpert ionization gauges can be utilized to measure pressures down to about 10^{-10} torr, in the 10^{-12} torr range these gauges are impractical for the following reasons:

1. the vapor pressure of the tungsten filament is about 10^{-12} torr at normal filament temperatures,
2. the gauge has a very low sensitivity,
3. the x-ray current is of the same order as the ion current and cannot be distinguished from it.

In the 10^{-12} torr range, however, the cold cathode magnetron gauge is the only commercially available gauge which claims any degree of accuracy. Since there is no reference pressure in this region, the accuracy of any gauge must be subject to some reasonable doubt. Nevertheless, this type of gauge does have two advantages over the

hot cathode gauge, namely, high sensitivity and very little apparent filament residual gas reaction. The principal disadvantages of this type of gauge are the fact that it does a considerable amount of pumping (about 1 liter/sec for nitrogen) and that fluctuations occur in the gauge under most operating conditions.

A mass spectrometer is an absolute necessity in order to determine which residual gases the gauges see (7 - 9). This instrument is also used to measure the partial pressures of molecular species present.

4.2 PUMPDOWN PROCEDURE

The system is put into operation by roughing down to 10 microns with the cryopump or to 0.01 microns with the cryopump-mechanical pump combination. A leak detection procedure is now followed using the helium detector. If the system is free of leaks, the pump down procedure is continued.

Now the bakeout furnace is placed in position and the bakeout temperature increased in 50°C increments over several hours until the desired temperature is reached (usually about 300°C). At this point the high vacuum valve is closed to eliminate the cryopump and the mechanical pump from the system and the lower 8 liter/second ion getter pump is turned on and is allowed to remain on throughout the baking cycle (usually about 24 hours). After adequate baking out - when the ion getter pump current drops sharply, indicating that the pressure in the system is falling - the Granville Phillips ultra-high vacuum valve is closed and the bakeout furnace is removed. As soon as the bakeout furnace is removed, the 8 liter/second ion getter pump on top of the chamber is started and electrical heating tapes, which were wrapped around the glass gauges before bakeout, are started. The heating tapes reduce excessive condensation and/or adsorption from occurring in the gauges as the entire system cools. This is felt to be necessary since the large mass of stainless steel of which the chamber is made cools much more slowly than the small glass gauges; thus the possibility of condensation and adsorption in the cooler part of the system (namely, the glass tubes) is present.

With this relatively simple pumpdown procedure pressures in the 10^{-10} torr range have been obtained.

REFERENCES
(Section 4.0)

1. S. Dushman, Vacuum Technique, John Wiley and Sons, 1949.

2. D. Alpert, "New developments in the production and measurement of ultra-high vacuum," J. of Appl. Phys. 24, 1953.

3. A. Venema, "The production of ultra-high vacua by means of a diffusion pump," Advances in Vacuum Science and Technology, Vol. 1, Pergamon Press, pp. 389-392 (1960).

4. B. D. Power, "Ultra-high vacuum by means of diffusion pumps," Unpub. lecture, Edwards High Vacuum, Inc., Niagara Falls, New York.

5. D. Alpert, "Recent advances in ultra-high vacuum technology," Advances in Vacuum Science and Technology, Vol. 1, Pergamon Press, pp. 31-38, (1960).

6. J. P. Hobson and P. A. Redhead, "Factors limiting ultimate pressure in ultra-high vacuum systems," Advances in Vacuum Science and Technology, Vol. 1, Pergamon Press, pp. 384-388 (1960).

7. W. D. Davis and T. A. Vanderslice, "A small, sensitive, bakeable mass spectrometer," General Electric Res. Lab. Report No. 60-RL-2501G, Sept. 1960.

8. H. W. Ehlbeck, K. H. Loecherer, J. Ruf and H. J. Schuetze, "The operation of the r-f mass spectrometer at high r-f voltage levels," Telefunken, Ulm (Donau), Germany, paper presented at the 1960 National Symposium on Vacuum Technology.

9. J. H. Reynolds, "High sensitivity mass spectrometer for noble gas analysis," Rev. Sci. Inst. 27, p. 928, (1956).

5.0 EXPERIMENTAL RESULTS

5.1 BAKE-OUT PHENOMENA

Apparatus. It was desired to determine the composition of the "residual" gas during various stages of bake-out of a system similar to that pictured in Fig. 4.2. To accomplish this, the 4000 Gauss omegatron magnet was placed inside the furnace, and the omegatron was operated during bake-out.

The system used was the same as in Fig. 4.2, except that the cryopump was replaced by the leak detector. On the chamber were the NRC Bayard-Alpert gauge, the NRC Redhead gauge, an omegatron, an Ilikon Bayard-Alpert gauge, a thermocouple probe and a Vac Ion pump. A General Radio bridge oscillator and Keithley model 410 micro-microammeter were used with the omegatron. The approximate total glass surface was 1100 cm^2 and the approximate total metal surface area was 2800 cm^2. The NRC gauges were not operated during these tests. There were no heating tapes used.

Procedure. The system was first checked with a helium leak detector and then the Vac Ion pumps started. The Ilikon was then outgassed and started; and a room temperature sweep was made with the omegatron. The furnace was then turned on. When the thermocouple probe read about 50°C, another sweep was made with the omegatron. This omegatron data was obtained for 100°C, 150°C and 200°C; the time interval between each of these sweeps was about two hours. In the interests of preserving the magnets, 200°C was set as the upper limit.

This test was run twice. During the first run, there were 2 sets of data taken for each temperature: one set with the furnace on, one with the furnace off. The reason for doing this was to separate the effects caused by the fact that the glass bulbs were at a higher temperature relative to the chamber wall when the furnace was on. Between runs, the system was opened to the atmosphere for about one hour. During this time a new Vac Ion pump was mounted on the chamber in place of the old one. During the first run, the Vac Ion was not water cooled; during the second run, the Vac Ion was water cooled. All of the data taken during the second run was with the furnace on.

It should be noted that great care was taken to sort out harmonics and sporadic readings from the omegatron data. There was also a constant check made on the noise level of the micro-microammeter.

There were no detectable leaks at the end of either test.

Results. The results of the second test are shown in Figs. 5.1 through 5.5. The results of the first test showed identical trends, but with slightly different percentages. The values used here are all corrected for relative ionization sensitivity. P_T is obtained by

adding all of the corrected partial pressures.

The results in the first test of turning the furnace off and on were as follows: the relative abundance of masses 58, 71, 83 and 200 appeared to be comparatively dependent upon whether the furnace was on or off. These represent a very small percentage of the total, however. A typical example is mass 83 at 100°C. With the furnace off, its abundance was 0.4%; with the furnace on, its abundance rose to 1.4%. Masses 28, 16 and 2 (H_2) were slightly dependent upon the furnace being off or on. For instance, H_2 at 150°C had a relative abundance of 30.5% with the furnace off and 33.6% with it on. The relative abundances of masses 26, 18 and 17 were virtually unaffected. In every case, when the furnace was turned off, there was a drop in total pressure by a factor of about 4, even though the thermocouple probe and furnace thermostat indicated no change of temperature.

Discussion. It is apparent that the admixture of exposed glass and stainless steel in the system is going to introduce experimental problems, especially when the desired data is measured by an omegatron whose effective wall is platinum. The effect of envelop material on gauge sensitivity will be discussed later. For the purposes of this report, the effect of the platinum on the omegatron readings will be neglected.

As noted earlier, there was a drop in pressure by a factor of 4 when the furnace was turned off, in spite of the fact that both the thermocouple probe and the furnace thermostat indicated no change in temperature, either inside or outside the chamber. Evidently, when the furnace was on, the glass envelopes were at a considerably higher temperature than the stainless steel, due to direct radiation. When the furnace was off, their temperatures dropped to a value nearly that of the steel. It is possible that the glass temperature was as high as 400°C.

First Test. The fact that the relative abundance of masses 58, 71, 83 and 200 is comparatively dependent upon whether the furnace elements are on or off would indicate that these are baked off the glass at temperatures around 200°C. Evidently, masses 2, 28 and 16 are baked off the glass at slightly higher temperatures, say 400°C. Apparently, water and mass 26 either have no preferential temperature, or come off at somewhat higher temperature. Probably the former is true of water, the latter true of mass 26. As has been mentioned in various references, the water may come from within the glass.

Second Test. Since all the data for this test was taken with the furnace on, the glass bulbs were constantly at a higher temperature than the steel chamber's inside wall. This introduces a certain amount of ambiguity into the results, but trends can be discerned.

As can be seen, all components of the residual gas had a dip at around 120°C. Before this temperature there is a maximum; and if the

tests had been extended to higher temperatures, say 400°C, another maximum (different for each component) would most likely have been found. The first maximum is probably due to the discharge of all the loosely bound gases, those with physical adsorption (this can be thought of as the first few layers of the several molecular-layers). It follows naturally that the more tightly adsorbed layers will need higher bake-out. As can be seen from these curves, another 100°C or so would probably see peaks in H_2, mass 28 and CO_2.

Figures 5.4 - 5.7 show that some of the components exhibit "group" behavior, i.e., masses 58, 71, 83 and 200 follow very similar trends, as do CH_4, masses 15 and 26. This "group" behavior is helpful in the determination of products of fragmentation at the filament, and differentiating, with the help of the furnace on - furnace off results of the first test, between fragments and "whole" desorption species. Judging from a study of these trends and the results of the first test, masses 58, 71, 83 and 200 are all fragments of the same molecule, probably a hydrocarbon from the oil of the forepumping system. Mass 15 probably is CH_3; mass 26, though it follows the same trend in Fig. 5.5 as mass 15 and CH_4, did not exhibit the same behavior as CH_4 in test one (furnace on - furnace off), so it is fairly certain that CH_4 is not produced as a fragment of mass 26.

The reasons behind the results indicated in Fig. 5.7 are as yet unknown.

The somewhat "confused" trends of Figs. 5.4 and 5.5 are very nearly reproducible. The decreasing percentage at 200°C is due mostly to the rapid increase in H_2 at this point.

Differences Between Tests. The slight differences in trends, the differing percentages and the comparatively large deviation in the behavior of mass 28 between the two tests may be attributable to the use of a different Vac Ion pump. The pump used in the second test was a so-called "Super Vac Ion Pump" with a modified cathode; also, this pump was water cooled, whereas the one used in the first test was not. History of the system is probably also a cause of some of these differences.

Identification of Species. Mass spectrometer data is always somewhat ambiguous by virtue of the fact that several kinds of molecules may have the same mass; for instance, mass 28 could be either CO or N_2; mass 17 could be CH_5^+ or $(OH)^+$; mass 16 could be O^+ or CH_4; etc. About the only two that one can be sure of are H_2 and He. To determine whether mass 28 is CO or N_2, one must look for masses 14 and 12 (N^+ and C^+), fragments caused by the ionization process. We have both, but in varying amounts. This aspect should be pursued further to determine if a differentiation can be made. Mass 26 may be C_2H_2. Mass 18 is very probably H_2O. Mass 16, in view of the work by Hickmott, et al (1) is probably CH_4. This would be the result of dissociation of H_2 at a hot filament. Mass 15, then, is CH_3.

For mass numbers above 30, the omegatron leaves much to be desired. It becomes very difficult to sort out the masses above this point. CO_2 is fairly certain from observations which have been carried out on pure gas systems, and from Hickmott's work. The mass numbers above 50 are a near guess.

Method of Temperature Measurement. The tip of the thermocouple probe used was about in the center of the chamber and was in "radiation equilibrium" with the chamber wall; it, therefore, was indicating some average wall temperature. The total temperature change of the wall temperature, as measured by thermocouples in the wall itself, was of the order of 30°C at 100°C, and 40°C at 150°C. Even with the thick wall which would tend to "smooth out" the temperature difference on the inside, there were large temperature variations on the inside wall.

Decrease of Omegatron Magnet Strength. During the course of these two experiments, the strength of the magnet decreased from 4200 to 4000 Gauss, due to the relatively high temperature. This was compensated for in the readings so that there was no confusion of masses. This would not affect the values of per cent composition as reported.

Experimental Uncertainties in Omegatron Readings. In our work, the omegatron was tuned twice for each set of data, once for masses 1 - 38, and again for masses 39 to 250. By not tuning it again for H_2, an accuracy error of about 3 - 5% was introduced, but this does not interfere with the trends. Considering this, plus the 4% precision of the micro-microammeter, the following approximate precision errors apply:

Omegatron readings for room temperature:	± 8%
Omegatron readings for 50°C	± 7%
Omegatron readings for 100°C	± 6%
Omegatron readings for 150°C	± 6%
Omegatron readings for 200°C	± 6%

The nominal sensitivity of the omegatron is 10/torr for nitrogen. But this gauge is notorious for its ability to change apparent sensitivity. This change occurs when the omegatron is retuned or when there is a large change of pressure. This is one of the main reasons for reporting percent compositions along with partial pressures. The above figures for probable error apply only within any given tuning; it follows that the trends of percent composition are more accurate than the trends of partial pressure.

Conclusions and Recommendations. The residual gases after a 125°C bake-out would be H_2, CH_3, CO, CO_2, CH_4, N_2 and H_2O. There would be few, if any, hydrocarbons left. This low bake-out rids the system of most of the loosely sorbed materials. Plotting omegatron data as a function of temperature helps to identify and relate various

species, besides indicating qualitatively their adsorption characteristics.

These tests should be repeated, using a wider range of temperatures (- 180°C to + 400°C) as well as systematically studying the effect of the history of the system. In future tests, less glass should be in the system and what glass there is should be shielded from direct radiation from the furnace elements. The work should be carried on with different wall materials as well.

5.2 DIFFERENCES IN GAUGES

We are interested in the differences encountered in the various types of ionization gauges; for instance, do we expect any difference in performance between a Bayard-Alpert gauge having a metal film on the envelope and, say, the Nottingham variation of the gauge, which has the protective grid and ordinary Pyrex glass envelop? Apparently, the differences are primarily due to (1), the effect of the gauge on the composition of its local residual gas, (2), time response of the gauges and (3), ejection of charged particles from electrodes and surface ionization. Each of these things apparently cause differences in performance between the various types of gauges. The first category, effect of the gauge on the composition of residual gas, can be subdivided as follows:

(a) effect of the hot filament, including chemical reactions at the walls,

(b) "secondary emission" of neutral particles from electrode and wall surfaces by bombardment of electrons and ions (2),

(c) wall potential and accommodation effect on composition.

Only (a), effect of the hot filament, has been experimentally examined to any extent.

5.2.1 Effect of Hot Filament

The pumping of the hot filament was first investigated by Langmuir in 1912 (3). Langmuir found that when a tungsten wire is heated to a temperature of between 1300°K and 2500°K, that H_2 was slowly cleaned up. Furthermore, this is a temperature dependent phenomenon, i.e., the higher the temperature, the greater the rate of clean up. With nitrogen or CO, such disappearance or clean up never occurs below about 2200°K, and seems to be a chemical or electrical effect, while the clean up of hydrogen seems to be purely thermal. There is a distinct saturation of the pumping, but the substitution of a new section of wire does not restore the action. If one wire is brought to incandescence, and pumped to saturation, and then another clean wire in the same system is also brought to incandescence, there is no more clean up. So the H_2 is not absorbed by the wire. Langmuir showed

that it is deposited on the glass, especially when the latter is cooled by liquid air. If the wire is allowed to cool and the liquid air is then removed, ordinary H_2 is set free, which will not recondense when liquid air is replaced. If this gas is pumped out and oxygen is admitted (or some other active gas), the oxygen will disappear and in its place a small quantity of hydrogen will appear. Langmuir found that with platinum and palladium this effect is much more marked; it is a function also of the surface properties of the filament as well as its chemical composition. These effects are not due to the presence of metal on the surface of the glass. Langmuir accounted for these by showing that the H_2 dissolves in the material of the wire in the atomic condition, but the atoms leaving the wire do not meet other atoms (because of the large mean free path), but diffuse to the envelope and are absorbed there in the atomic condition. They retain all the chemical activity inherent in the atomic hydrogen.

Hickmott (1) and others have shown that atomic hydrogen reacts with a glass envelop to produce contaminant molecules CO, H_2O and CH_4. This effect may vary with the type of glass used.

In the case of a metal envelop, the atomic hydrogen recombines to form molecular hydrogen much more easily, and therefore the pumping effect is more quickly saturated. However, Fox, et al (4) have found that the recombination of atomic hydrogen is poisoned under some circumstances; this poisoning has been attributed to contaminant species produced by reactive hydrogen atoms.

It was found that when hot cathode gauges with glass envelopes were first turned on, they became very high speed hydrogen pumps. This would cause a local scarcity of H_2 in the gauge and a general decrease in the quantity of H_2 in the chamber, as well as a decrease in total pressure. Since ionization gauge sensitivity is very composition-dependent, one would expect a change in apparent sensitivity due to this. Therefore, differences can be expected from, say, two different types of hot cathode gauges with different envelope materials and filaments (different sizes and resistances) which are operating at the same emission current. Since the filaments will operate at different temperatures, depending on the resistance and size for the same emission current, the filament at the higher temperature will pump faster; and, since the saturation of the pump depends upon the wall material, one gauge will pump longer than another.

To study these effects, the meaningful parameter is the ratio of the collector currents. In the work noted here, each Bayard-Alpert gauge was compared with the Redhead gauge. If the gauges have large conductances and low pumping speeds, one would expect a straight line for these ratios versus time for non-varying emission currents, since

$$I_c = I_e \, k \, p \qquad [5.2.1]$$

where I_c is the measured ion current, I_e is the emission current (held

constant throughout our testing), p is the actual pressure in the gauge, and k is the gauge sensitivity defined by Eq. [2.5. 1]. Actually,

$$I_c = \sum_i I_e k_i p_i = I_e \sum_i k_i p_i \qquad [5.2.\ 2]$$

where p_i is the "partial pressure" k_i is the gauge sensitivity of the i-th component. So, for two gauges measuring the same volume, there would have to be a change of composition of gas for them to read differently relative to each other (if the ratio of the pumping speed to the conductance is small). If we use the quantity

$$r_i \equiv k_i/k_{Argon} \qquad [5.2.\ 3]$$

which has been found to vary slightly from gauge to gauge, Eq. [5.2. 2] becomes

$$I_c = I_e k_A \sum_i r_i p_i \qquad [5.2.\ 4]$$

For small pumping speeds near equilibrium we could expect the variation in pressure between gauges to be nearly zero, i.e., at

$$dp/dt \sim 0, \qquad \Delta p/p \sim S/F \sim 0 \qquad [5.2.\ 5]$$

where S is the pumping speed of the gauge and F its conductance. But these effects are also composition-dependent, i.e.,

$$\left(\frac{p_c - p_g}{p_g}\right)_i = \frac{S_i}{F_i} \qquad [5.2.\ 6]$$

where p_{c_i} is the partial pressure in the reference chamber, and p_{g_i} is the partial pressure in the gauge. Even when not in equilibrium, changes of pumping speed of a gauge of one gas relative to another is going to cause a change in gauge sensitivity and a change in measured ion current.

Consider the ratio (ρ) of two measured ion currents, say, of an Ilikon Bayard-Alpert gauge and a Redhead cold cathode gauge. The primes in the following equations refer to the Redhead parameters:

$$\rho \equiv \frac{I_c}{I'_c} = \beta \frac{\sum_i r_i p_i}{\sum_i r'_i p'_i} \qquad [5.2.\ 7]$$

where

$$\beta \equiv \text{constant} = \frac{S_A}{S'_A} \frac{I_e}{I'_e} \qquad [5.2.\ 8]$$

ρ can change if the partial pressure of the gas components in one gauge is different from that in the other for $r_i = r_i'$, or by a varying of p_i ($p_i = p_i'$) where $r_i \neq r_i'$.

A change in composition of gas in the system (whether or not the change is felt equally throughout the system, including the gauges) could result in a change of the ratio I_c/I_c'.

Apparatus. The system described in Section 4 (Fig. 4.2) was used here. The gauges compared were an Ilikon Bayard-Alpert gauge, an NRC Bayard-Alpert gauge, a nude Bayard-Alpert gauge made by Hughes, and the inverted magnetron gauge of Redhead (also by NRC). The Ilikon gauge has the Nottingham variation, that is, the protective grid around the inner electrodes, auxilliary filament and screens on the end of the inner grid structure. Its tubulation had a relatively high conductance, about 35 ℓ/sec for hydrogen. The Bayard-Alpert gauge by NRC has the Redhead modification - the metal film on the inside of the envelope to eliminate the effects of Barkhausen oscillations. The envelope is kept at zero potential, the same potential as that of the collector. The disadvantages here are that there is ion bombardment of the walls, which may contribute to instability in readings, and a conductance of only about 5 ℓ/sec for H_2. The Hughes nude gauge is a miniaturized gauge with high electrode surface area. Its x-ray limit corresponds to ~ 5×10^{-9} torr. The Redhead gauge is a cold cathode gauge; and has the distinct advantage that it does not need outgassing. It has the effect of inducing hydrogen into the atmosphere; hydrogen that has already been pumped by this gauge is re-emitted. It is almost impossible to get a pure gas system with this gauge in the system. The conductance on the Redhead gauge was very good, of the order of 40 ℓ/sec for hydrogen.

A Keithley micro-microammeter (model 410) with an auxilliary control were used interchangeably with the NRC Bayard-Alpert gauge control (model 751) for the Bayard-Alpert gauges. The Redhead was controlled and monitored by its own NRC unit.

Procedure and Results. The system was baked out just enough to put the tests into the range between 1×10^{-9} and 1×10^{-7} mm Hg. After the system was baked out, the ultra-high vacuum valve was closed, and ultimate pressure attained. The actual test procedure was as follows: with the Vac Ion pump and Redhead running continuously, the Bayard-Alpert gauge or gauges to be studied were electron-outgassed at 100 ma, 500 Volts, for 15 minutes, and then switched on. In all cases the hot-cathode emission current was 1 ma. The collector currents were recorded for the Redhead and for the Bayard-Alpert gauge(s) from one minute after outgas to 24 hours after outgas. Ratios of these two collector currents (the collector current of the Bayard-Alpert gauge/the collector current of the Redhead gauge) were then plotted as a function of time.

The results of three typical tests are plotted in Figs. 5.9, 5.10,

and 5.11. In each case there is a rapid decrease in the ratio during the first few minutes (even in the nude gauge) and then a slow increase (the increase is of a different nature for the nude gauge). The rate of increase of this ratio is different for each of the glass gauges. There was a much greater fluctuation of the data for times greater than 100 min. for the NRC than for the Ilikon gauge.

The calculations for the nude gauge curve include an assumed x-ray limit of 1×10^{-11} amps.

To make sure that the dip in the ratio curves was not due to non-linearity of the Redhead gauge at higher pressures, the test was repeated twice, using one hot-cathode gauge to monitor the other. In the first of these, the monitor was another glass envelop gauge; in the second, a nude gauge was used. In each repeated test, the monitor gauge was outgassed for 15 minutes at 100 ma and then turned on. After 30 minutes, the Ilikon gauge was similarly outgassed and the test begun. The results of the first of these are shown in Fig. 5.12. The results of the second were completely similar to the tests with the Redhead. The time, again, was measured relative to the end of outgassing of the test gauge.

Some details of hydrogen pumping at a hot filament were studied with the aid of the omegatron. The curves of Fig. 5.13 show typical partial pressure (%) curves of H_2 for the cases of the Vac Ion pump alone, and for the Vac Ion plus an NRC Bayard-Alpert gauge. The H_2 pumping of the hot filament is apparent.

When the Vac Ion pump is not on, the Bayard-Alpert gauge in one minute is capable of pulling the hydrogen level of the system about to that obtainable with the Vac Ion (Figs. 5.14, 5.15)(this also shows that the gauge's hydrogen pumping speed is ~ 10 ℓ/sec, since the Vac Ion pump is rated at about 15 ℓ/sec for hydrogen). It should be noted (Fig. 5.14) that the total pressure at t = 30 min. in the case of the Vac Ion plus NRC is about 10^{-8} torr, while in the case of the NRC alone it is about 10^{-6} torr. These curves also illustrate the fact that the Vac Ion actually re-emits H_2. This was further proven when attempts were made to obtain a pure gas with the Vac Ion operating. Invariably, although a pure gas was admitted, there was an increase in H_2 in the system.

When the NRC gauge was shut off, there was a rapid increase in H_2 in the system (from 2×10^{-8} torr to 1.3×10^{-6} torr partial pressure in 30 minutes), and a rapid decrease and then an increase of Mass 28 (from 8.7×10^{-7} to 2.2×10^{-7} torr in 15 min. and then back to 4×10^{-7} torr in another 15 min.).

When the gauge is outgassed (electron bombardment) there is a rapid increase in both CO and H_2, but then a slow decrease in H_2. This rate of decrease is much smaller than that discussed above, because of the filament being at too high a temperature for effective pumping.

The initial increase is due to the outgassing of the grid and the bake-out of the envelop. Hickmott (1) has shown that the atomic hydrogen on the envelop is all desorbed at or before 250°C; during electron-bombardment outgassing, therefore, the hydrogen pump is regenerated.

Discussion.

Changes of Apparent Sensitivity With Time. When a hot cathode gauge is turned on just after outgassing, it is not only a very effective pump of hydrogen, but as Alpert and Tomaschke* have shown, it is also momentarily a high speed pump for CO. This CO pump saturates much more quickly than does the hydrogen pump. So, immediately after outgassing, the CO and H_2 pressures in the gauge are somewhat lower than those of the chamber. But then the CO pump begins to saturate and eventually the gauge becomes a source of CO, rather than a sink (1). To illustrate the effect that this has on the gauge, consider a typical test comparing the Ilikon gauge to the Redhead gauge with the Vac Ion on. Let us assume for the Ilikon, H_2 conductance of approximately 35 ℓ/sec, with a pumping speed of 10 ℓ/sec; and a CO conductance of 11 ℓ/sec, with a pumping speed of about 2 ℓ/sec initially, which drops to 0.5 ℓ/sec in about 6 minutes. After about 15 minutes, the gauge becomes a source of CO until the gauge CO partial pressure is about 5% above that of the chamber (these approximations for the pumping characteristics of CO have been derived from the work by Tomaschke* and Hickmott (1). We have assumed here a constant temperature envelop).

An estimate of the results expected from these phenomena are shown in Table 5.1. The partial pressures in the chamber were obtained from an omegatron. It is assumed that the omegatron and the Redhead both are monitoring the chamber relatively accurately. Partial pressures for the Ilikon were calculated from Eq. [5.2. 6]. As can be seen from the table, the increase of ρ/β from 6 minutes to 30 minutes is about 5.7%. In Fig. 5.9, the increase in ρ/β over the same period of time is about 13.6%. In the calculations for Table 5.1, no account has been taken of the fact that a glass gauge is also a source of masses 15, 16 and 18, whose pumping characteristics resemble those of CO. The lack of a sizeable increase in ρ after the dip (Fig. 5.12) can also be explained by these ideas.

In these tests, the temperature of the envelop was not constant; in fact, it dropped from the 300°C temperature attained during outgassing to very near its normal operating temperature in about 6 min. This explains the initial dip in the durves (except, possibly, for the nude gauge); the drop is partially due to Knudsen's relationship,

$$\frac{p_A}{p_B} = \sqrt{\frac{T_A}{T_B}}$$

and also to the fact that the gauge is becoming less and less a source

*Private communication.

of contaminants as the bulb cools, until eventually it becomes a pump.

The causes of the dip and then the late increase in the curves of ρ vs. time for the nude gauge are still unclear. Quite possibly the dip is due to some localized outgassing (similar to that of the gauges) which decreases, or it may be due to some pumping phenomenon. The rise in ρ after several hours may be due to a changing x-ray limit of a type similar to that noted by Achley, Lothrop and Wheeler (5).

All these conditions affect when a gauge should be read, how often to out-gas, etc. In the system here, for instance, it was found that the Ilikon gauge should not be outgassed more than once every 24 hours in the range 10^{-8}, and should not be read for at least an hour after outgassing. The NRC, on the other hand, had to be outgassed every two hours to get reproducible readings, and could not be read for the first 30 minutes after outgassing. Not only do these reading times change from gauge type to gauge type, but from system to system; depending upon whether the system has a Vac Ion pump or mercury diffusion pump, what size the system is, its material, etc. It is suggested that, when a system is set up, it be tested as a unit to find out where the gauge is stabilized so that reproducible readings can be obtained. In a well trapped system having no cold cathode devices, one would probably not have to wait as long for the hydrogen content to stabilize; and readings probably could be made for a longer period of time before having to outgas.

5.2.2 Re-emission of Neutral Particles

Besides the contaminants produced in a glass hot-cathode gauge due to H_2 pumping, there are other causes of changing composition in a gauge. One of the primary mechanisms of this change is the re-emission of previously pumped particles from surfaces by subsequent bombardment by ions and electrons.

When the intermittent filament technique (2, p. 351) is employed, there is a momentary surge of gas (Fig. 5.17). The type of gas given off during this peak was analyzed. The amount of mass 28 given off was much greater than that of H_2, even though there was more H_2 in the system as a whole than mass 28.

A similar phenomenon occurred when emission current was increased during operation. Again, CO was momentarily given off, though in small amounts. Redhead (6) has noted that a quick drop of emission current in a Bayard-Alpert gauge activates a chemical pump. Evidently, during normal operation the gauge is constantly removing particles from the grid by electron bombardment. This partial cleaning of the grid is proportional to the adsorption energy of the gas involved, the electron impact energies, and the current. So when the current is decreased, one would expect an increase in adsorption on the grid. When the current is increased one would expect an increase in desorption, with the gases with the lowest adsorption energies coming off in

the greatest proportion.

If H_2 and CO are adsorbed on a tungsten grid, an increase in grid current would cause the evolution of an additional amount of CO, since CO has the lower adsorption energy on tungsten (7). This serves to explain why the gas given off at the intermittent filament peak was rich in CO.

5.2.3 Wall Potential and Accommodation Coefficient

The wall potential and accommodation coefficient vary with pressure, or, rather, with the number of monolayers on the surface in question. In a different way, with different materials and different gases, they may gradually induce a change in composition, or they may cause the gas in the volume enclosed in the envelop to be at a different temperature and, therefore, different pressure relative to the chamber and other gauges. This effect has yet to be studied in detail.

Time response. In systems which are varying rapidly with time, and when all the densities, partial pressures, etc., are known, there is still a problem of time response; which was investigated by Soo (8). The parameter here is the characteristic time of response which can be defined by:

$$\tau = \frac{V}{S + F} \qquad [5.2.9]$$

where S is the pumping speed, V is the volume of the gauge envelop, F is the conductance.

In our situation, the time response was not a problem, the τ was very small. In general, though, this is a factor to consider when using gauges of different types in systems that have rapidly changing pressure with time (see Section 3).

Ejection of charged particles from surfaces and surface ionization. Since the amount adsorbed on the collector varies with time and outgassing, the secondary emission of electrons from the collector will also vary with time (9, 10). This may contribute to the present experimental curves to the order of 2% to 5%.

It would seem that there is a certain amount of surface ionization at the grid. The amount ionized would be proportional to the amount adsorbed on the grid and the grid current. Some of these ions would be accelerated to the wall, but some would be drawn to the collector and would contribute to the reading of the gauge. Because of the buildup of gas on the grid after outgassing, for constant grid current one would expect a slow increase in ion current as a result of this. This would add to the increase of ρ vs. time. How much this

contributes is presently unknown.

Differences at lower pressures. What has been said here would apply in the 10^{-10} range. However, in the x-ray region, we are forced to go to indirect techniques, especially when using Bayard-Alpert gauges. The problem here is so highly individualistic--there is so much variation from one gauge to another, that it does no good to compare types of gauges in this region. Even the variation of one gauge within itself is extreme, changing from one time to another, when used with the indirect methods. Each gauge must be calibrated and continuously recalibrated both for partial and for total pressures.

5.3 EXPERIMENT ON GAUGE RESPONSE

The principal objective of the following experimental investigation is to verify the present method of determination of low pressure. In order to determine the effect of surface adsorption of an available ultra-high vacuum pressure gauge (Fig. 5.18) on the low pressure measurement, a suggested experimental method is presented in the following:

The schematic sketch for experimental method is shown in Fig. 5.19. The vacuum chamber is brought down to the range of about 10^{-7} mm Hg by the pump down procedure which has been presented previously. The pressure change (p_o) in the vacuum chamber is caused by "turning on" and "turning off" of the Redhead gauge. Here we assume that the nude ionization gauge measures the true pressure of the vacuum chamber (p_o). We can see what is the pressure response from the NRC ionization gauge (p) which is effected by adsorption and desorption from the surface and conductance of the gauge sensing tube.

It is assumed that the sensitivities of the NRC ionization gauge and the nude ionization gauge are constant and here we use the gauge constants which are specified by the gauge manufacturers, i.e., the sensitivity for the NRC ionization gauge,

$$K'_{NRC} = 27.5 \frac{1}{\text{mm Hg}}$$

and the sensitivity for the nude gauge,

$$K'_{nude} = 12 \frac{1}{\text{mm Hg}}.$$

The NRC ionization gauge, as well as the nude ionization gauge, measures the ratio of ion current (i_+) to electron current (i_-) to give an indication of pressure (p). The relation can be expressed as follows:

$$\frac{i_+}{i_-} = K'p \qquad [5.3.1]$$

where K' is the sensitivity of a gauge and has the dimensions of $\frac{1}{\text{mm Hg}}$.

The experiment was undertaken under room temperature condition. The ion currents (i_+) were measured by the NRC ionization gauge as well as by the nude ionization gauge while maintaining the electron current (i_-) at 1 ma. The experimental results computed from Eq. [5.3. 1] are shown in Fig. 5.20.

For the long time range, the pressure change inside the chamber (the measurements of the nude gauge) can be expressed by an equation of the type (see Fig. 5.21)

$$p_o = p_2 + C_1 e^{-b_1 t} \qquad [5.3.\ 2]$$

where

$$p_2 = 3 \times 10^{-8} \text{ mm Hg}, \quad C_1 = 1.85 \times 10^{-8} \text{ mm Hg}, \quad b_1 = 7.83 \times 10^{-5} \frac{1}{\text{sec}}.$$

From Section 3, the analytical solution which the NRC ionization gauge should read for Eq. [5.3. 2] is:

$$p = p_2 + C_1 e^{-b_1 t} - 2 \beta_o \beta_2 - \frac{1}{2} \beta_o \theta_1 \operatorname{erf}\left(\frac{1}{2\sqrt{t^*}}\right)$$

$$+ \frac{4}{3} \beta_o'(\beta_5 - 2 \beta_2 \beta_8^2)\left[1 + \exp\left(-\frac{1}{4t^*}\right)\right] + \frac{1}{\pi} \beta_2 C_o'$$

$$- \frac{2}{\pi} \beta_2 \sqrt{r_t C}\left[C_1 \sqrt{b_1}\, e^{-b_1 t} \int_o^{\sqrt{b_1 t}} e^{\tau^2} d\tau\right] \qquad [5.3.\ 3]$$

where $V_g = 110 \text{ cm}^3$, $L = 17.5$ cm, $r_o = 0.85$ cm, $r_t = 0.9$ cm,

$A = 133 \text{ cm}^2$, $C = 1.9 \times 10^{-6}$ sec cm ($T = 300^\circ C$),

$\alpha \simeq 0.5 \times 10^{-7}$, $\beta_o = \frac{\alpha\sqrt{C}}{\sqrt{r_t}} = 0.725 \times 10^{-10}$,

$\beta_o' = 0.95 \times 10^{-13}/\sqrt{t}$, $C_o' = 2.42 \times 10^{-11}/\sqrt{t}$,

$\beta_2 = 150$, $\beta_3 = 180$, $\beta_4 = 164$, $\beta_5 = 185$, $\beta_6 = 19.4$,

$\beta_7 = 20.6$, $\beta_8 = 1.06$, $\theta_1 = 136$, $t^* = 493\ t$.

For the numerical computation, we used the ILLIAC computor to compute the integral,

$$\int_0^{\sqrt{b_1 t}} e^{\tau^2} d\tau$$

and we get the results shown in Table 5.2, and in Fig. 5.21.

Here we have presented a new method for the determination of very low pressure measurement by a gauge in an envelop. This study has been made under the simplifying assumptions of an isothermal system and a semi-classical and semi-empirical model of adsorption and desorption. The usefulness of the method is tested by experimental results (Fig. 3.6 and Fig. 5.21).

The study of detailed mechanisms of physical and chemical adsorption in ultra-high vacuum range shows that physical adsorption follows Henry's Law and plays a necessary prerequisite role to chemisorption. A comparison of the present results with Hobson's measurements of the helium adsorption isotherm on Pyrex glass at $4.2^{\circ}K$ (11) shows that the present theory [Eq. 2.5. 7] is adequate in an ultra-high vacuum range ($p \leq 10^{-9}$ mm Hg)(Fig. 2.3). Although physical adsorption of nitrogen on Pyrex glass over the range of pressure, $10^{-9} \leq p \leq 10^{-3}$ mm Hg follows the Dubinin-Radushkevich formula (12) very closely, it is expected that adsorption isotherms will switch to the present formula (Eq. [2.5. 7]) in ultra-high vacuum range ($p \leq 10^{-9}$ mm Hg) as shown in Fig 2.4 (although there is presently no experimental result available for ultra-high vacuum range) for two reasons: First, the Dubinin-Radushkevich formula is based on the theory of condensation and might not be expected to apply to physical adsorption at very low coverage. Second, most of the adsorbents to which the Dubinin-Radushkevich formula have been applied (13) have been porous, whereas Hobson concluded that Pyrex glass is nonporous for nitrogen in his experimental paper (14).

A typical system for measuring pressures in an ultra-high vacuum range consists of a vacuum gauge connected to the vacuum chamber by a length of tubing, usually with an orifice of diameter smaller than that of the tubing at the end (Fig. 3.1). The above study shows that pressure measurements by this vacuum gauge system are affected by the physical properties (adsorption and desorption) as well as by the geometry of tubulation. The physical parameter α which plays the main role in this method can be calculated analytically (Section 3) and obtained experimentally.

In Fig. 5.21, a comparison between the experimental results and the theoretical results for a particular α (here, $\alpha = 0.5 \times 10^{-7}$) is shown. It is suggested that an experimental determination of α can be made so long as it is assumed that sensitivities of the NRC ionization gauge and the nude ionization gauge are constant. Further study, which includes the gauge sensitivity as well as the corrections for thermal effects, is now being carried out by our group.

REFERENCES
(Section 5.0)

1. T. W. Hickmott, "Interaction of atomic hydrogen with glass," J. App. Phys. 31, 128 (1960).

2. S. Dushman and J. M. Lafferty, "Scientific Foundations of Vacuum Technique," John Wiley and Sons, Inc., New York (1962) pp. 669-673.

3. C. Guy Suits, Ed., "The Collected Works of Irving Langmuir," Vol. 1, Pergamon Press, New York (1960), pp. 69-82, 194-207. Also Vols. 8 and 9.

4. Fox, Smith and Smith, "The variability of the recombination of hydrogen atoms on metal surfaces," Proc. Phys. Soc. (London), 73, 533 (1959).

5. Achley, Lothrop and Wheeler, "Anomalous behavior of ionization gauges operated at low grid currents," Vacuum Technology Transactions, (1962) (In publication).

6. J. P. Hobson and P. A. Redhead, "Factors limiting ultimate pressure in ultra-high vacuum systems," Advances in Vacuum Science and Technology, Pergamon Press, Vol. 1, p. 384-386 (1960).

7. P. A. Redhead, "The desorption spectrometer as an analytic tool in ultra-high vacuum investigations," Vacuum Technology Transactions, Pergamon Press, New York (1960), p. 12.

8. S. L. Soo and A. B. Huang, "Transient measurements by vacuum gauge systems," Trans. Am. Vacuum Society (in press)(1962). Report to AEDC, USAF, Arnold AF Sta., Tenn., Contr. No. AF 40(600)-909, Proj. # 7776, Task # 77794, April (1962).

9. H. O. Hagstrum, "Effect of monolayer adsorption on the ejection of electrons from metals by ions," Phys. Rev., 104, 1516 (1956).

10. J. D. Cobine, "Gaseous Conductors," Dover Press, New York (1958), p. 115.

11. J. P. Hobson, "First adsorbed layer of helium at 4.2°K," Can. J. Phys. 37, p. 300 (1959).

12. M. M. Dubinin and L. V. Radushkevich, Doklad, Akad. Nauk., CCCP, (Proc. Acad. Sci., USSR), 55. p. 331, (1947).

13. M. G. Koganer, "A method for the determination of specific surfaces from the adsorption of gases in the monomolecular region,"

(English translation), Proc. Acad. Sci. USSR, 116, p. 603 (1957).

14. J. P. Hobson, "Physical adsorption of nitrogen on Pyrex at very low pressures," J. Chem. Phys. 34, p. 1850 (1961).

6.0 CONCLUSIONS

To obtain a reasonable estimate of the sensitivity of a gauge a number of factors were examined. Since the number of gas atoms which are ionized depends upon (1) the path length of electrons inside the grid which are energetic enough to ionize, (2) the number of electrons inside the grid, (3) the energy of the gas molecules, and (4) secondary electron emission. These points were studied. It was found that, because of space charge effects, the electrons, although emitted from a small filament, enter the grid in essentially a uniform fashion. Despite the space charge effect, the electrons are sufficiently energetic to ionize over most of the region inside the grid. The number of electrons inside the grid depends on the capture cross-section of the grid. The determination of this, based on the electric fields inside the gauge, requires more analysis. If the gas molecules stream through the gauge with even a small energy compared to the grid-collector potential drop, the sensitivity of the gauge should decrease considerably because of the flatness of the electrostatic potential inside the grid. The secondary emission of electrons from the collector, due to energetic ion bombardment, may also alter the sensitivity by 5% to 25%, depending on the collector surface.

The absorption constant α can be determined thus from gauge flashing.

With the species determined by the omegatron, sensitivity of a gauge can be predicted accurately from calibration with a standard gas and subsequent modification for gas environment.

The response characteristic is such that accurate measurement of the upper atmosphere by a sounding rocket or artificial satellite should be made with a nude gauge. At usual orbiting speeds, a nude gauge calibrated on a static environment has to be corrected for species, streaming and radiation.

When several ionization gauges are installed in one simulation chamber, readings are affected by outgassing characteristics, pumping and exchange of adsorbed molecules.

In simulation chambers, the bakeout characteristics and replacement of species should be checked carefully.

TABLE 2.1

PHYSICAL PROPERTIES OF SUBSTANCES

(Parenthetical numbers within the Table are Reference numbers)

Molecule (atom)	Density (ρ) (g/cc)	(α_o) Atomic Polarizability ($\times 10^{24}$)	(x) Atomic Susceptibility ($\times 10^{29}$)	Ionization Potential (ev)
Ar	1.65 (52)	1.623(57)	3.24 (59)	17.5 (46)
C	2.24 (53)	1.02 (53)	3.79 (53)	11.2 (56)
Cu	8.92 (53)	2.14 (55)	2.17 (60)	7.68(56)
Fe	7.86 (53)	1.13 (55)	2.79*	7.83(56)
He		0.205(53)	0.292(59)	21.2 (62)
Kr	2.99 (52)	0.246(57)	4.65 (59)	14.7 (46)
Na	0.97 (54)	29.7 (46)	0.90 (61)	2.08(56)
Ne	1.20 (55)	0.393(57)	1.12 (59)	25.7 (46)
W	19.3 (54)	3.00 (58)	7.63*	8.1 (56)
Xe	3.56 (52)	4.00 (46)	7.04 (59)	12.2 (46)
N_2	0.81 (56)	1.74 (46)	2.00 (55)	15.8 (46)
O_2	1.14 (56)	1.57 (46)	2.57 (47)	13.6 (46)
CH_4	0.41 (56)	2.58 (46)	6.67 (56)	14.1 (46)
AgI	5.67 (53)	9.28 (53)	13.6 (53)	
CaF_2	3.18 (53)	2.53 (56)	4.68 (53)	
KCl	1.98 (56)	4.32 (56)	6.40 (56)	
NaBr	3.27 (53)	4.60 (56)	8.06 (56)	
NaOH	2.13 (53)	1.65 (56)	3.93 (56)	
Na_2O	2.27 (53)	2.71 (56)	3.83 (61)	
Alumina		4.52 (53)	1.66 (53)	
Porous Glass	2.32 (55)	3.96 (53)	4.91 (53)	
Saran Charcoal		1.02 (53)	3.79 (53)	

*Calculated from the polarizability by using the Kirkwood formula (Equation [2.5. 8]).

TABLE 2.2

NUMERICAL CALCULATIONS OF EQUATION [2.5.7]
FOR N_2 ON PYREX GLASS

$P = 10^{-12}$ mm Hg

T (^{o}K)	ε^*/RT	Log S'	S'	N_a/A_s (molecules/cm^2)
63.3	38	14.5	3.16×10^{14}	9.6×10^{11}
67.1	35.8	13.6	4.04×10^{13}	1.145×10^{11}
72.6	33.1	12.4	2.5×10^{12}	6.62×10^{9}
77.4	31.2	11.6	4.04×10^{11}	1.0×10^{9}
81.0	29.7	11.0	1.0×10^{11}	2.38×10^{8}
84.9	28.3	10.45	2.8×10^{10}	6.35×10^{7}
90.2	26.6	9.6	4.04×10^{9}	8.55×10^{6}

TABLE 2.3

ACTIVATION ENERGIES OF GASES ON VARIOUS GLASSES

Gas	Nature of Glass	Activation Energy E_o (cal/g-mole)	Sources of Data
Air	Fused silica	14,500	(76)
	" " after prolonged heating	19,000	(76)
A	Fused silica	32,100	(76)
	" " after prolonged heating	48,000	(76)
He	Fused silica	5,600	(71)
		5,700	(76)
		5,390	(77)
	Pyrex	8,700	(72)
	Thuringian	11,300	(78)
	Jena 16^{III}	8,720	(79)
H_2	Fused silica	8,500	(80)
		9,200	(81)
		12,000	(67)
	Fused silica I	9,300	(73)
		10,900	(76)
	Fused silica II	10,000	(73)
		10,800	(76)
	Fused silica III	10,000	(73)
	Fused silica IV	10,800	(73)
N_2	Fused silica	26,000	(81)
		22,000	(76)
Ne	Fused silica	9,500	(71)
O_2	Fused silica	31,200	(76)

TABLE 2.4

ACTIVATION ENERGIES OF GASES ON VARIOUS METALS

Gas	Metal	Activation Energy E_o (cal/g-mole)	Source of Data
H_2	Ni	14,600 - 13,100 (below Curie point)	(85)
		13,100 - 12,040 (above Curie point)	(85)
		15,420	(86)
		13,860	(87)
		13,400	(88)
		13,260	(89)
H_2	Pt	19,600	(90)
		18,000	(88)
		19,800	(91)
H_2	Mo	20,200	(89)
H_2	Pd	17,800	(92)
		4,620	(93)
		10,500	(94)
H_2	Cu	16,600	(89)
		18,700	(95)
H_2	Fe	9,600	(89)
		8,700 (below 900°C)	(96)
		18,860 (above 900°C)	(96)
H_2	Al	30,800	(97)
O_2	Ag	22,600	(98)
N_2	Mo	45,000	(89)
N_2	Fe	23,800	(99)
CO	Fe	18,600	(99)

TABLE 3.1

t^*	t sec	$x^* = 0$ $P^* \times 10^{-4}$	$x^* = 1/2$ $P^* \times 10^{-4}$	$x^* = 1$ $P^* \times 10^{-4}$
1	9.62×10^{-4}	87.296	27.96	54.26
10	9.62×10^{-3}	30.81	8.959	17.814
10^2	9.62×10^{-2}	10.505	2.8167	5.6775
10^3	9.62×10^{-1}	4.005	0.6984	1.1836
10^4	9.62	1.959	0.1442	0.28257
10^5	96.2	1.2423	0.0475	0.08913

(see also Figure 3.8)

TABLE 3.2

t (sec.)	t^*	P^* at x = 1	P^* at x = 0
9.6	10^4	9.84×10^5	10^6
48	5×10^4	9.18×10^5	10^6
96	10^5	8.36×10^5	9.98×10^5
605	6.3×10^5	1	-----
960	10^6	-----	9.94×10^5
9600	10^8	-----	3.32×10^5
14600	1.4×10^8	-----	6.8×10^4
15100	1.45×10^8	-----	3.14×10^4
15600	1.5×10^8	-----	3.68×10^3
15700	1.508×10^8	-----	1

(see also Figure 3.9)

TABLE 5.1

Time (min.)	*Partial Pressures of Chamber × 10^8 torr		Partial Pressures in Ilikon Gauge × 10^8 torr		$r_i p_i \times 10^8$ torr		$\frac{\rho}{\beta}$
	H_2	CO	H_2	CO	Ilikon	Redhead	
2	9.50	6.00	7.40	5.08	7.45	9.10	.82
6	3.98	2.05	3.10	1.96	2.97	3.39	.87
30	2.57	1.10	2.00	1.16	1.82	1.99	.92

* Corrected for relative sensitivity

Assume $r_{H_2} = .39$, $r_{CO} = .90$ for both gauges.

TABLE 5.2

τ	$C_1\sqrt{b_1}\, e^{-b_1 t} \int_0^{\sqrt{b_1 t}} e^{\tau^2} d\tau$	$\int_0^{\sqrt{b_1 t}} e^{\tau^2} d\tau$
7200	8.565×10^{-11}	9.19×10^{-1}
9000	8.790×10^{-11}	1.09×10^{0}
10800	8.857×10^{-11}	1.26×10^{0}
12600	8.816×10^{-11}	1.44×10^{0}
14400	8.704×10^{-11}	1.64×10^{0}
16200	8.542×10^{-11}	1.86×10^{0}
18000	8.349×10^{-11}	2.09×10^{0}

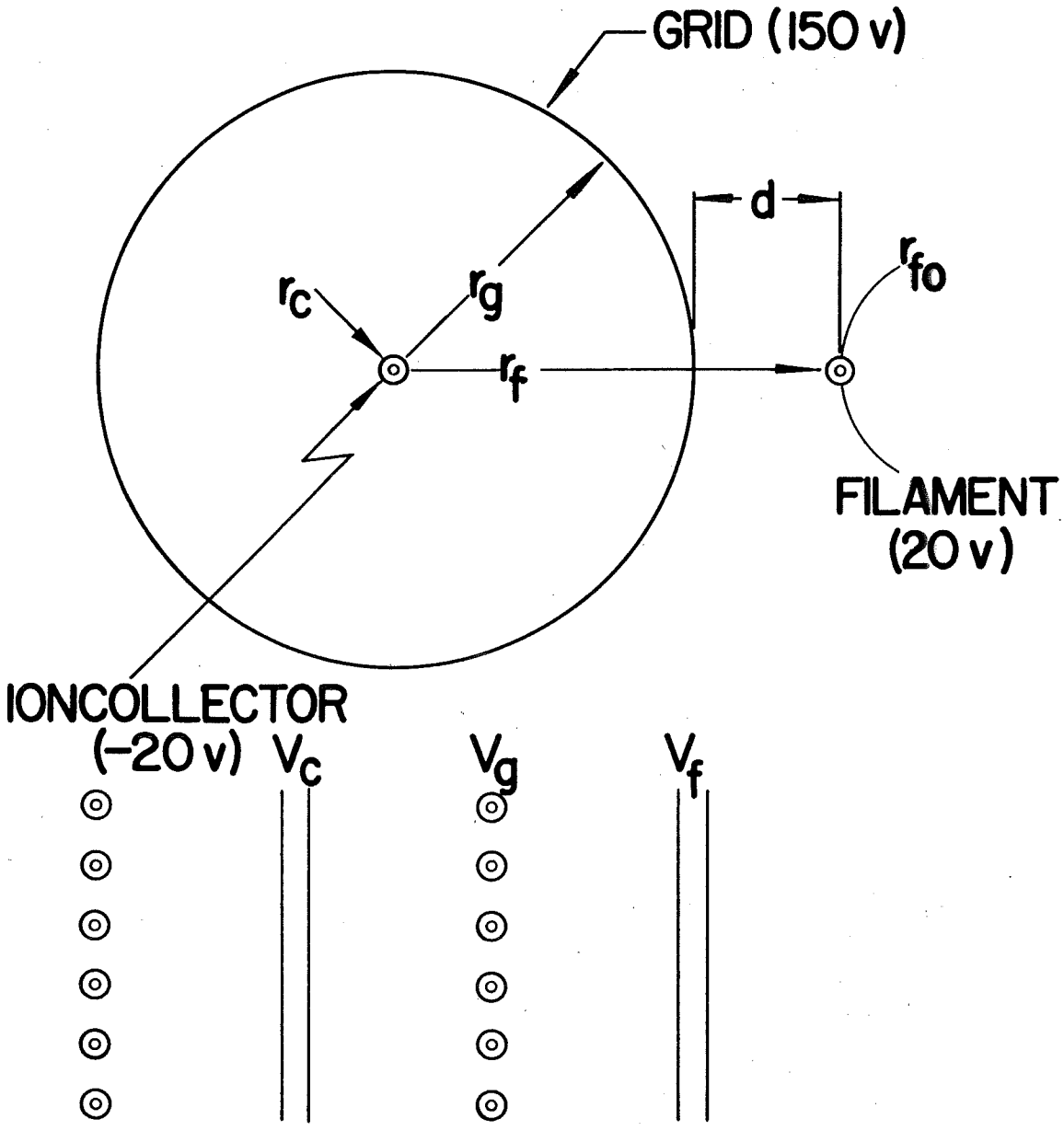

Fig. 1.1 Gauge Geometry

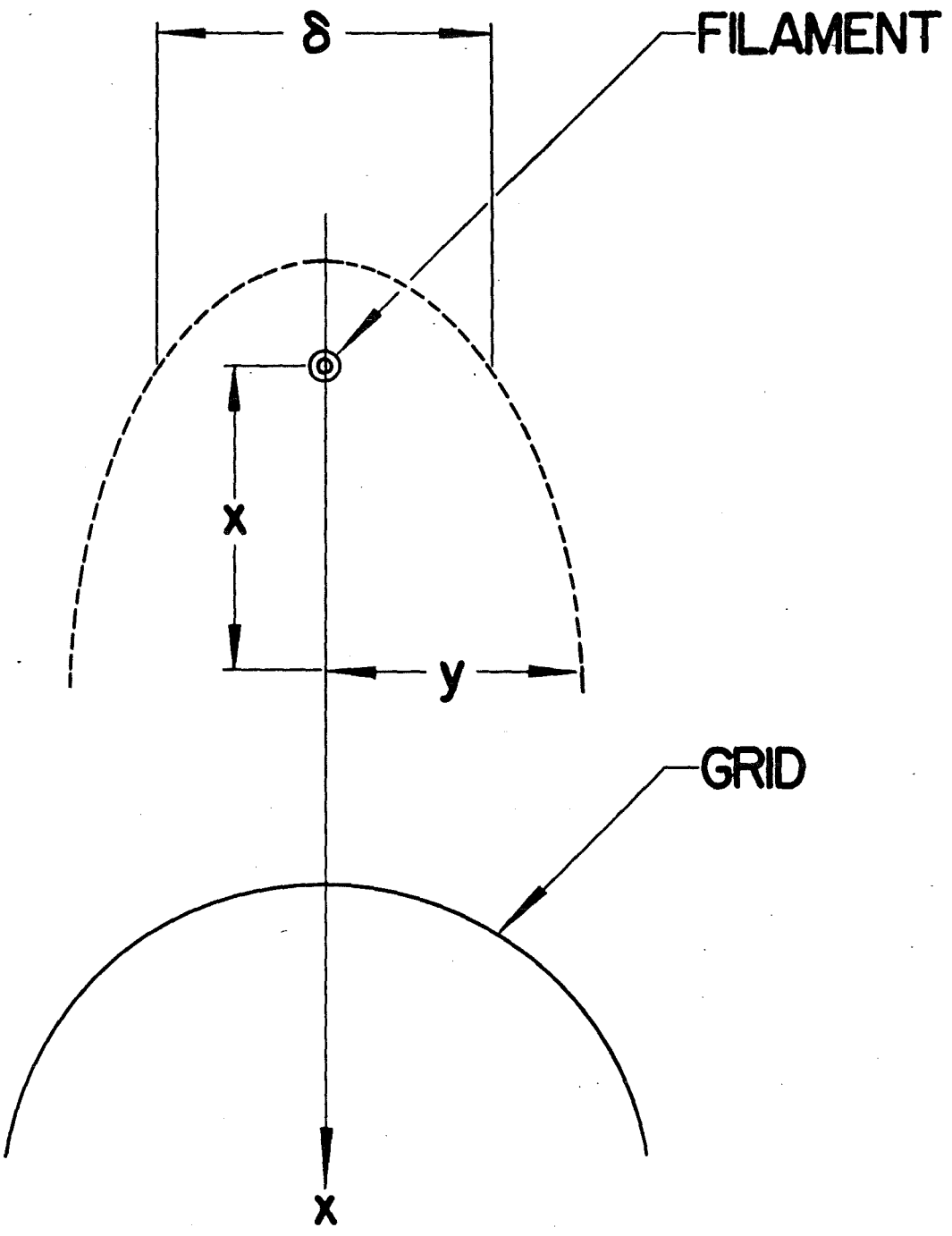

Fig. 1.2 Spread of Electrons

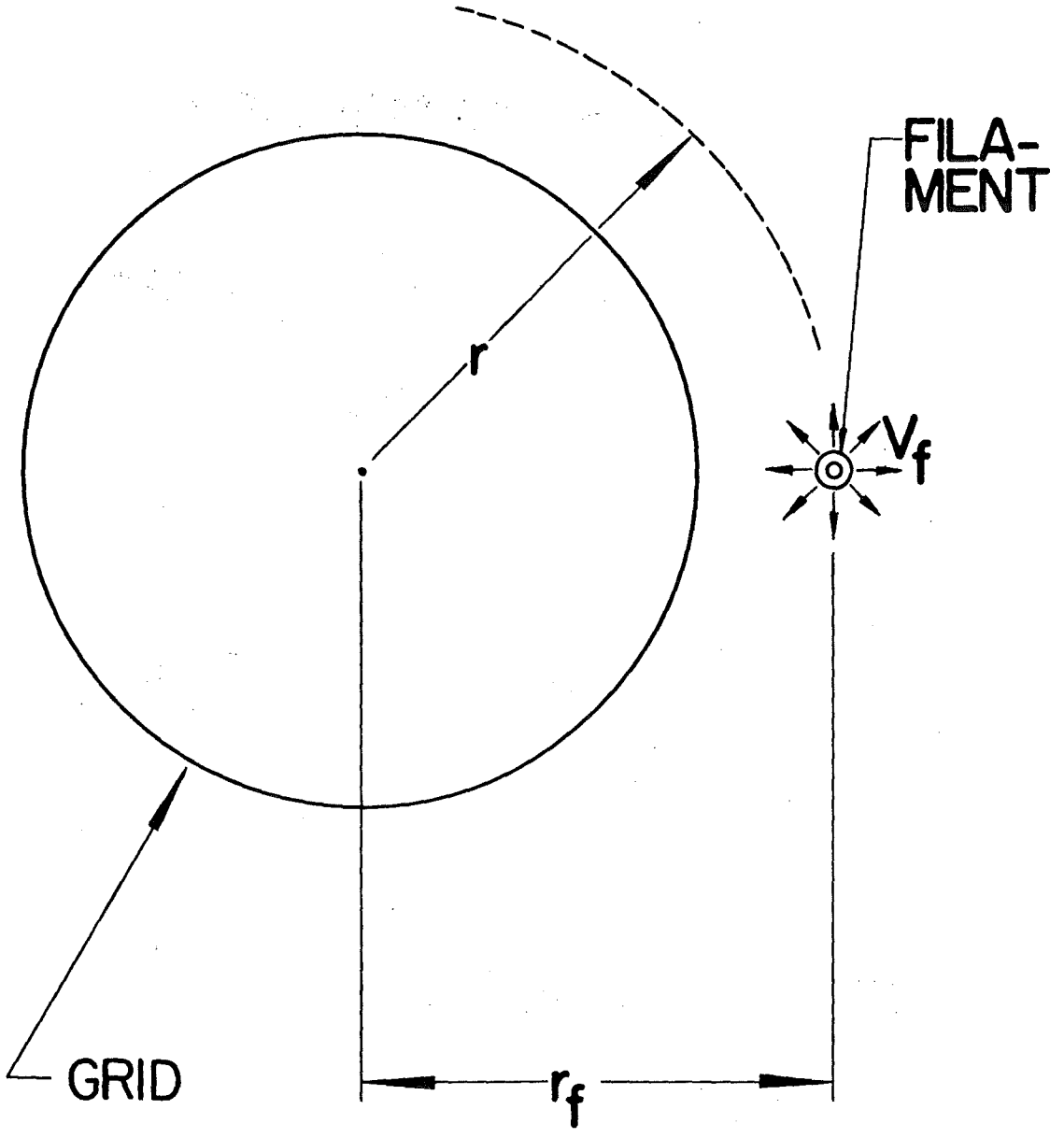

Fig. 1.3 Emission from Filament as Affected by Geometry

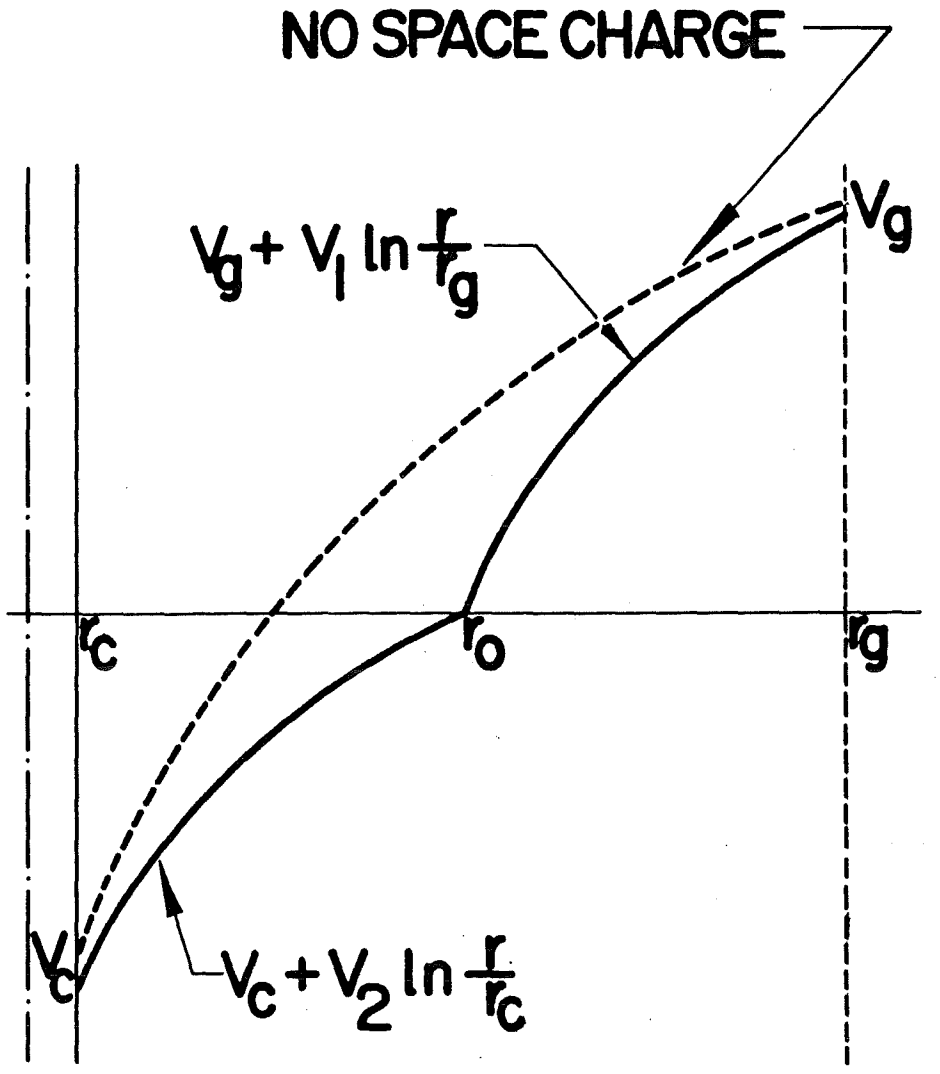

Fig. 1.4 Potential Distribution

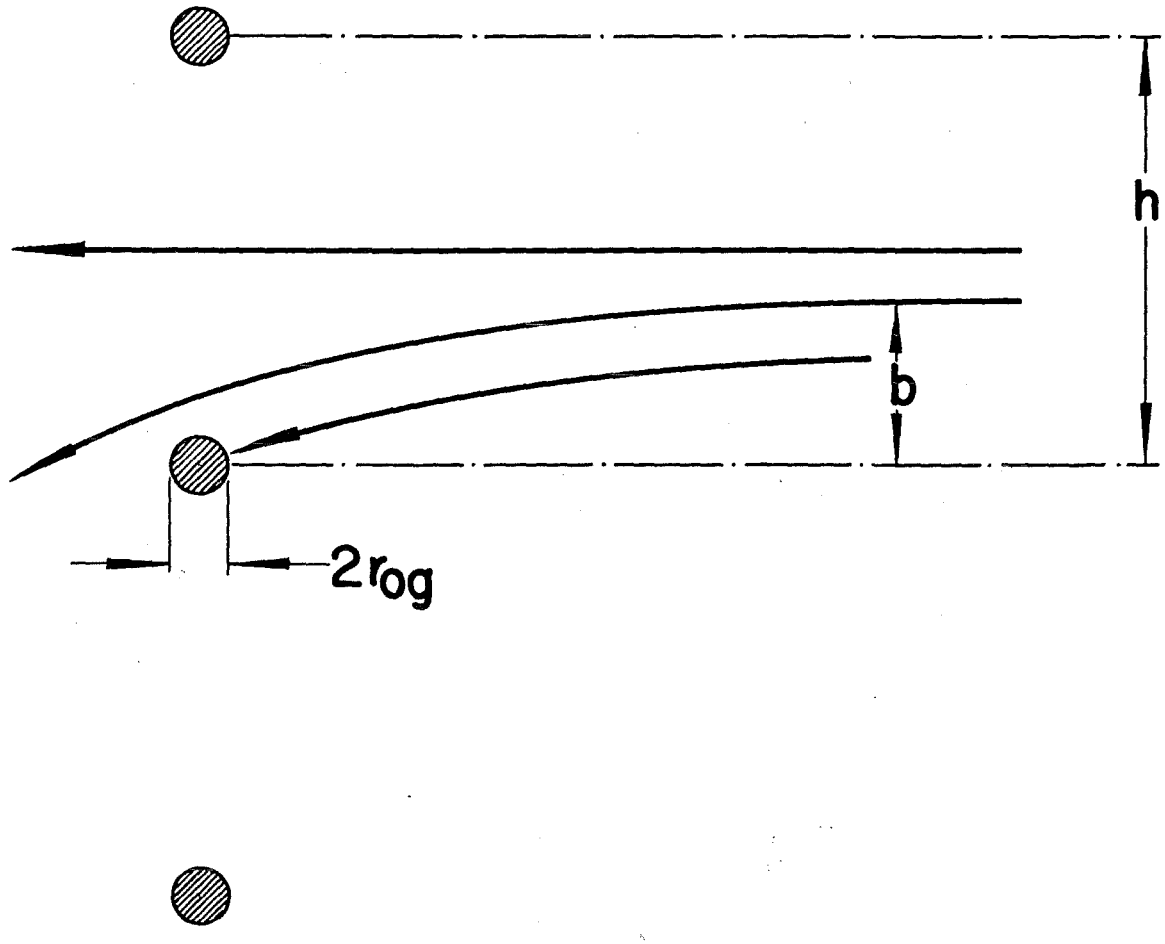

Fig. 1.5 Passage of Electrons through the Grid

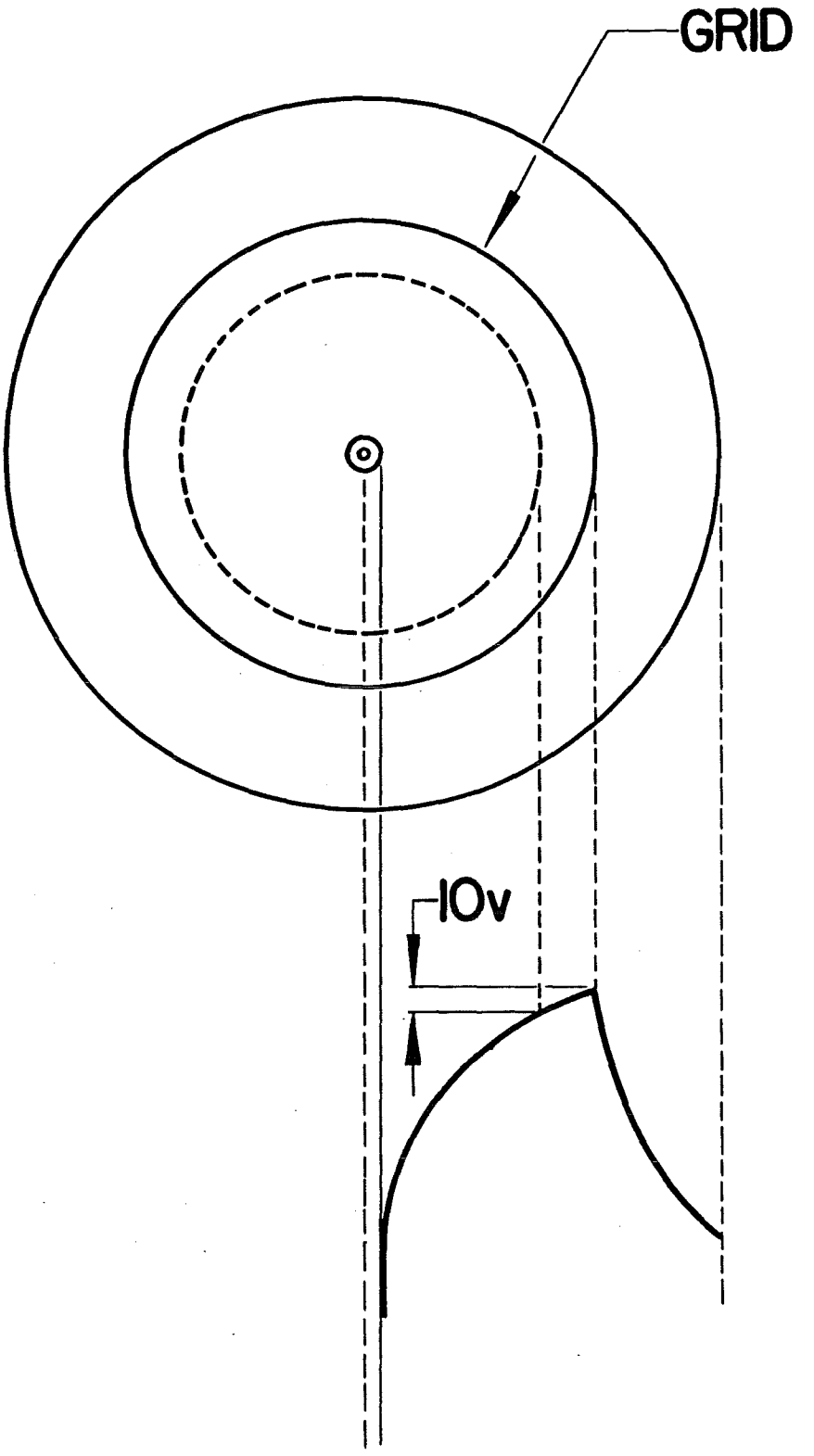

Fig. 1.6 Effect of Streaming

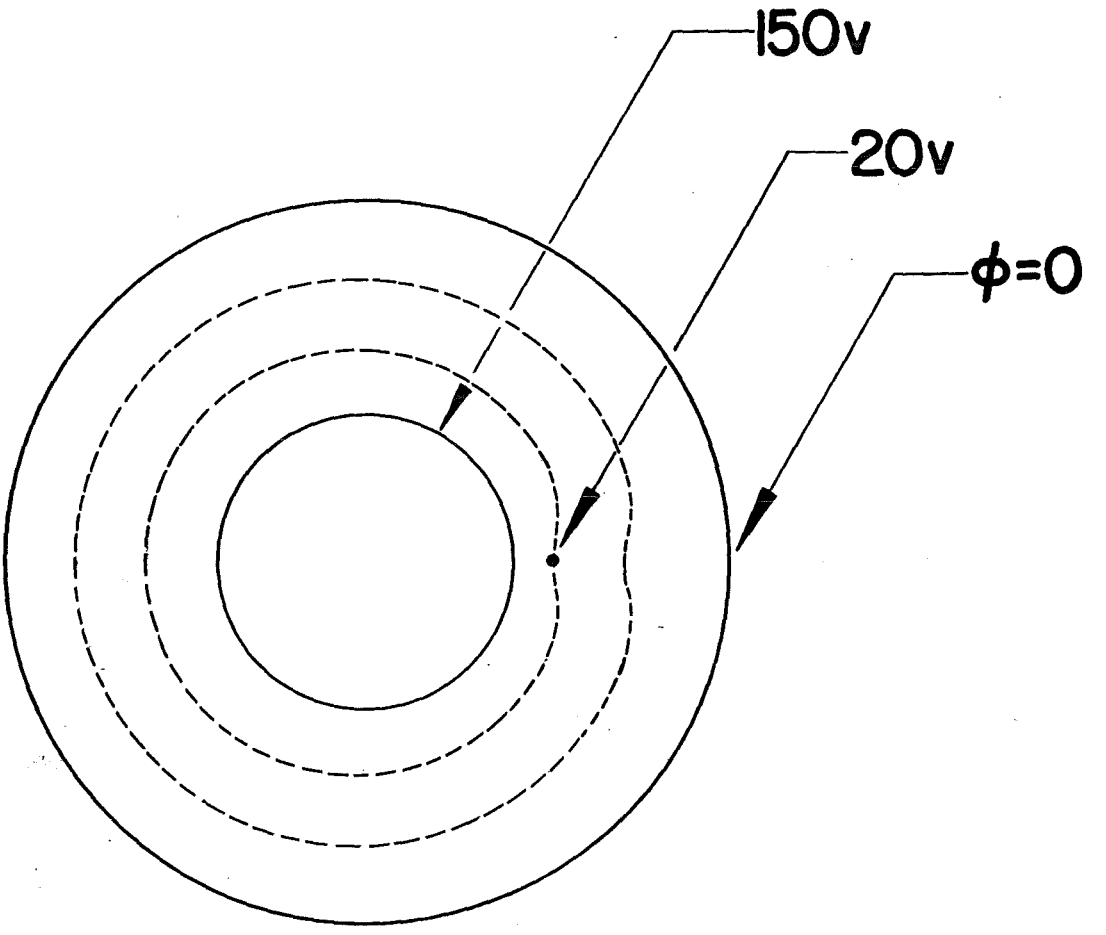

Fig. 1.7 Distortion of Field

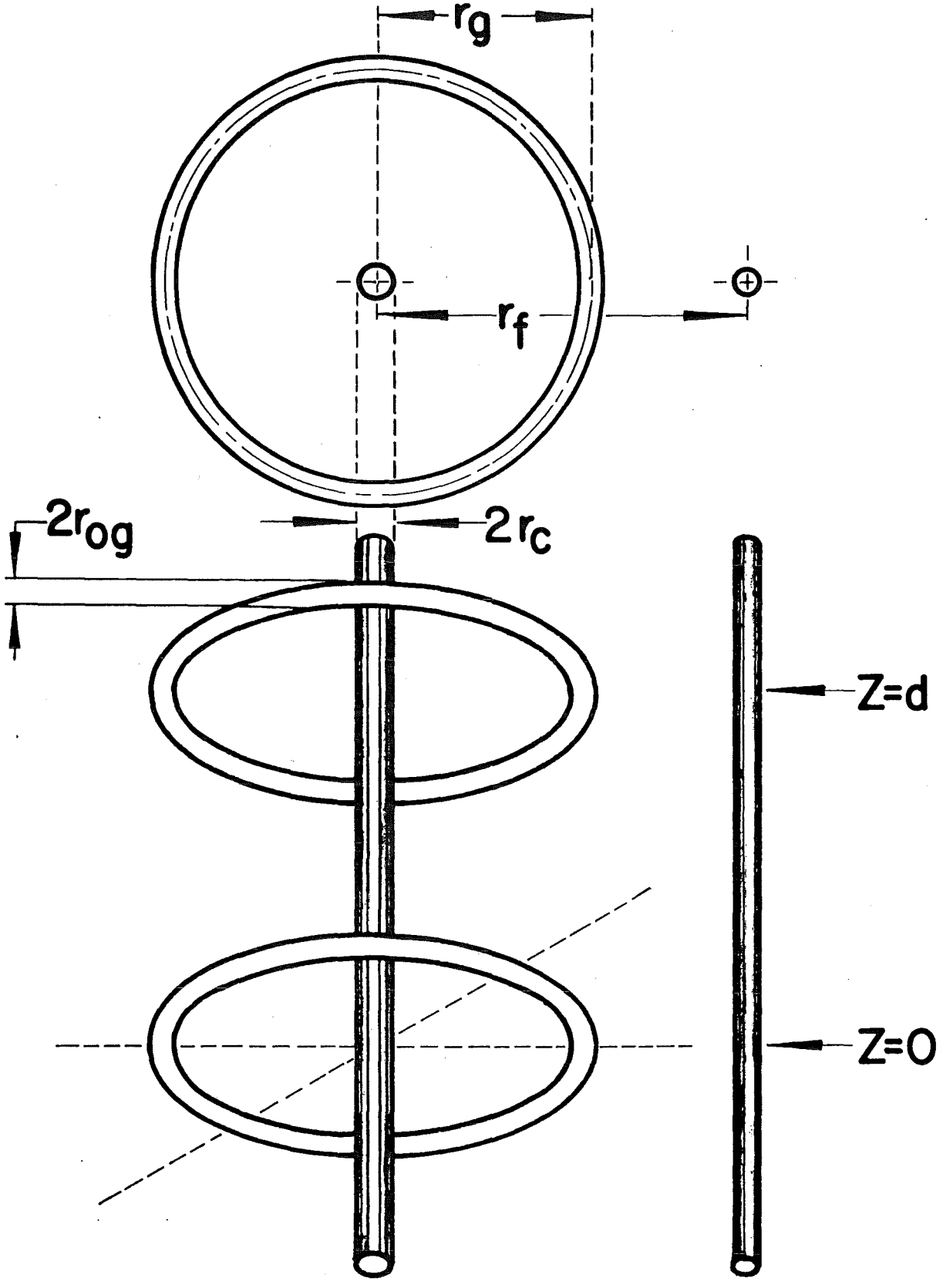

Fig. 1.8 Potential Distribution Due to Finite Dimension of Wires

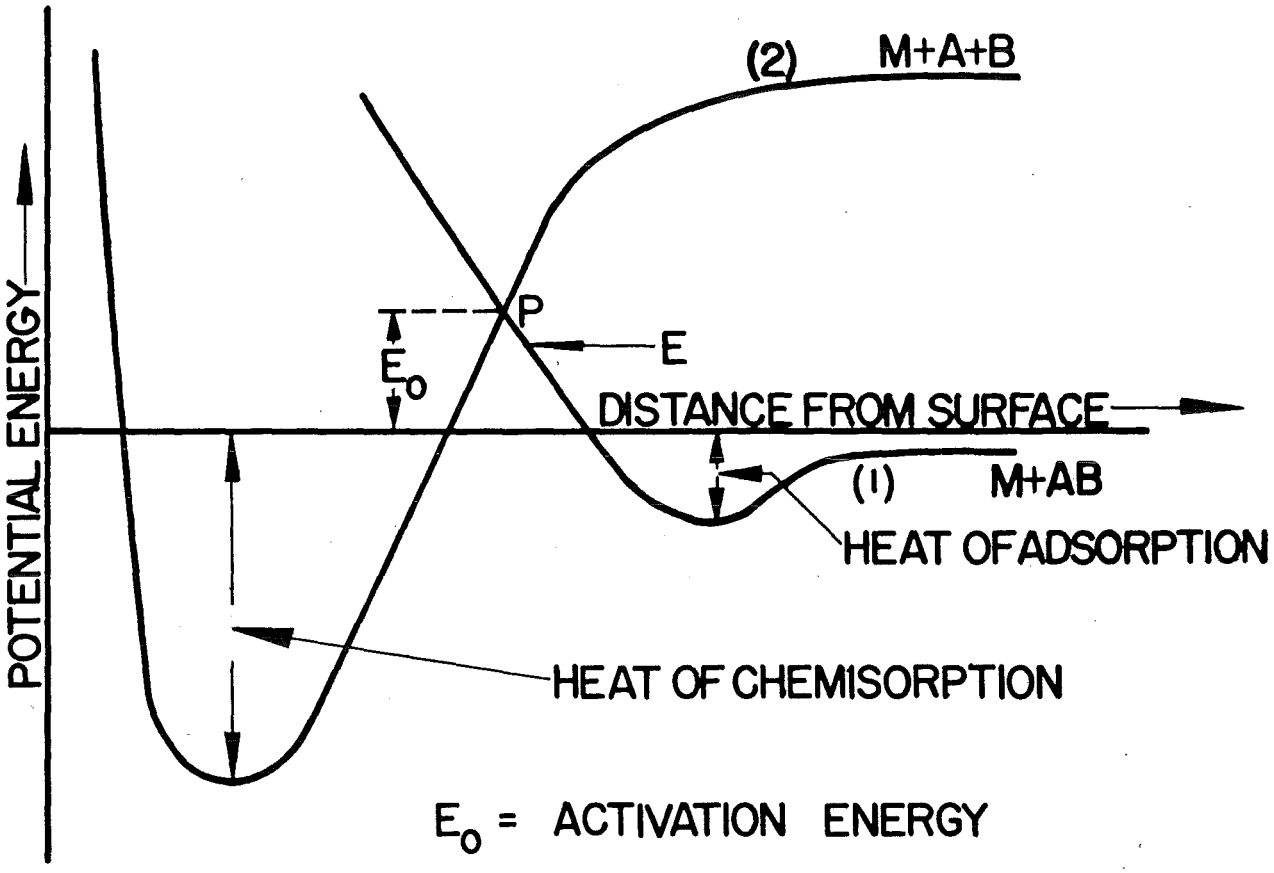

Fig. 2.1 Interaction of a Molecule and a Metal

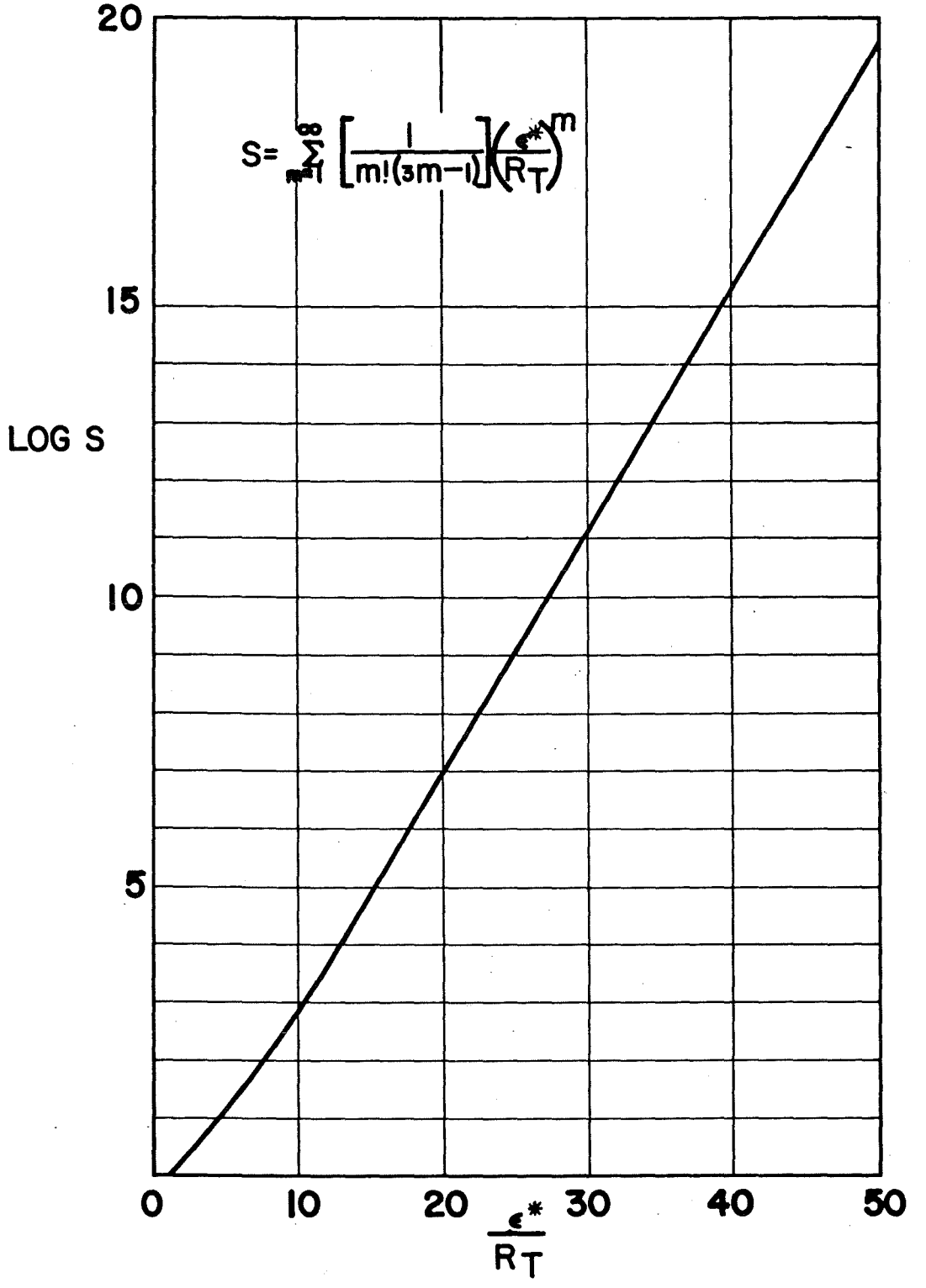

Fig. 2.2 Machine Computed Values of Gas-Solid Collision Sum

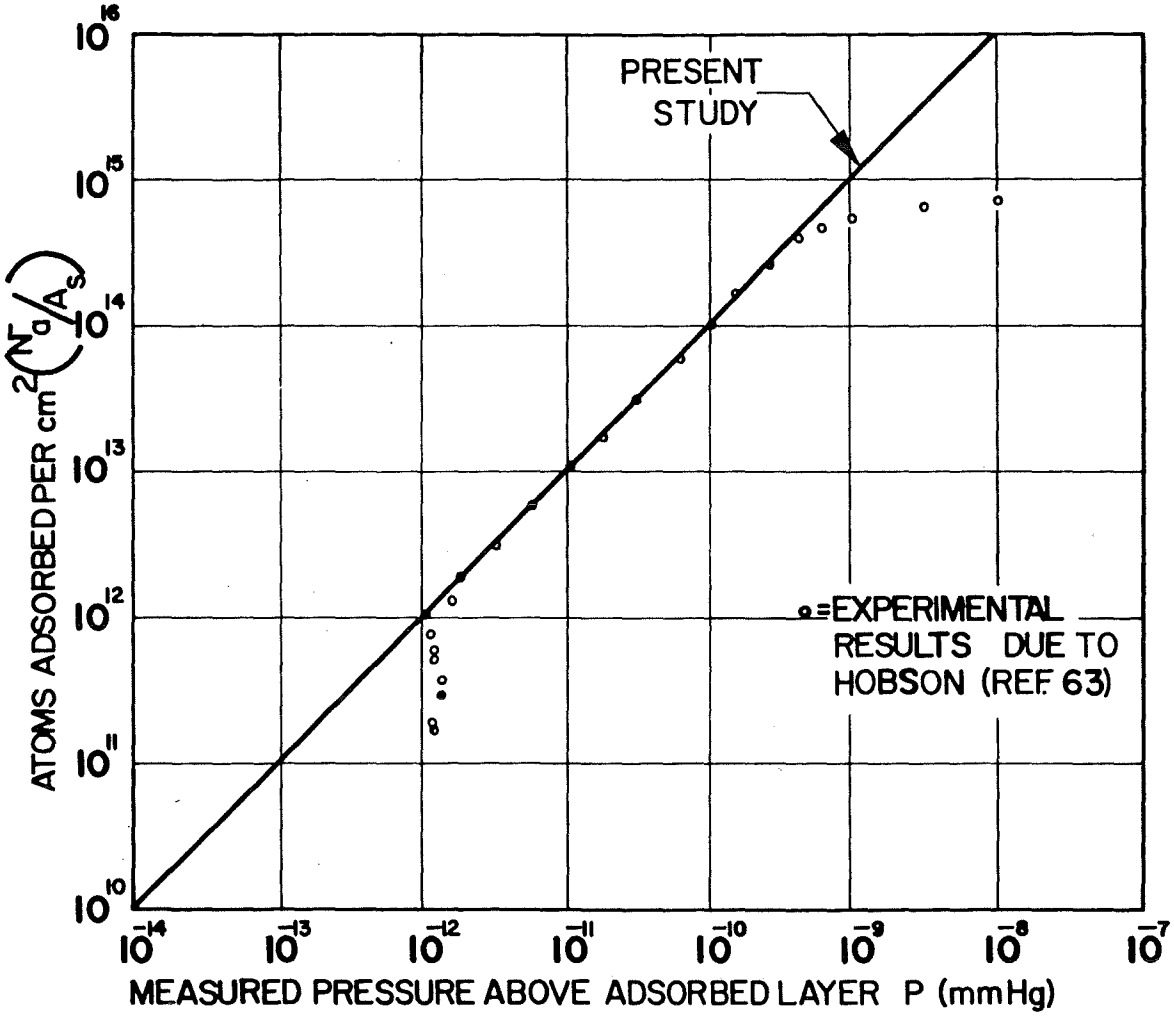

Fig. 2.3 Adsorption Isotherm Measurements for Helium on Pyrex at 4.2°K

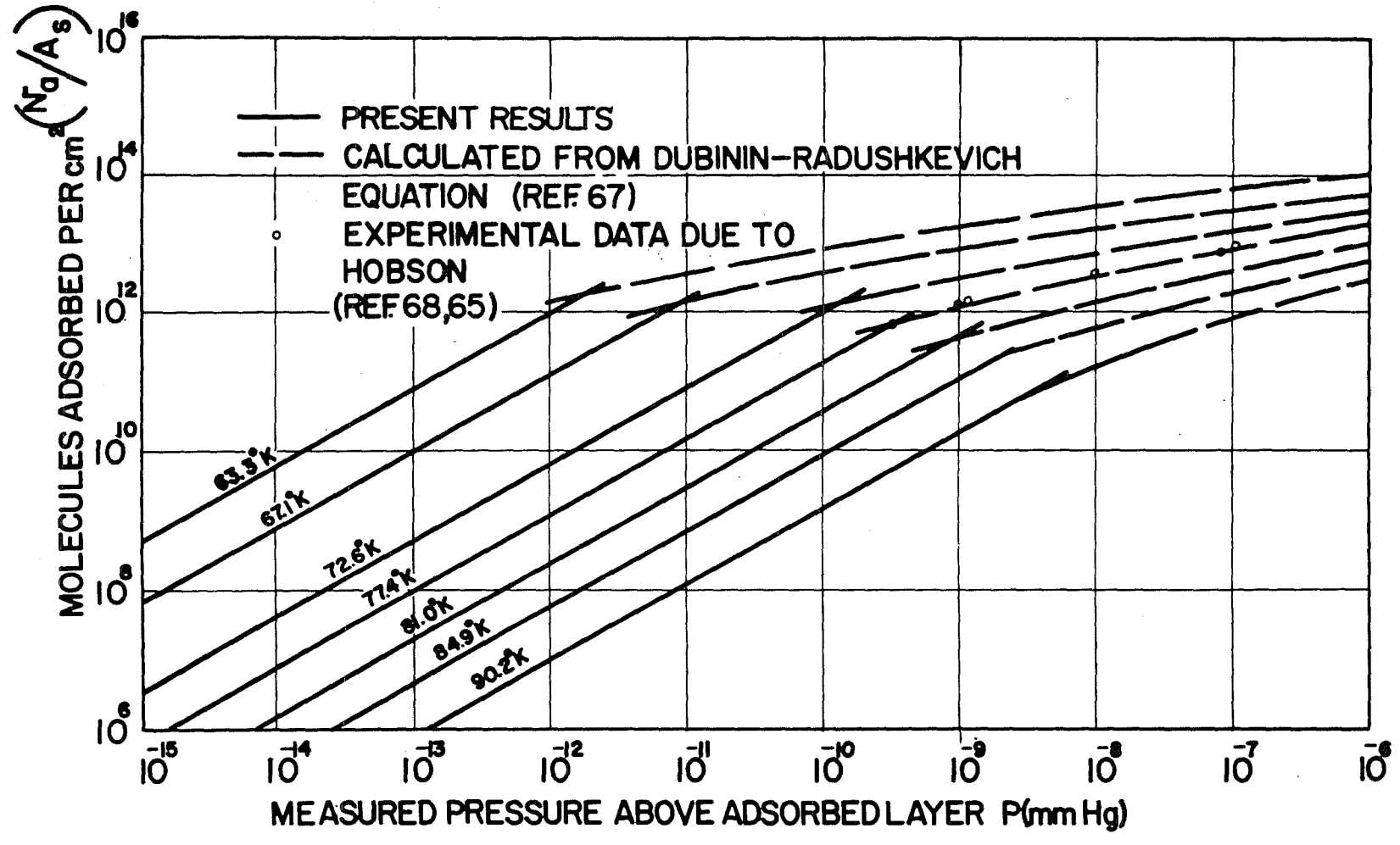

Fig. 2.4 Adsorption Isotherm of Nitrogen on Pyrex

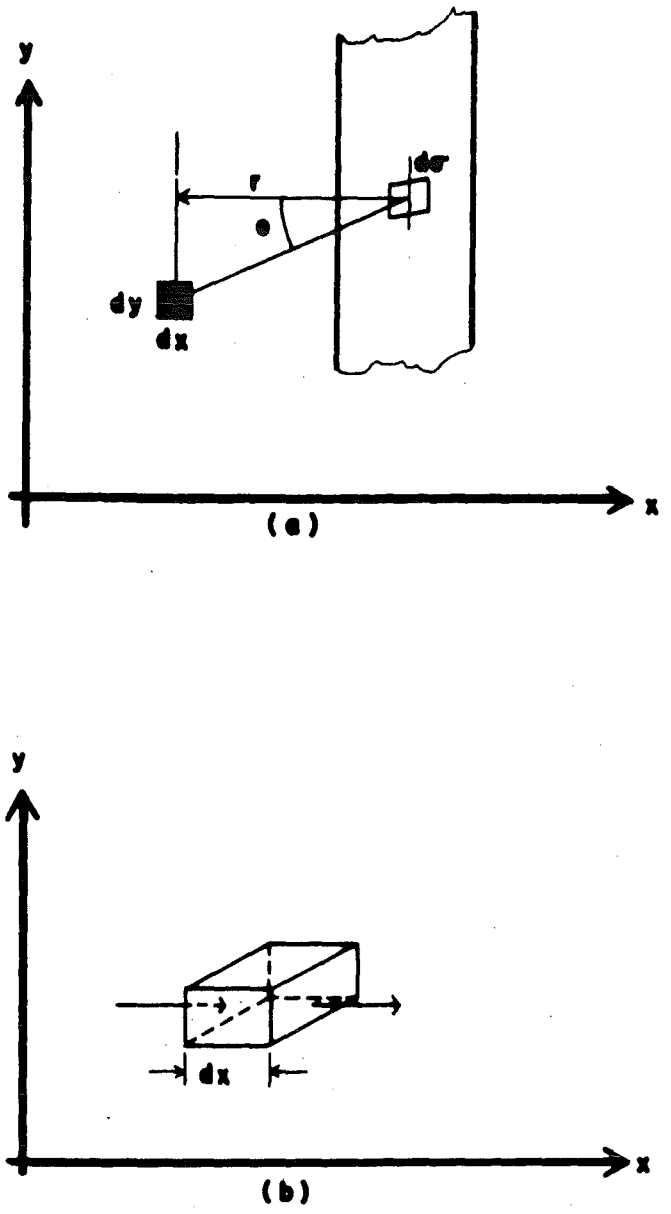

Fig. 2.5 Geometry of Adsorption in a Solid, and Diagrammatic Representation of a Solid Element

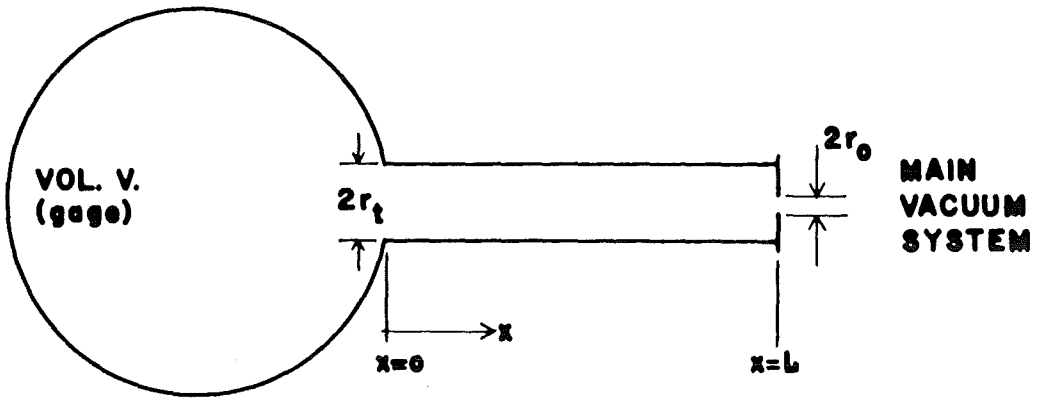

Fig. 3.1 Typical Probe Envelope and Connection

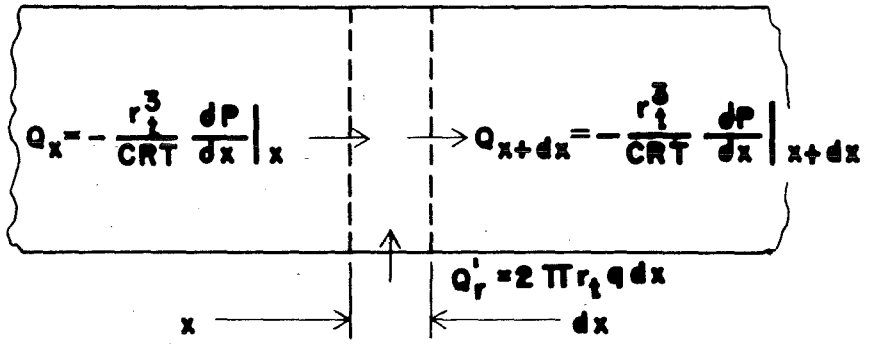

Fig. 3.2 Flow through a Control Volume

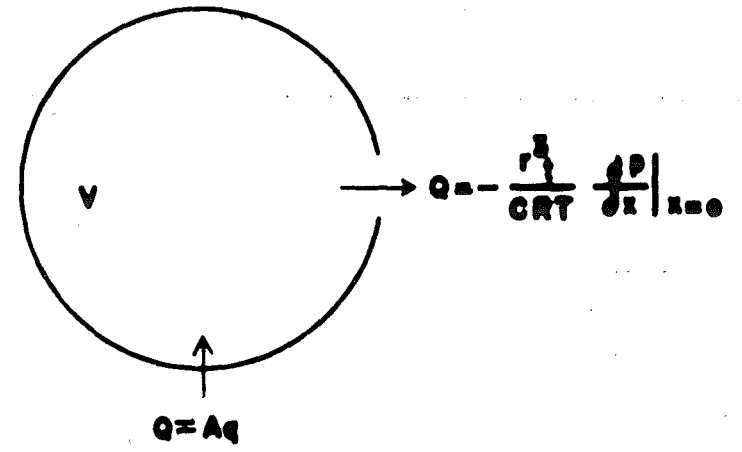

Fig. 3.3 Flow through a Spherical Control Volume of Gauge

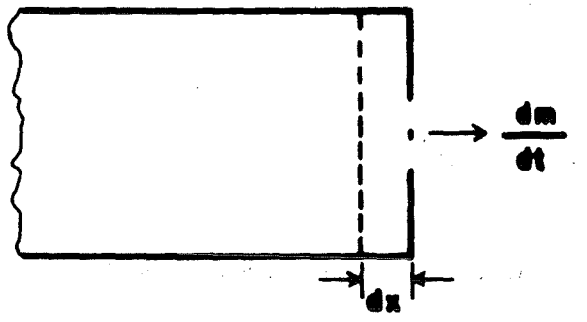

Fig. 3.4 Flow through a Control Volume at the End of Gauge

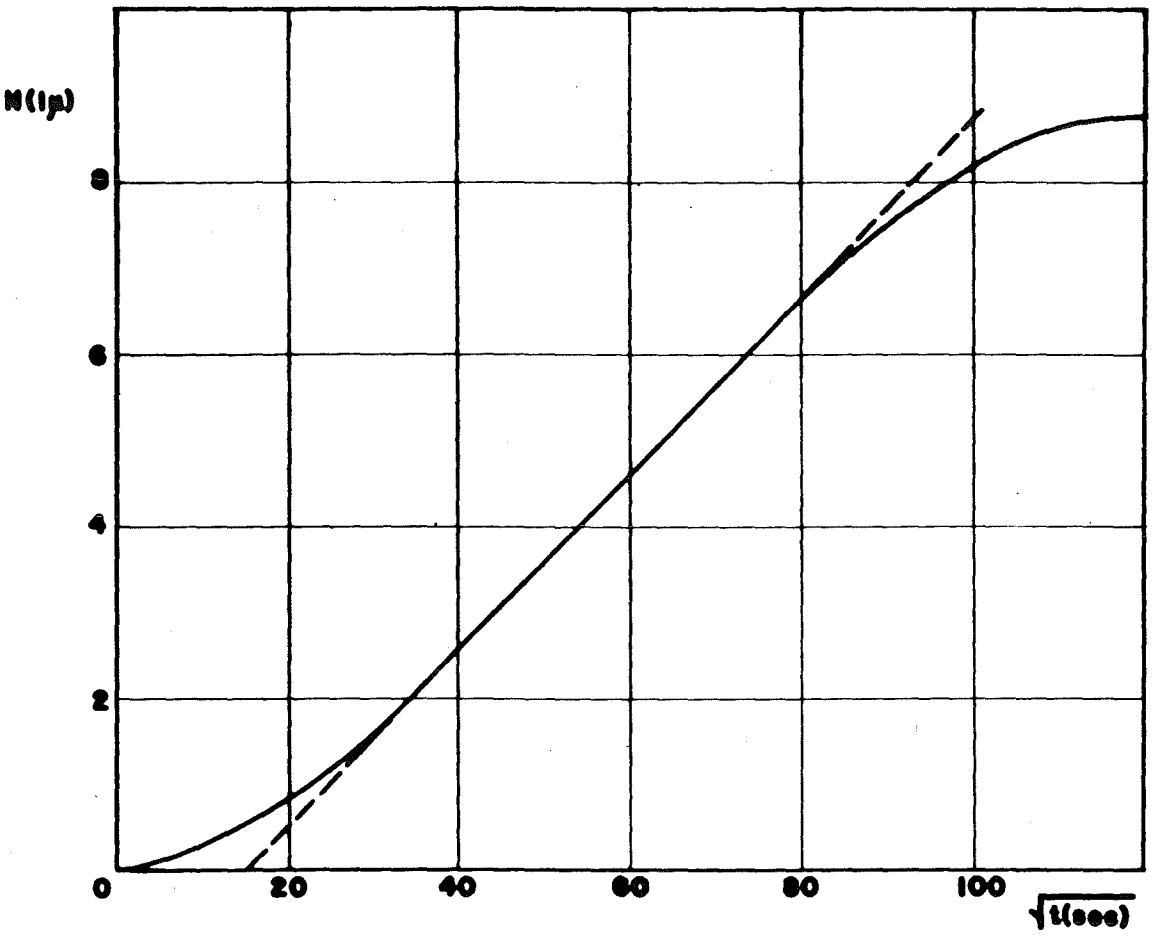

Fig. 3.5 Approximation of Adsorption Rate by Eq. [2.8.18] – Copper (Ref. 5)

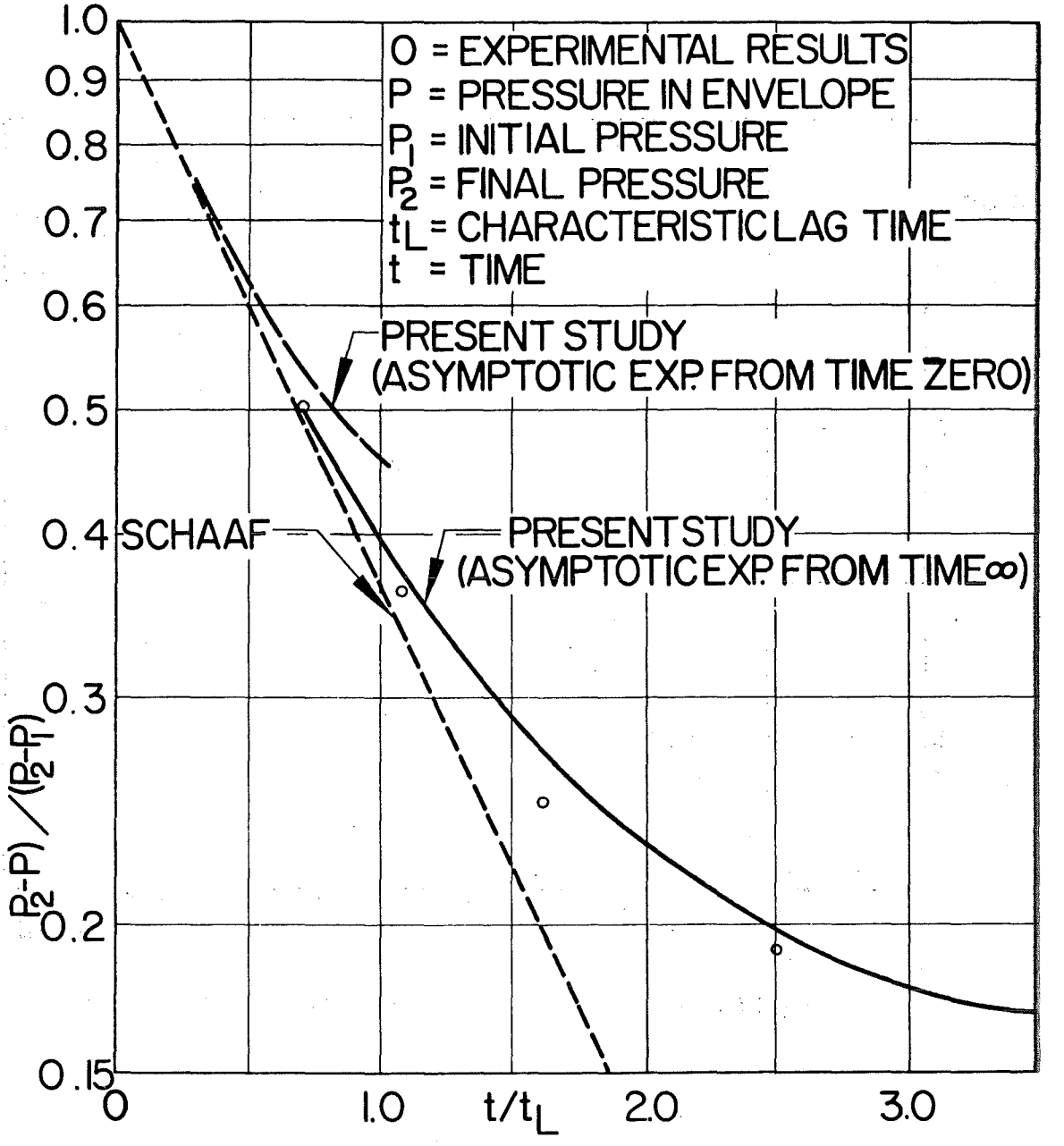

Fig. 3.6 Response to Stepwise Change in Pressure

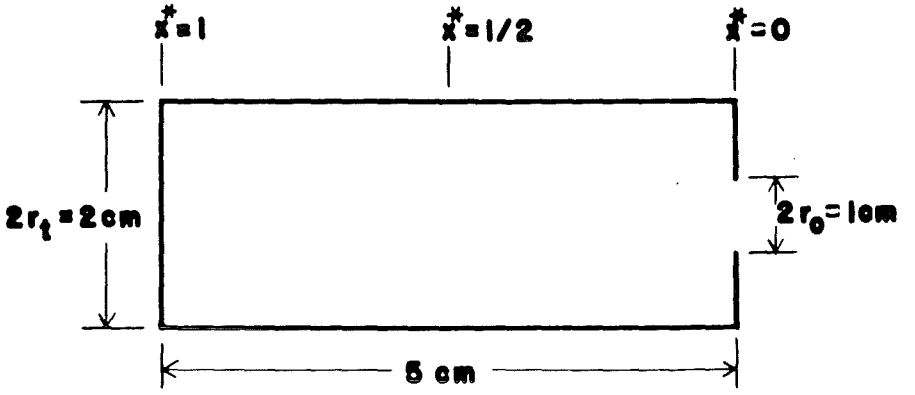

Fig. 3.7 Gauge Envelope System Schematic

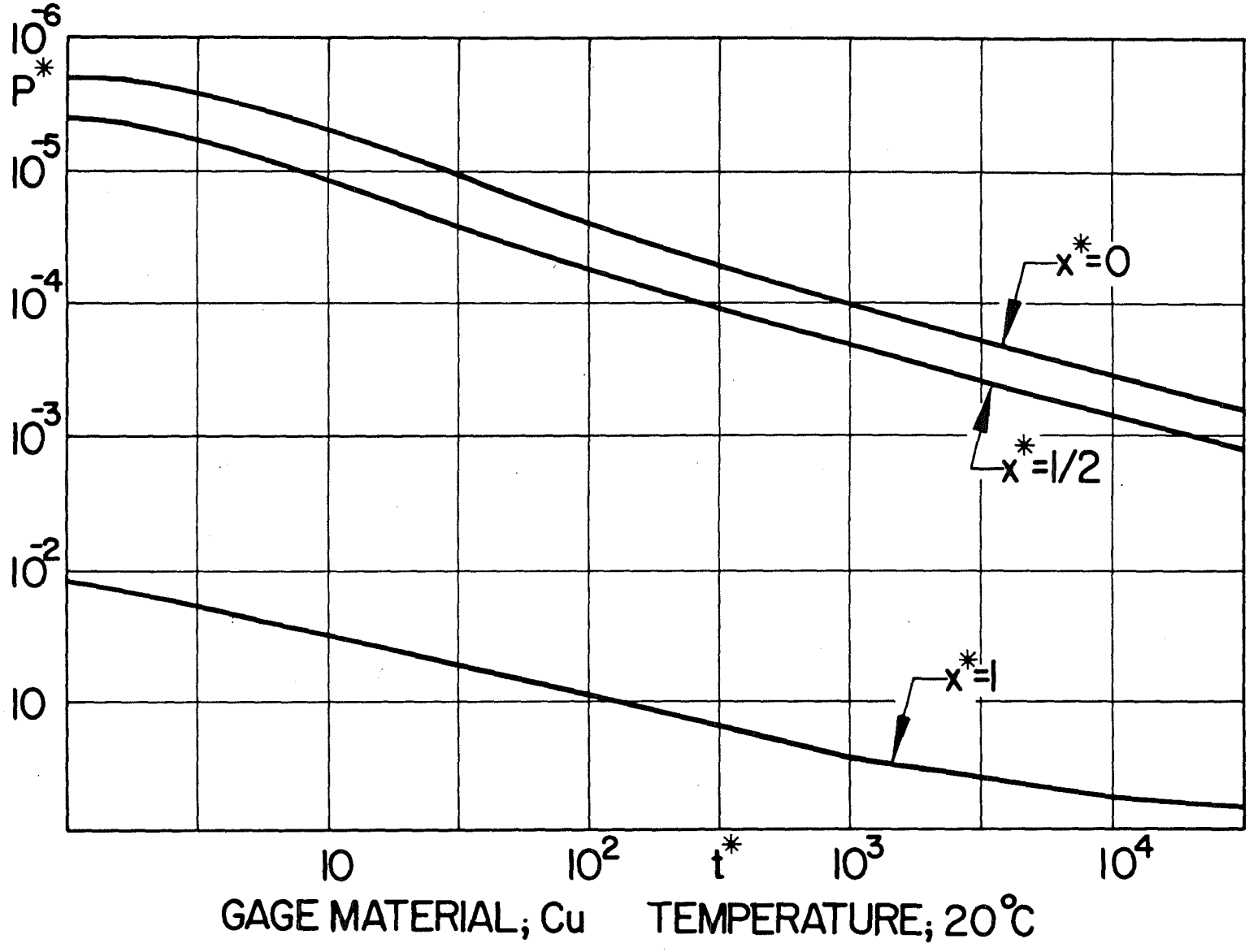

Fig. 3.8 Response of Gauge System to a Stepwise Change in Pressure of the Environment

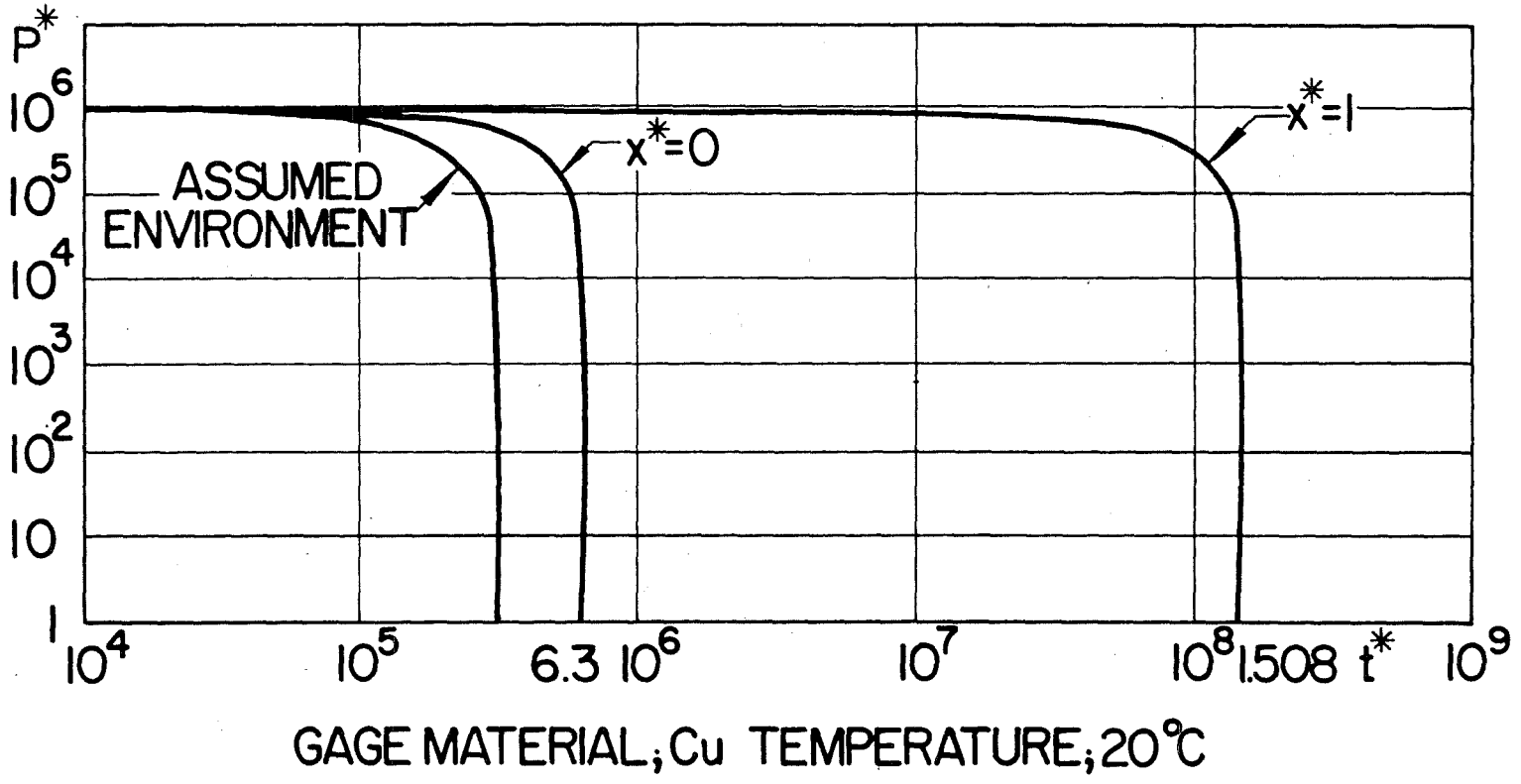

Fig. 3.9 Response of Gauge System to a Linear Variation of Pressure

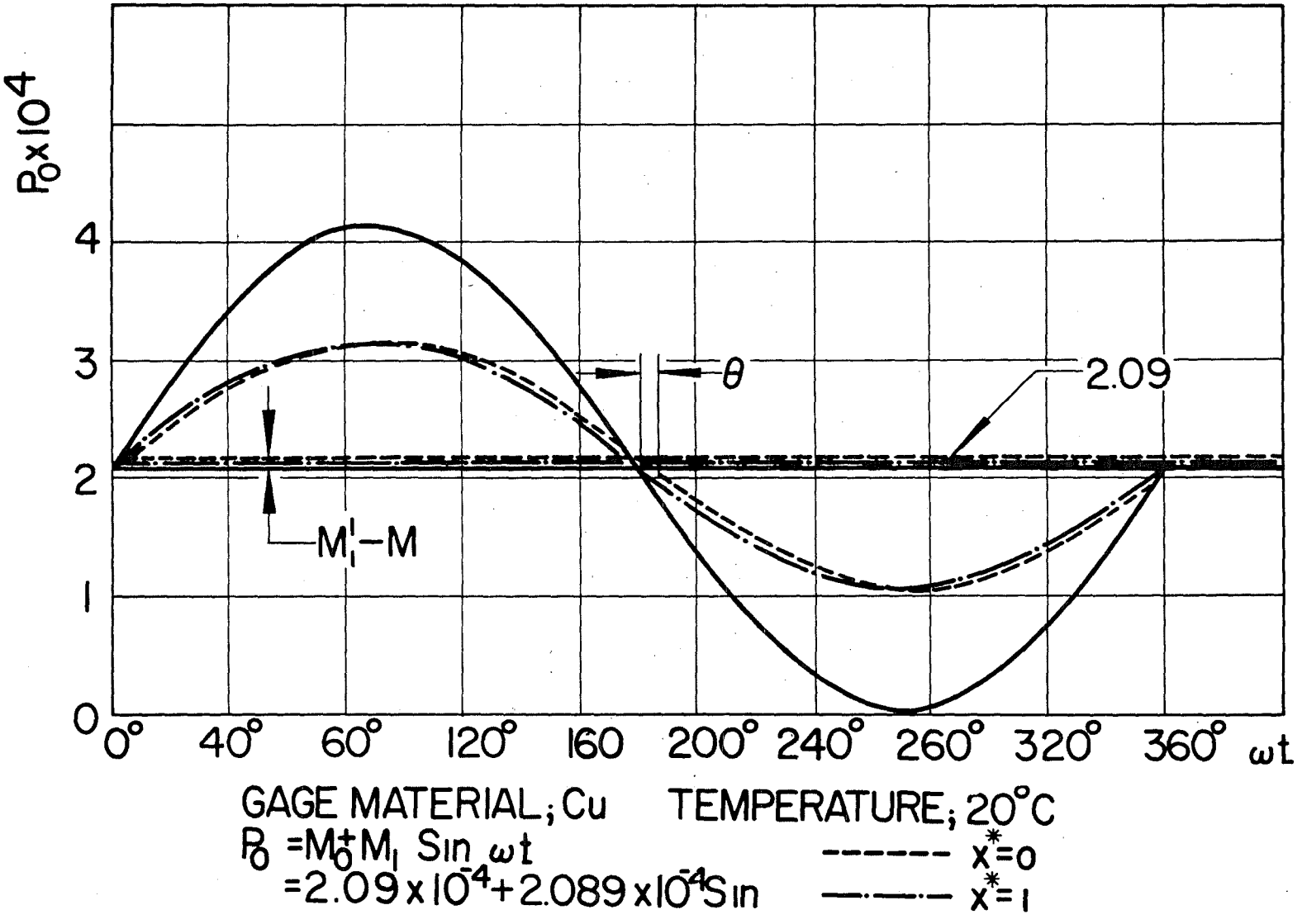

Fig. 3.10 Response of Gauge System to a Periodically Varying Pressure of the Environment

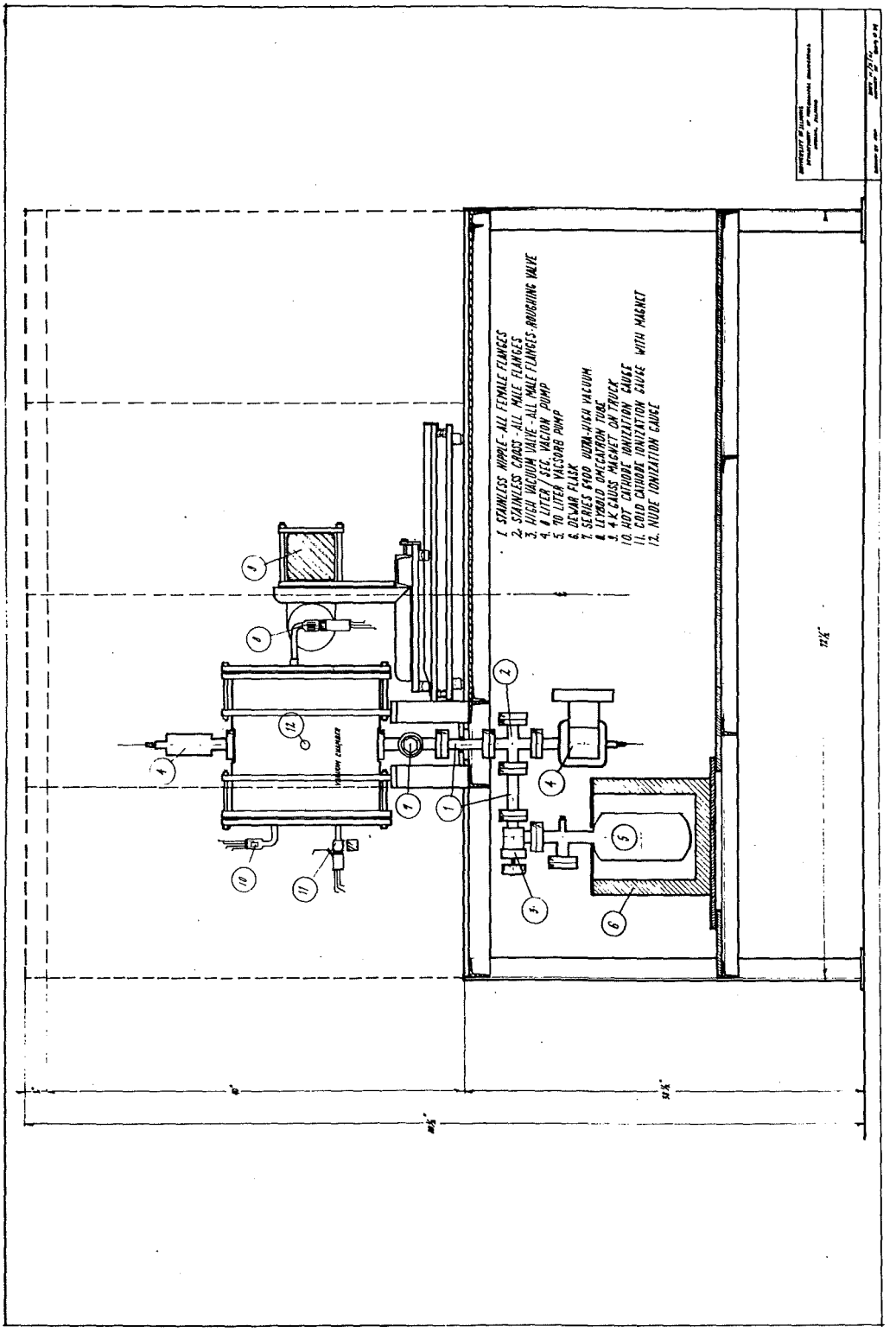

Fig. 4.1 Vacuum Chamber and Pumping Circuit

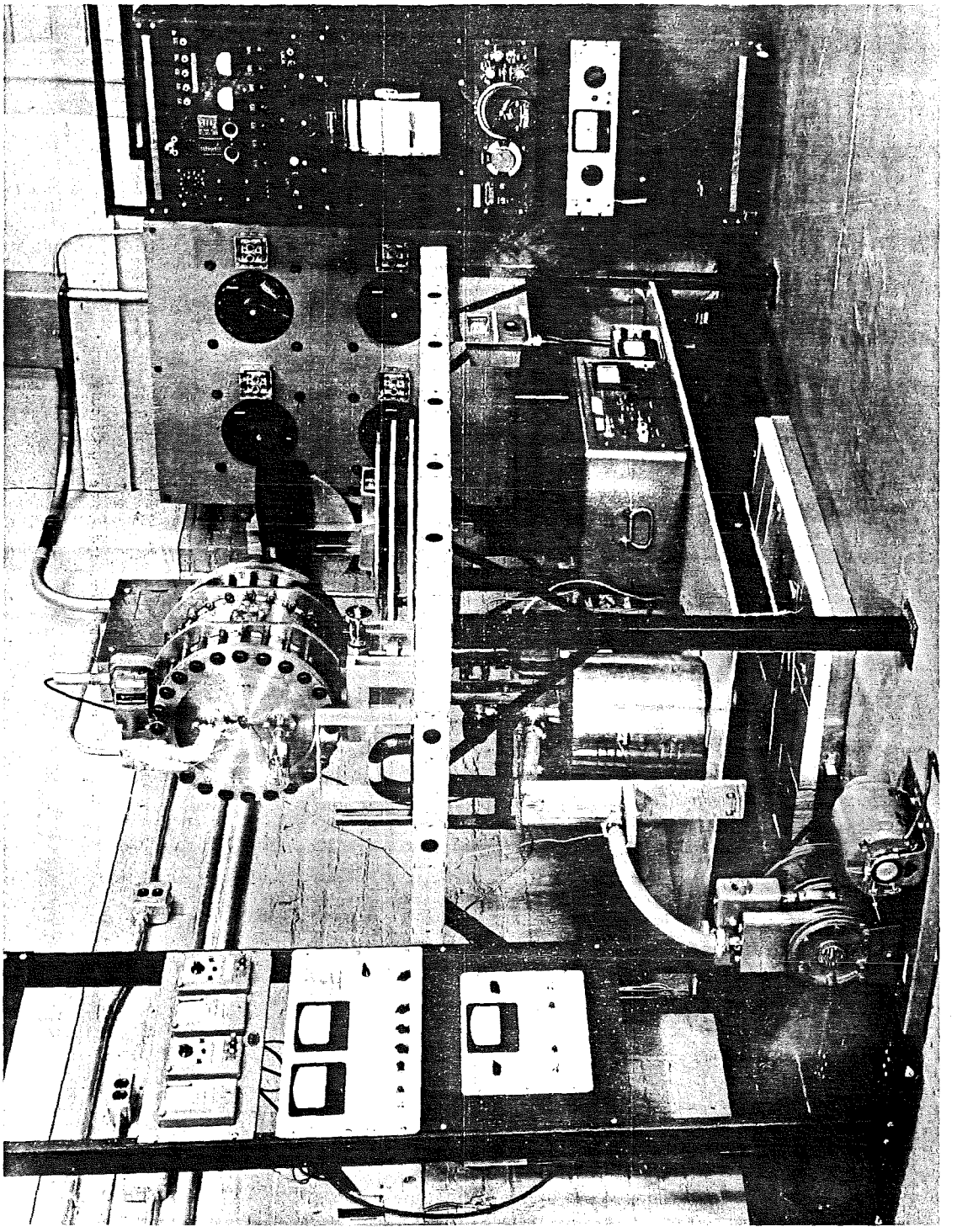

Fig. 4.2 Ultra-High Vacuum Chamber with Associated Equipment and Instrumentation

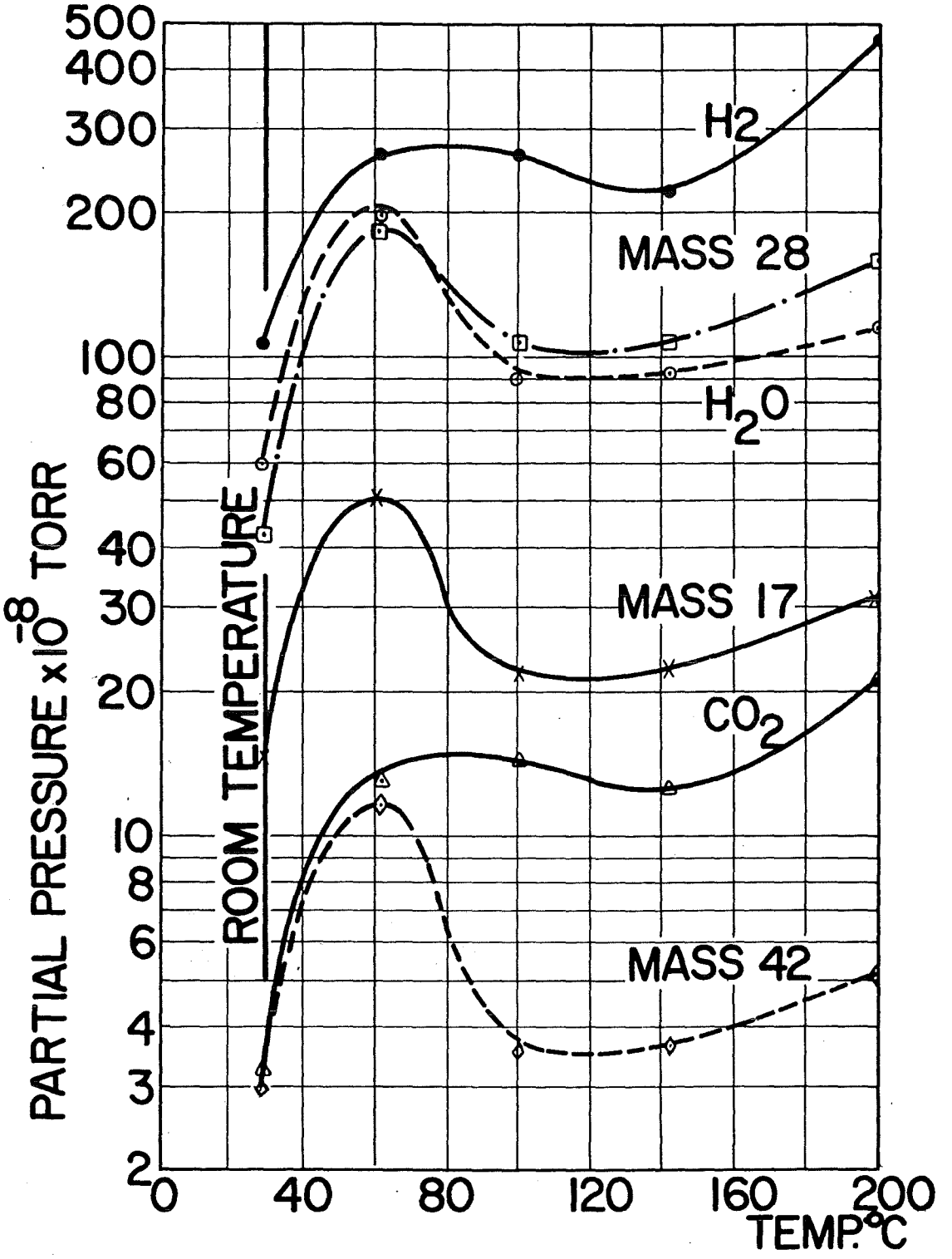

Fig. 5.1 Partial Pressures during Bakeout of Some Gases in a Stainless Steel-Glass System as a Function of Wall Temperature

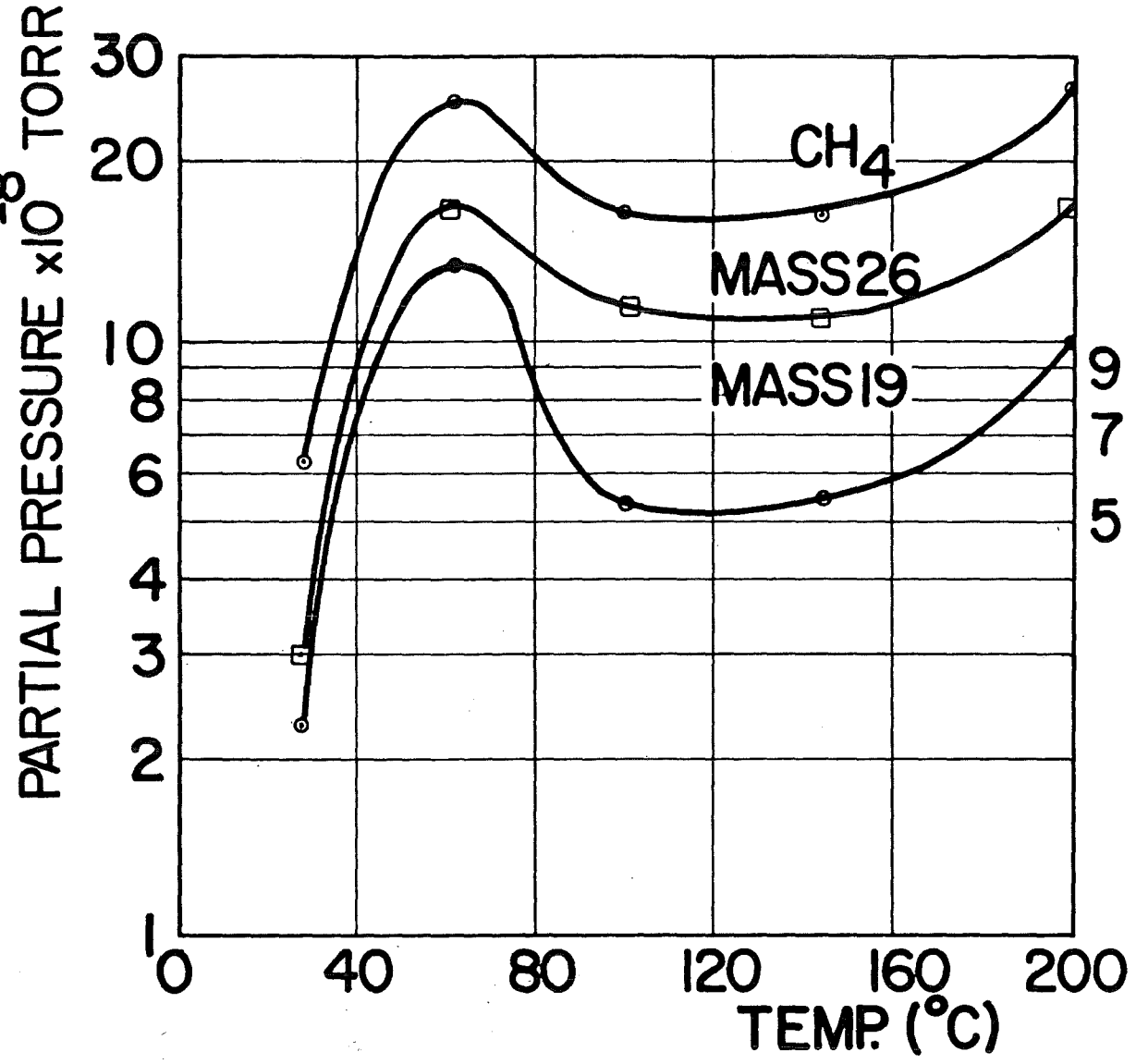

Fig. 5.2 Partial Pressure during Bakeout of Some Gases as a Function of Wall Temperature

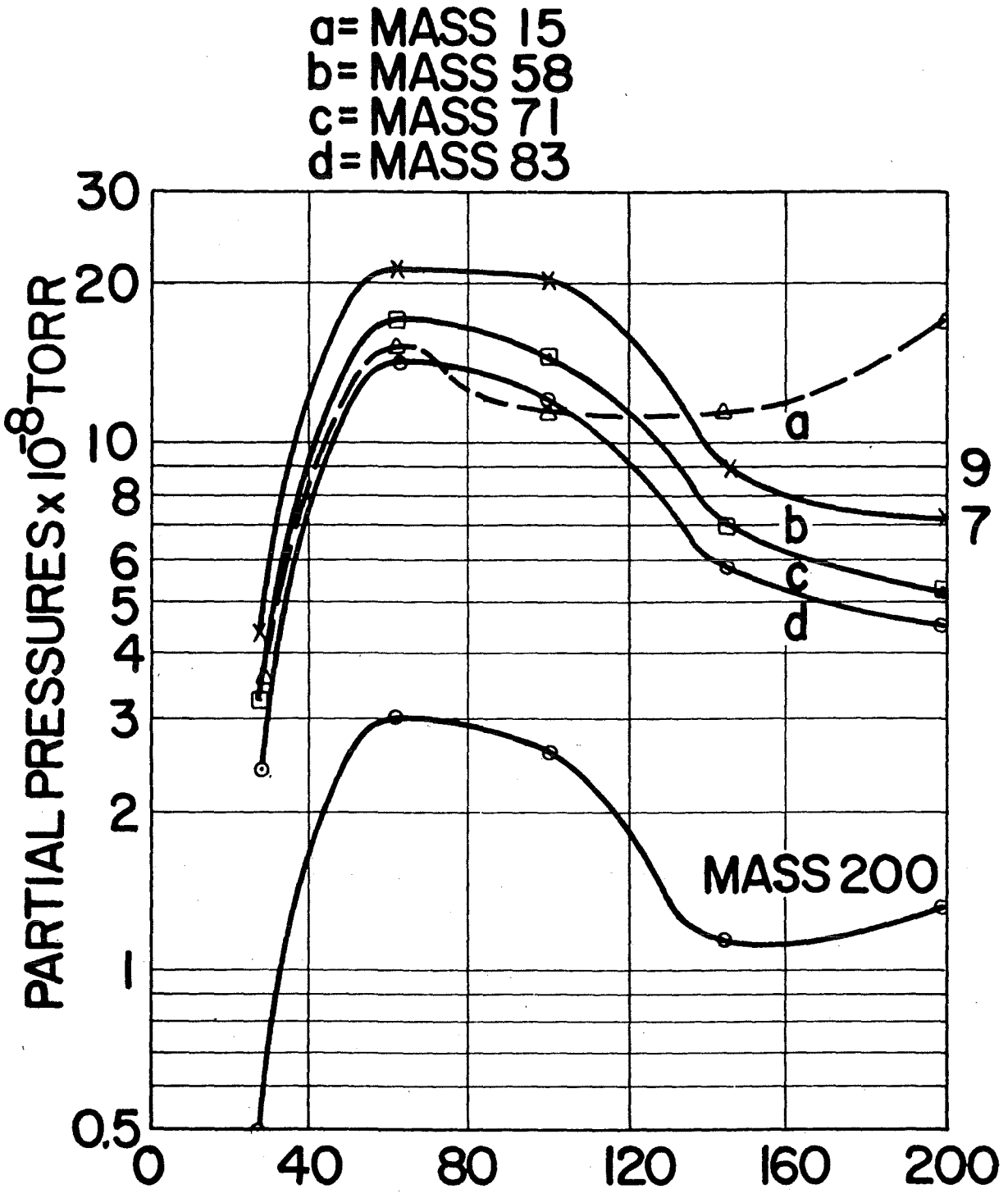

Fig. 5.3 Partial Pressure during Function of Temperature (Test 2)

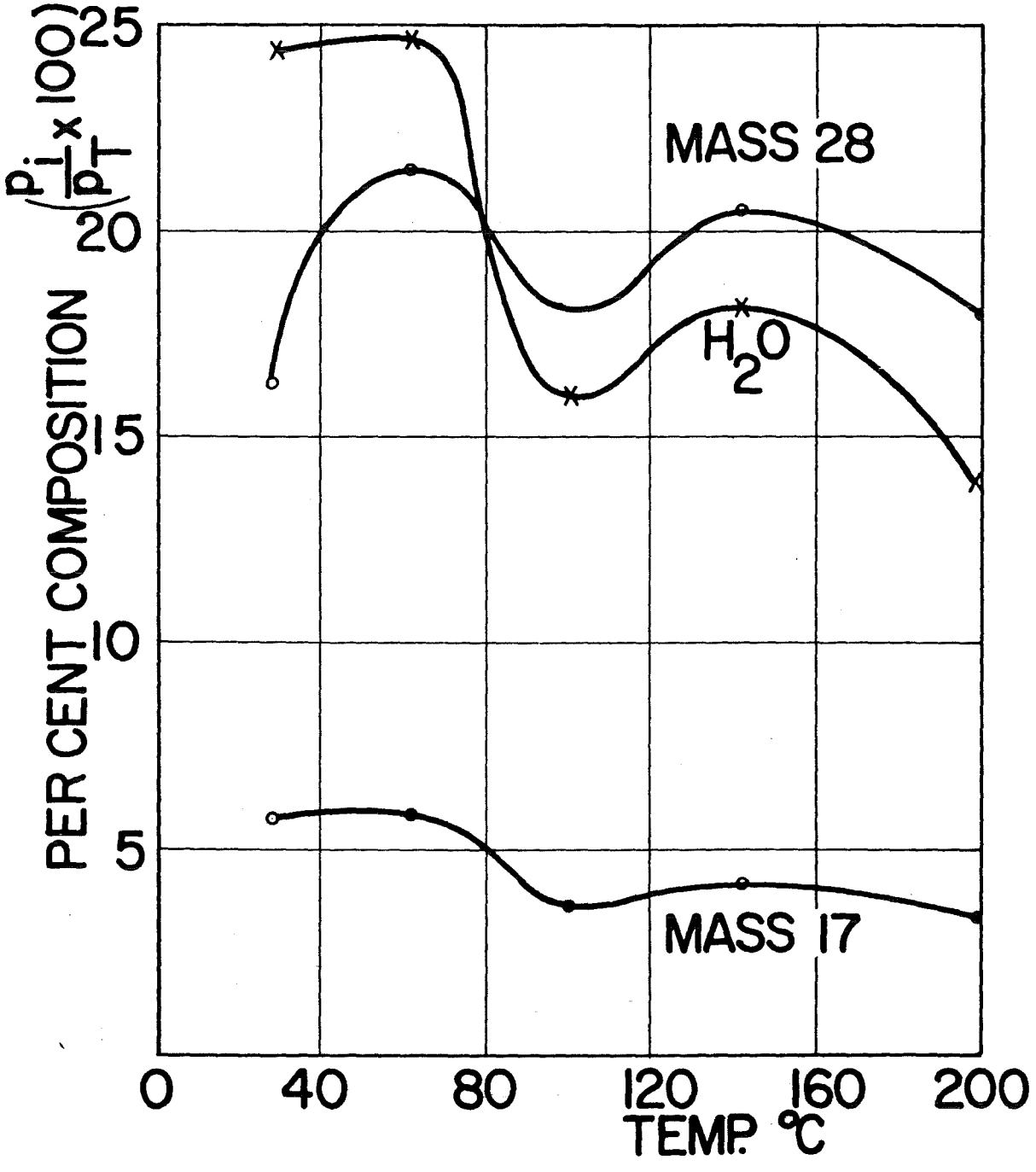

Fig. 5.4 Relative Change of Some Residual Gases as a Function of Temperature (Test 2)

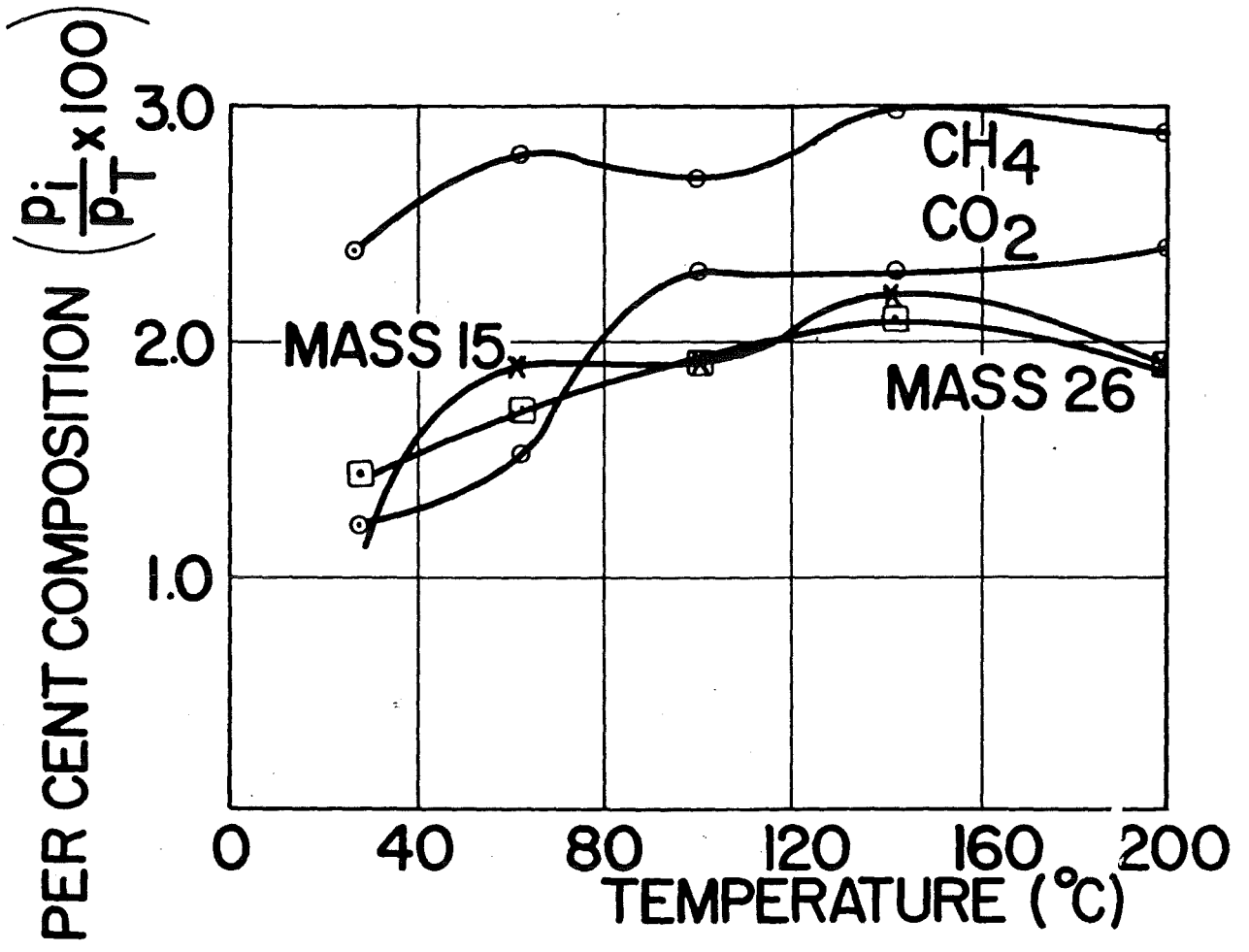

Fig. 5.5 Relative Change of Some Residual Gases as a Function of Temperature (Test 2)

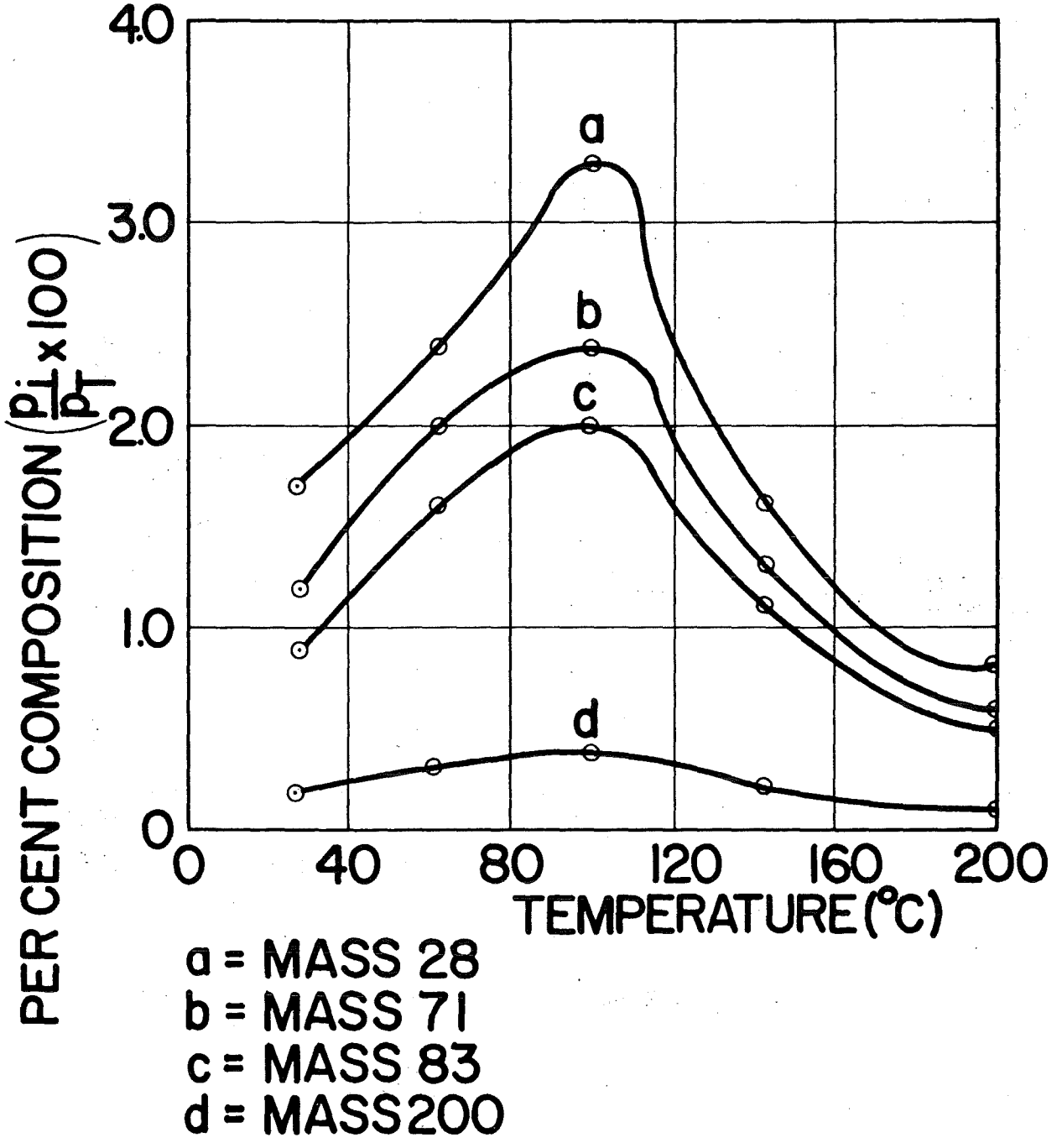

Fig. 5.6 Relative Amounts of Some Residual Gases as a Function of Temperature (Test 2)

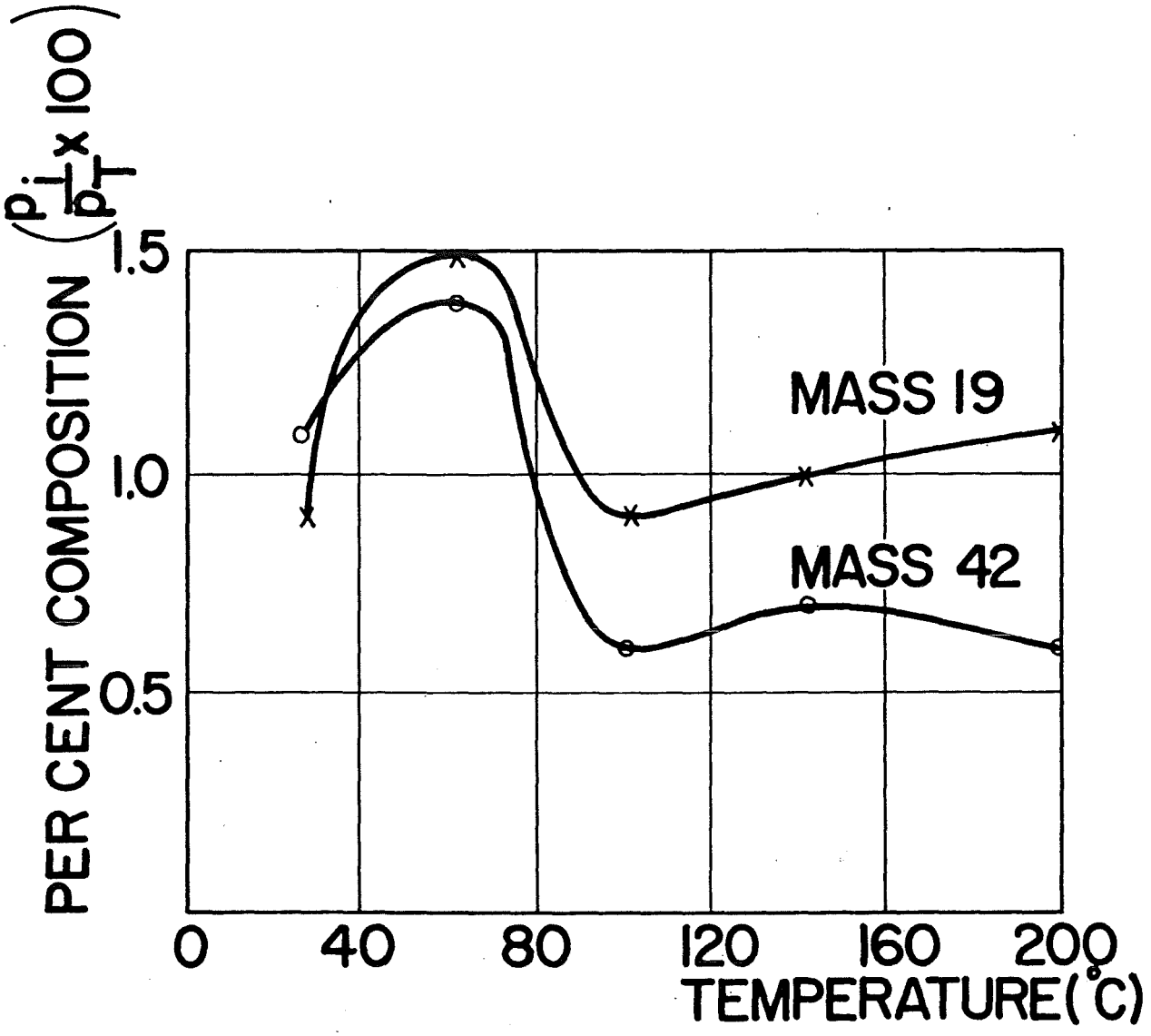

Fig. 5.7 Relative Change of Some Residual Gases as a Function of Temperature (Test 2)

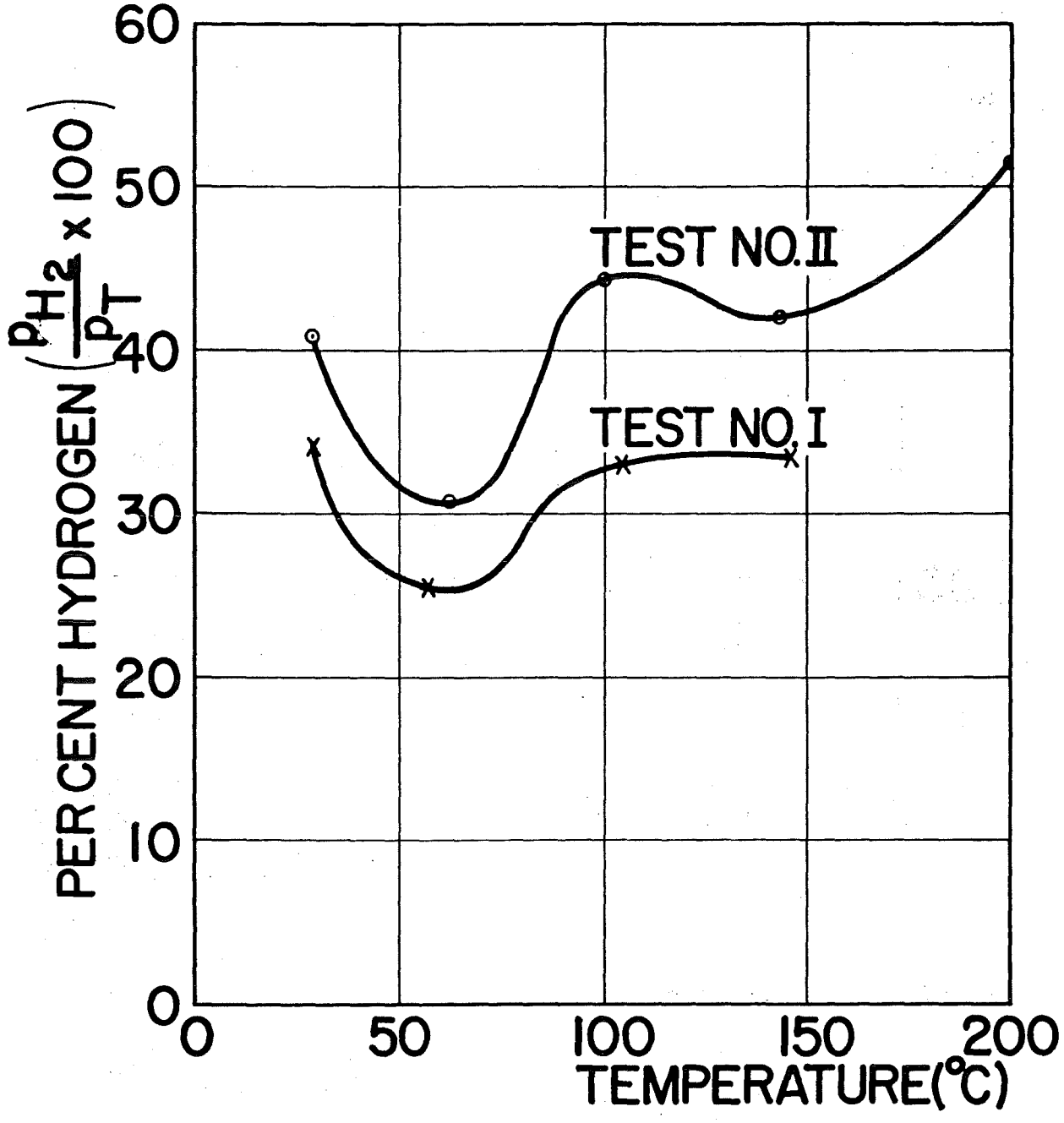

Fig. 5.8 Relative Change of Hydrogen as a Function of Temperature during Bakeout

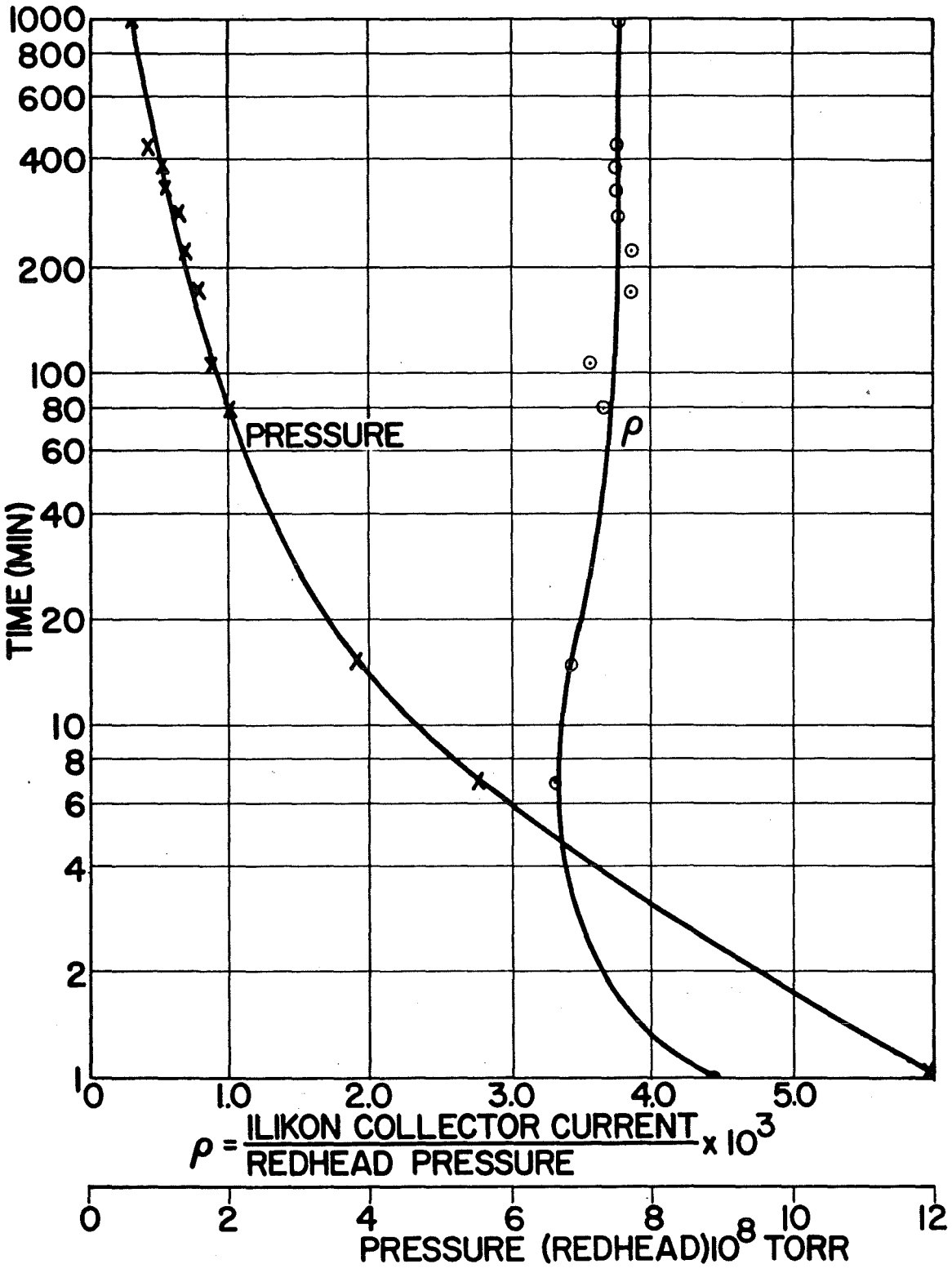

Fig. 5.9 Change of Apparent Sensitivity of Ilikon Gauge after Out-Gassing as Monitored by Redhead Gauge

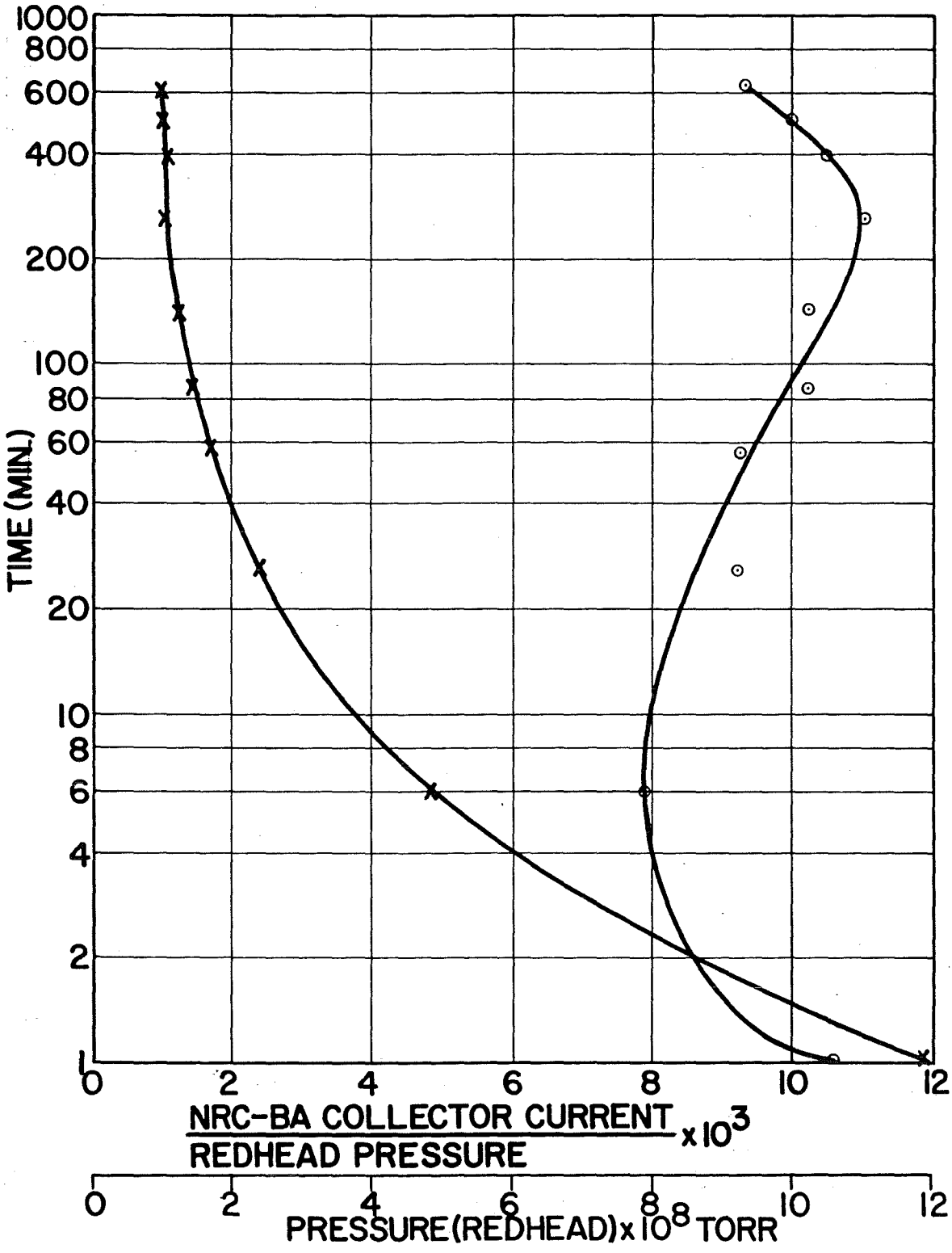

Fig. 5.10 Change of Apparent Sensitivity of NRC Bayard-Alpert Gauge after Out-Gassing as Monitored by Redhead Gauge

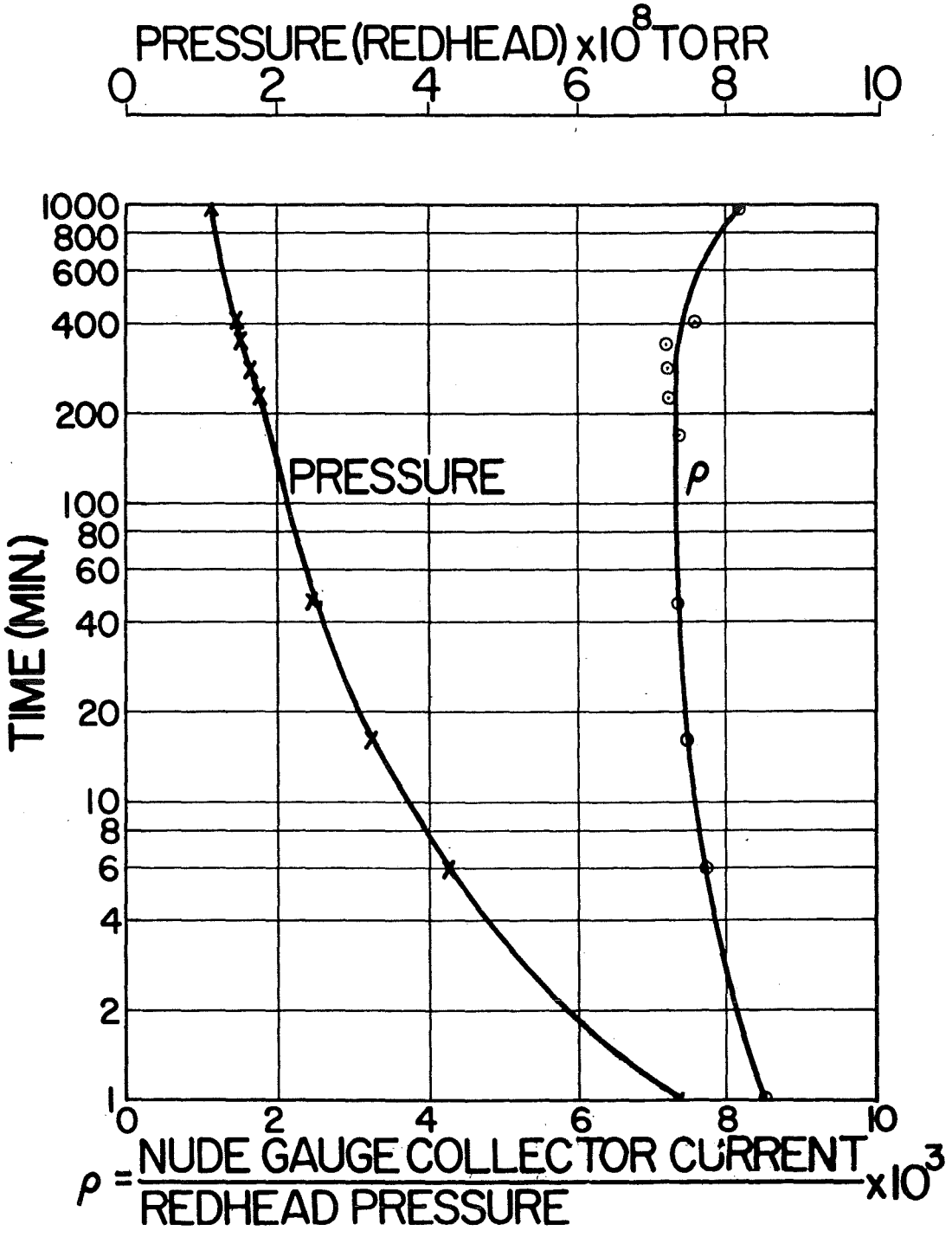

Fig. 5.11 Change of Apparent Sensitivity of Nude Gauge after Out-Gassing as Monitored by Redhead Gauge

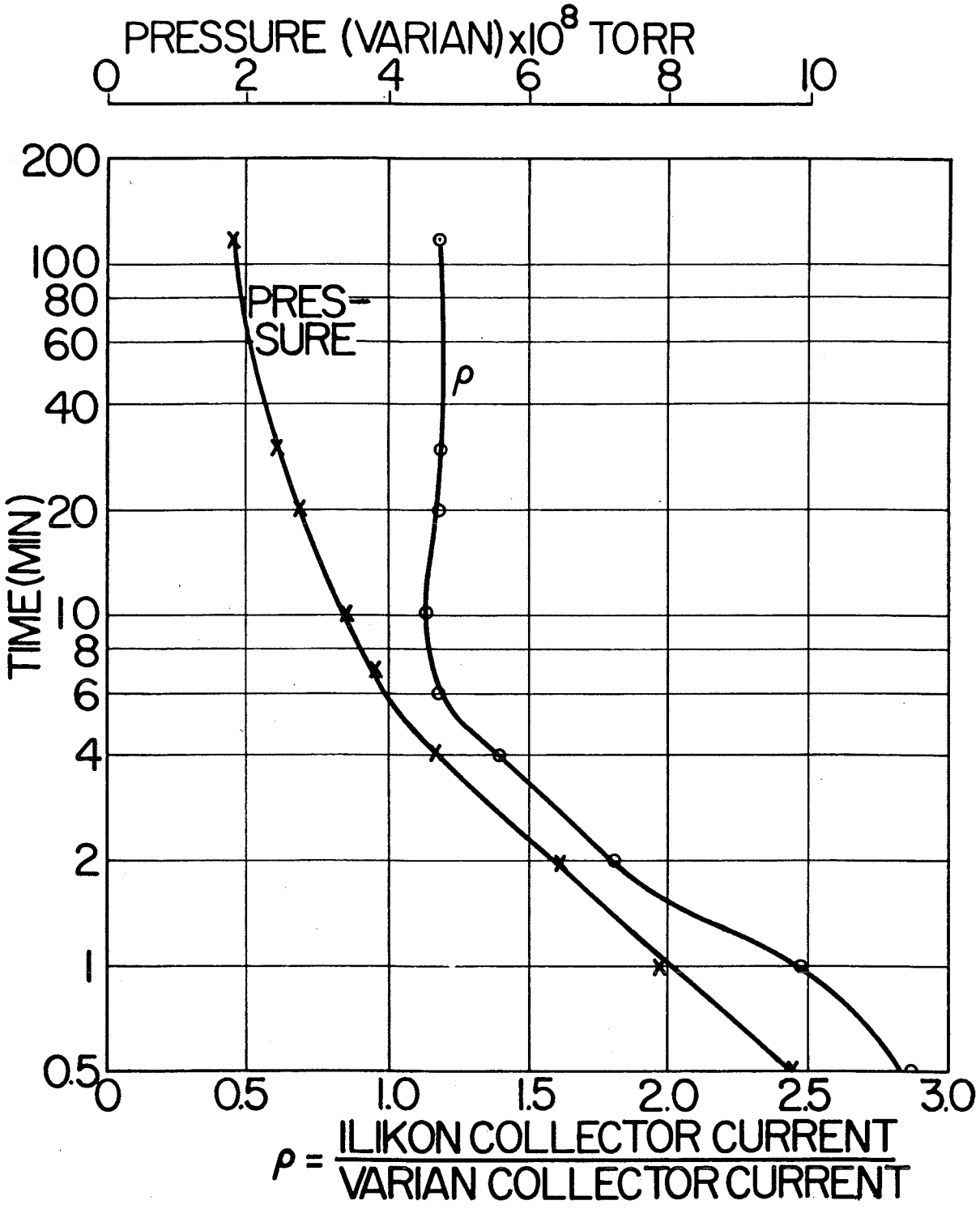

Fig. 5.12 Change of Apparent Sensitivity of Ilikon Gauge after Out-Gassing as Monitored by Varian Gauge

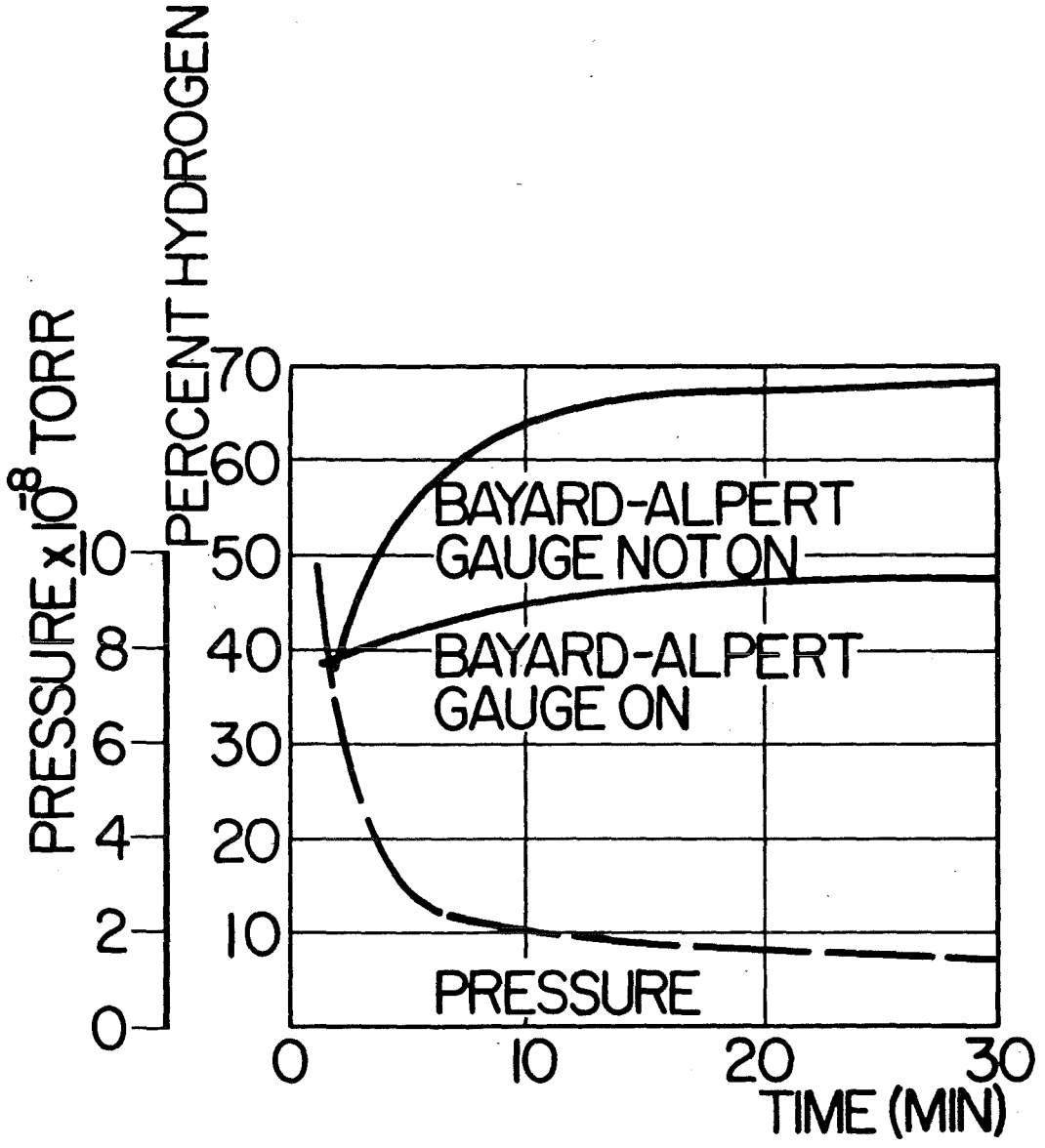

Fig. 5.13 Percent Hydrogen in System vs Time Vac-Ion Pump On

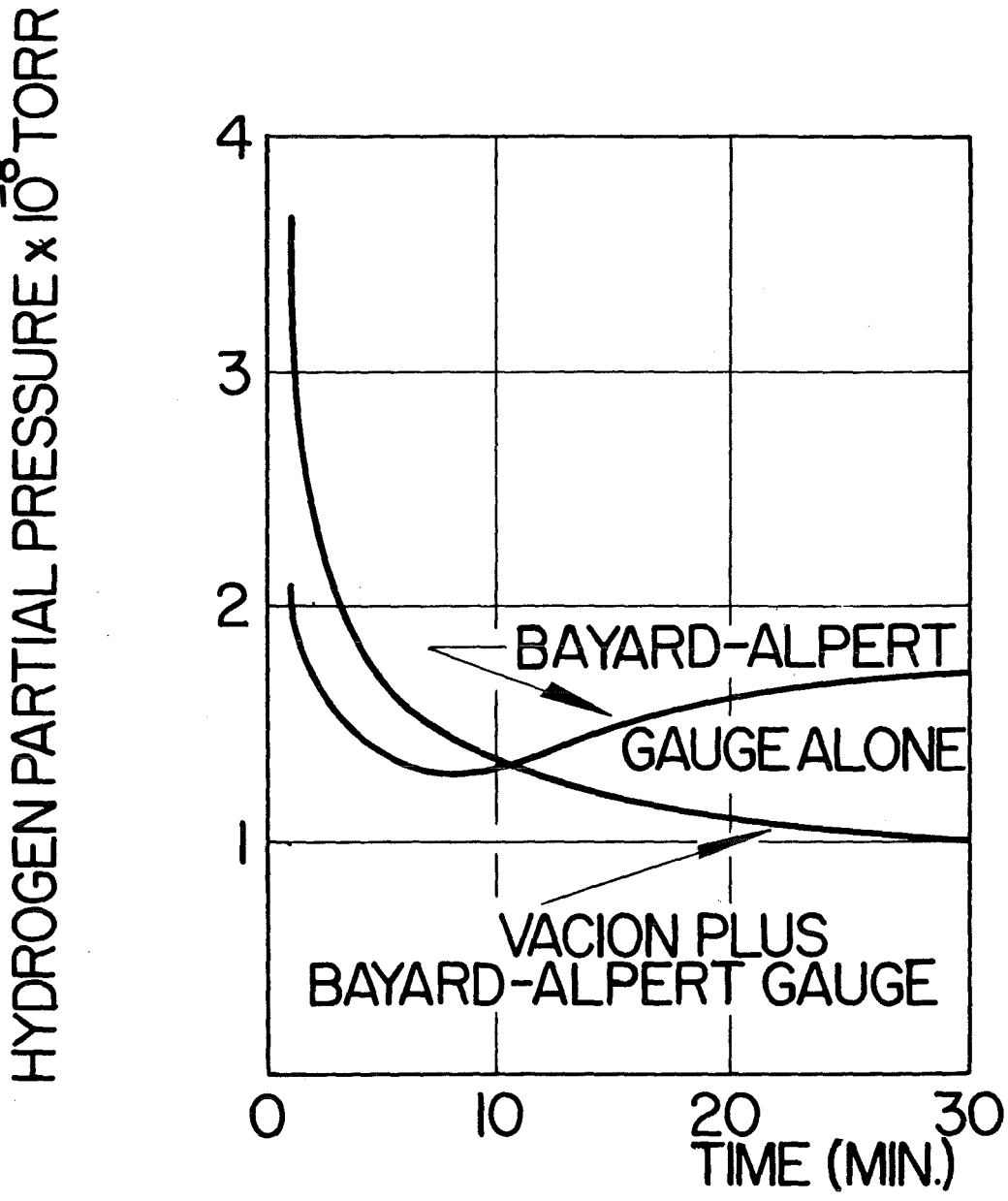

Fig. 5.14 Comparison of Pumping Speeds for Hydrogen

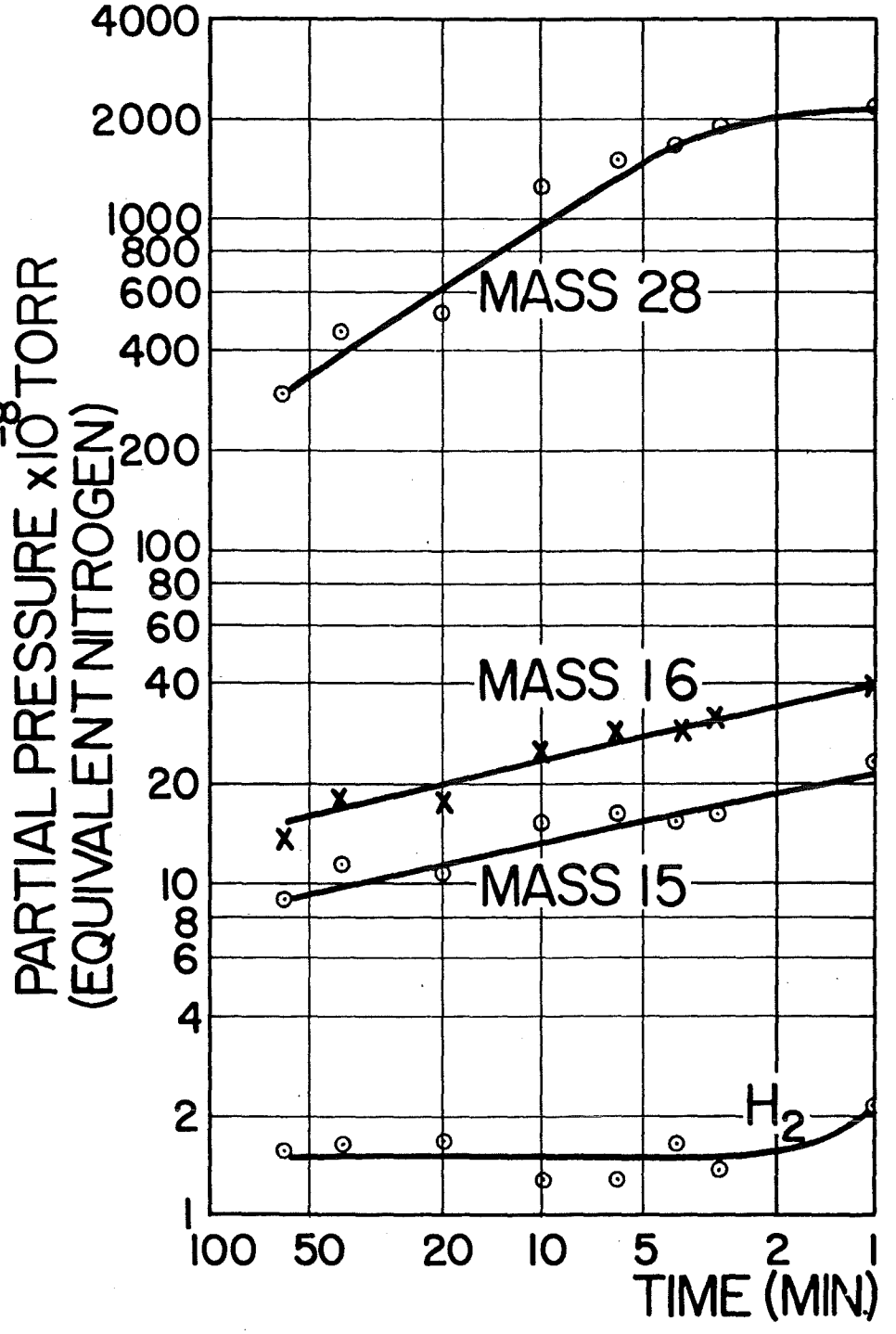

Fig. 5.15 Rate of Change of Various Species with NRC-Bayard-Alpert Gauge on – No Vac-Ion

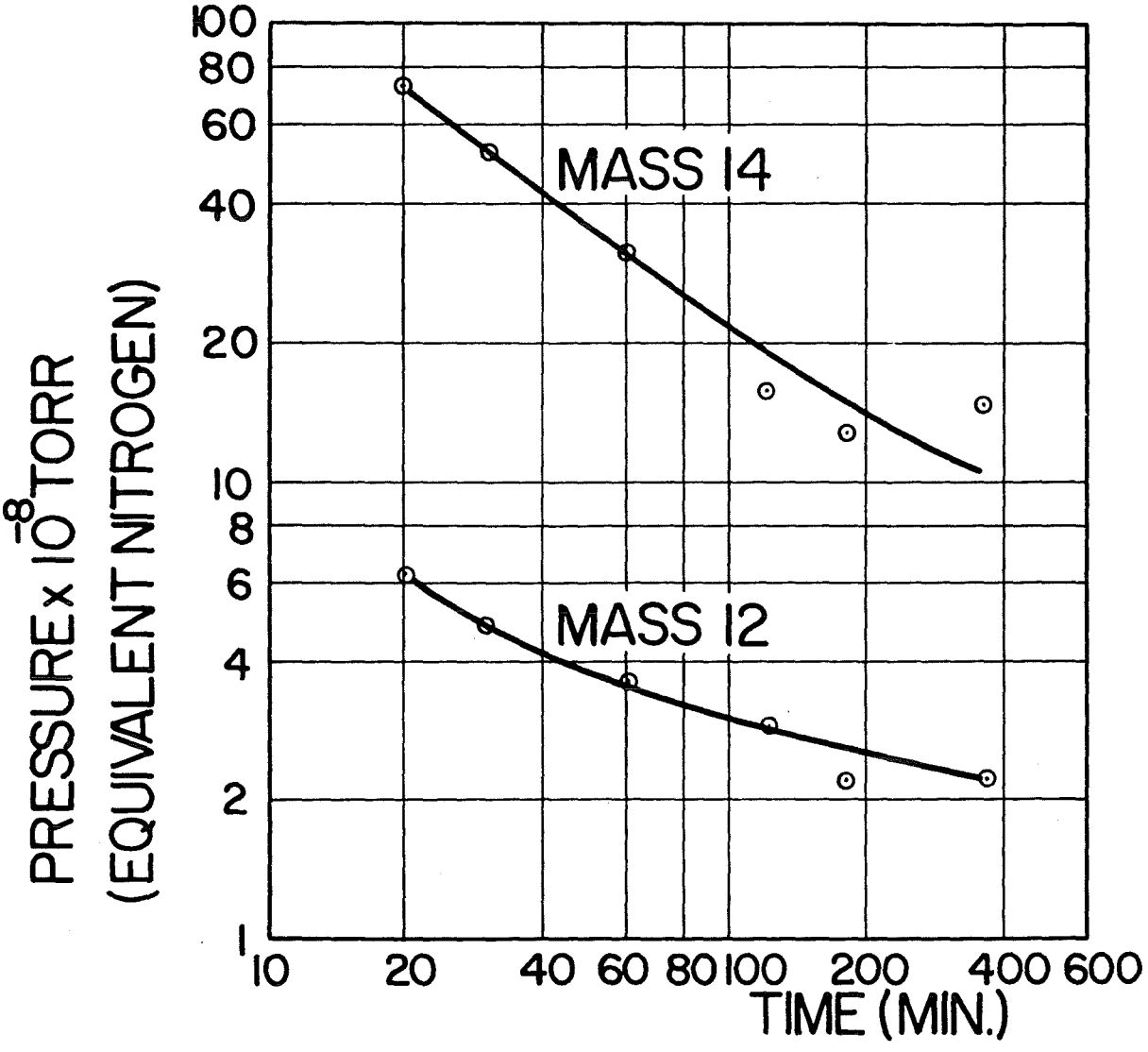

Fig. 5.16 Comparison of Changes of N_2 and CO as Indicated by Changes of N^+ and C^+. NRC Bayard-Alpert Gauge Only

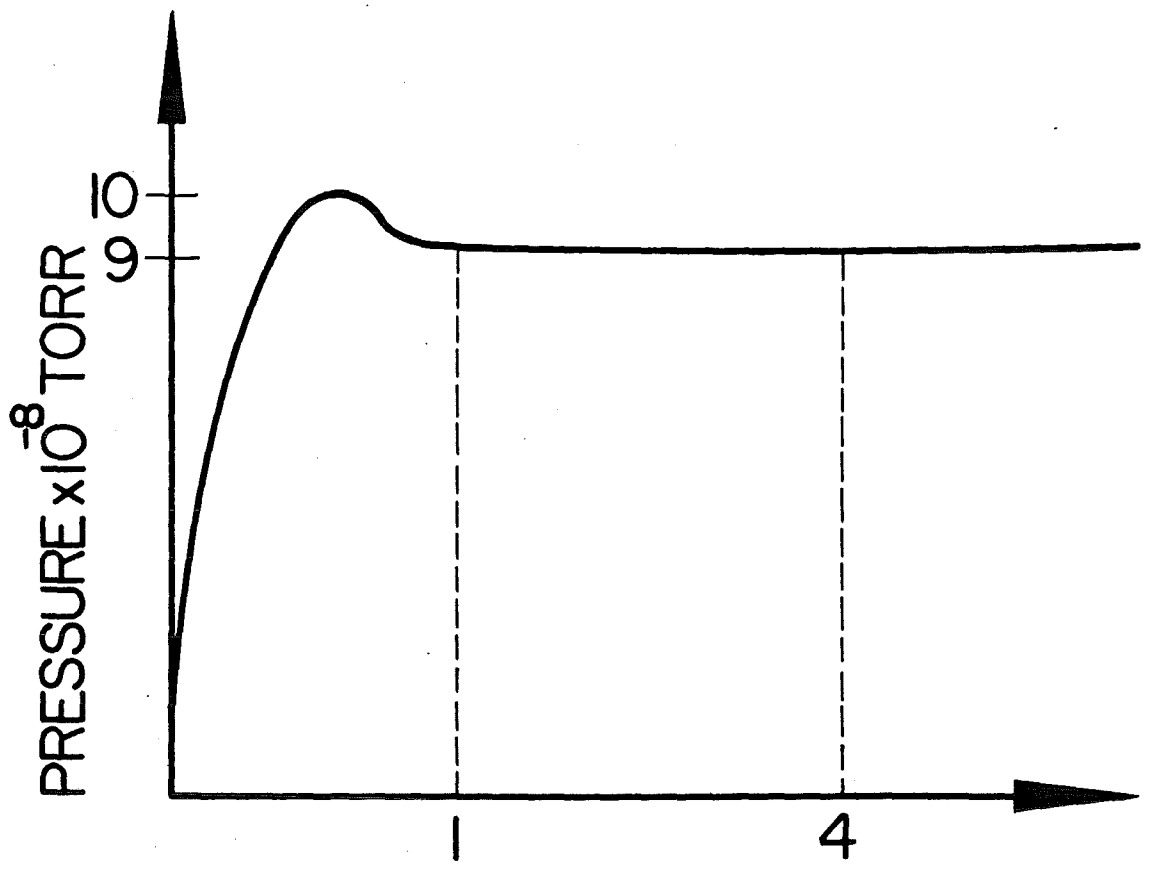

Fig. 5.17 Time after Applying Potentials

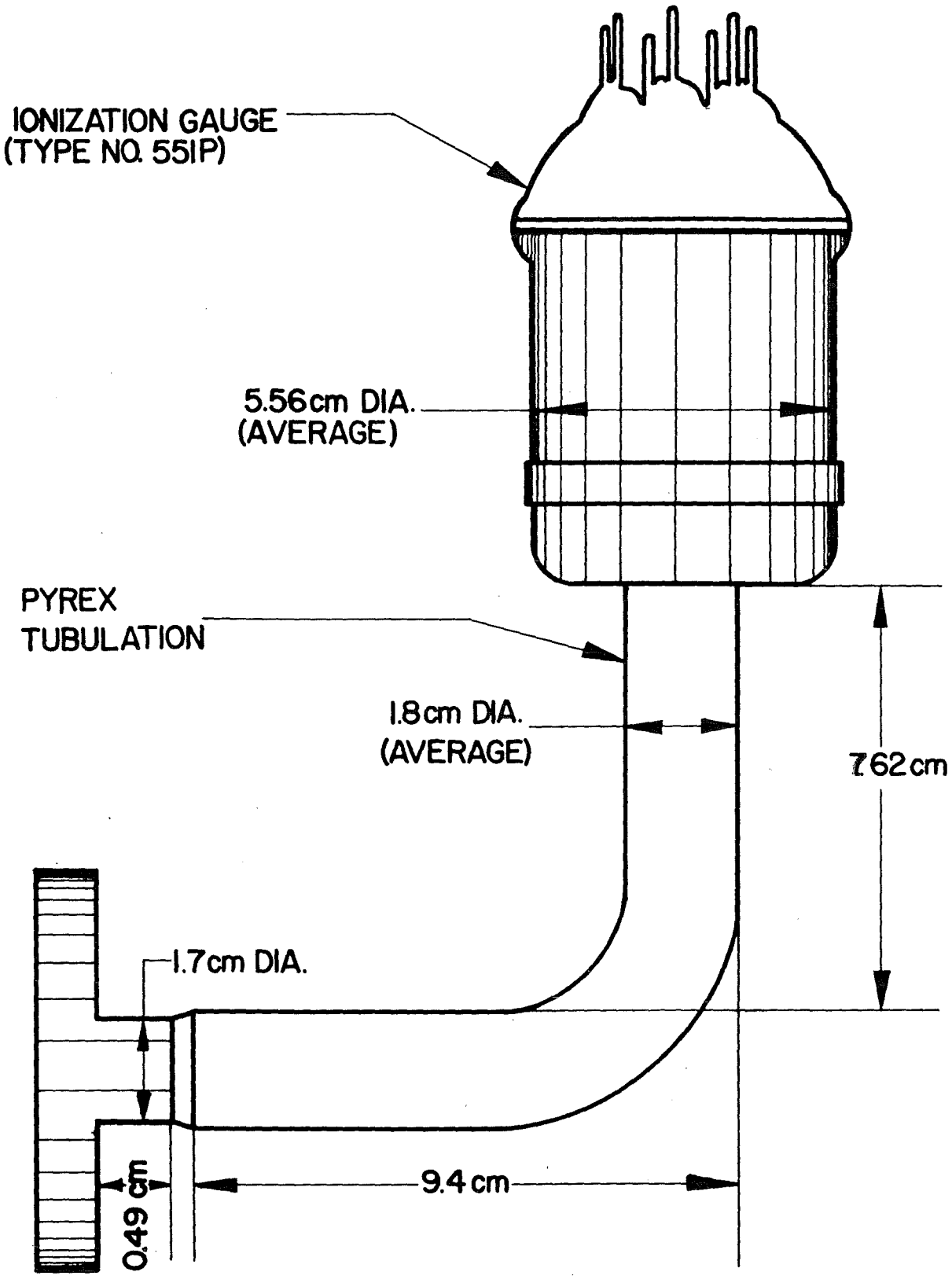

Fig. 5.18 Schematic Diagram of NRC Ultra-High Vacuum Ionization Gauge

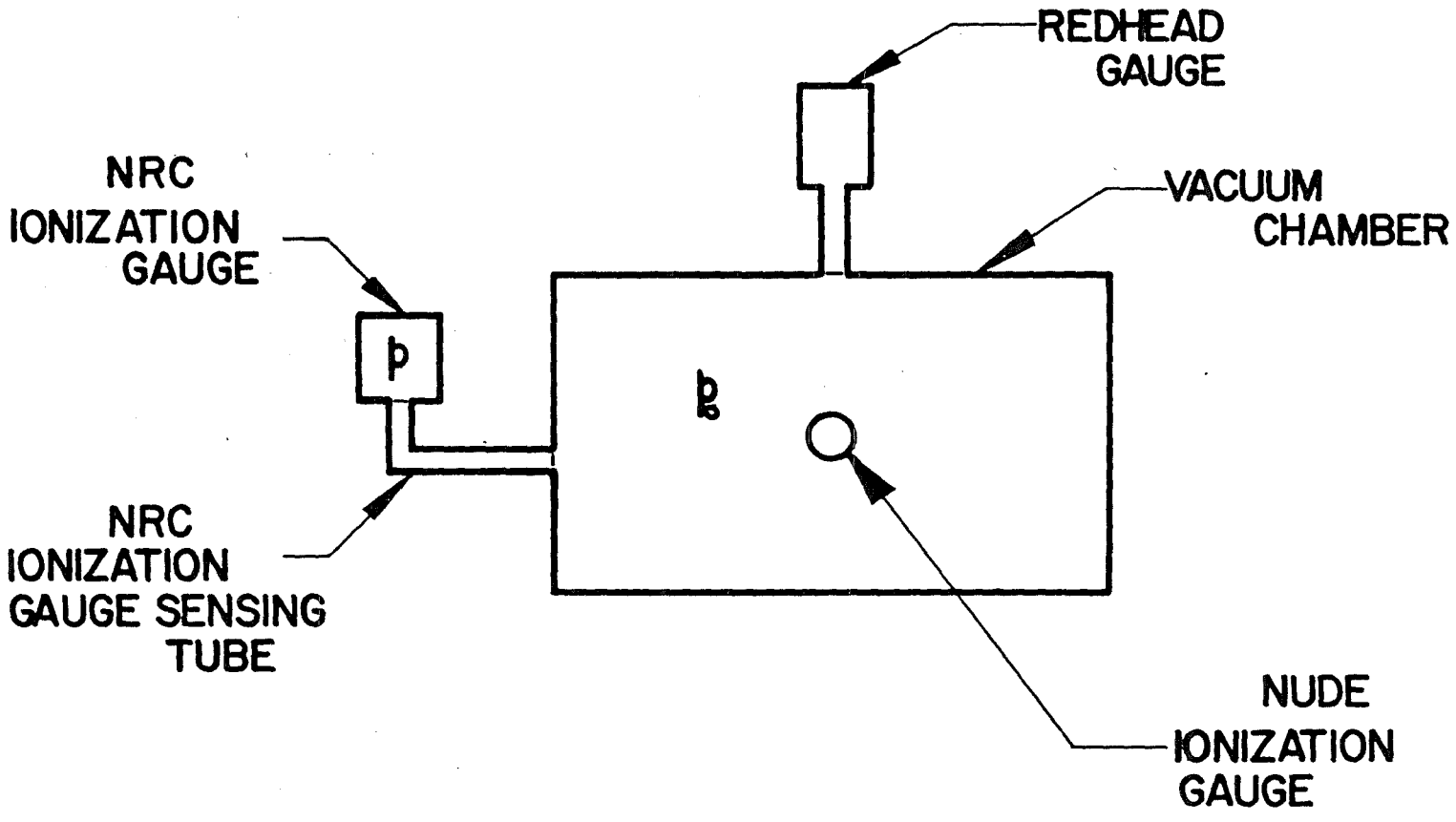

Fig. 5.19 Schematic Sketch of Experimental Method

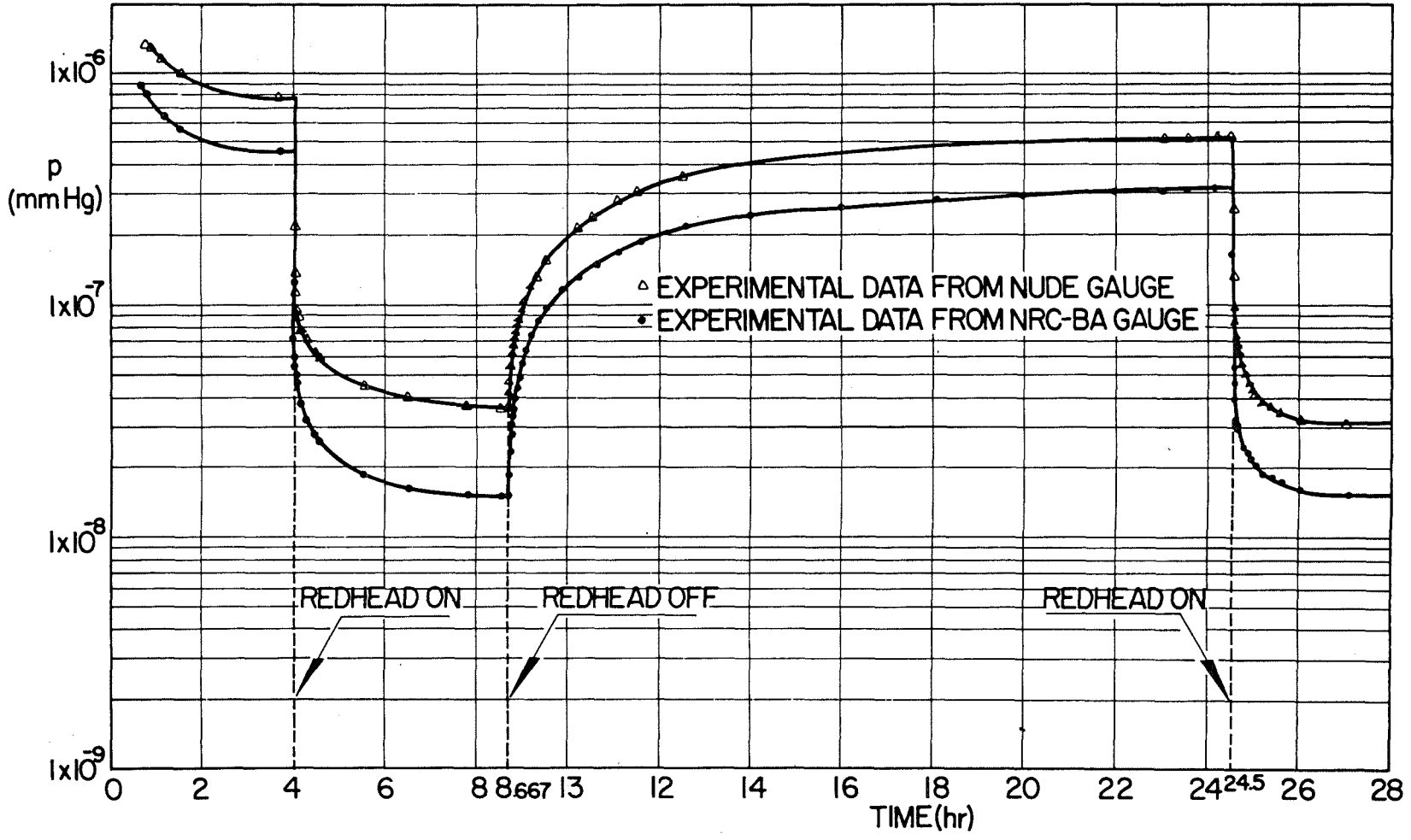

Fig. 5.20 Response of NRC Ionization Gauge to Pressure Change – Turn On, Turn Off of Redhead Gauge

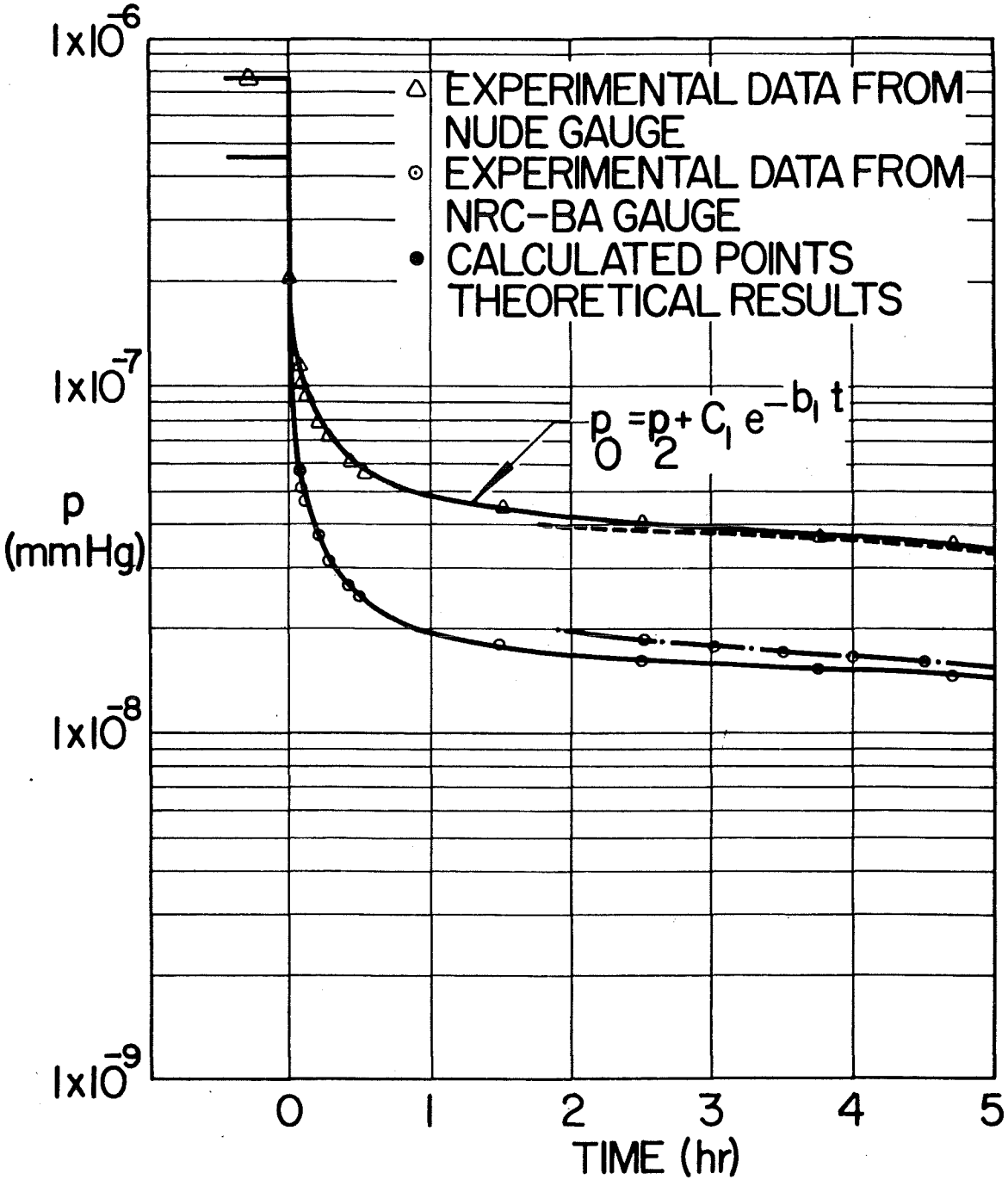

Fig. 5.21 Comparisons of Theoretical and Experimental Data

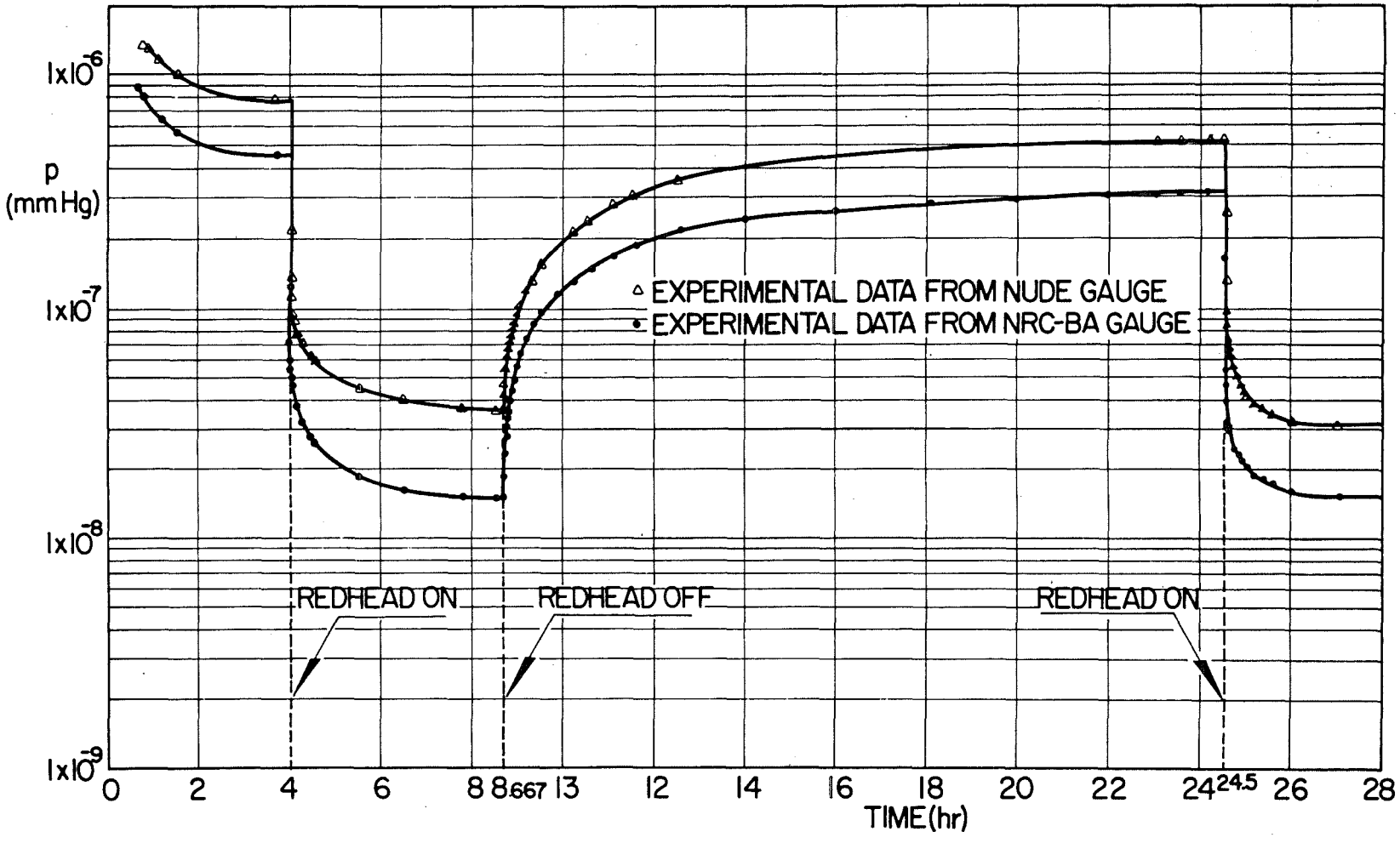

Fig. 5.20 Response of NRC Ionization Gauge to Pressure Change – Turn On, Turn Off of Redhead Gauge

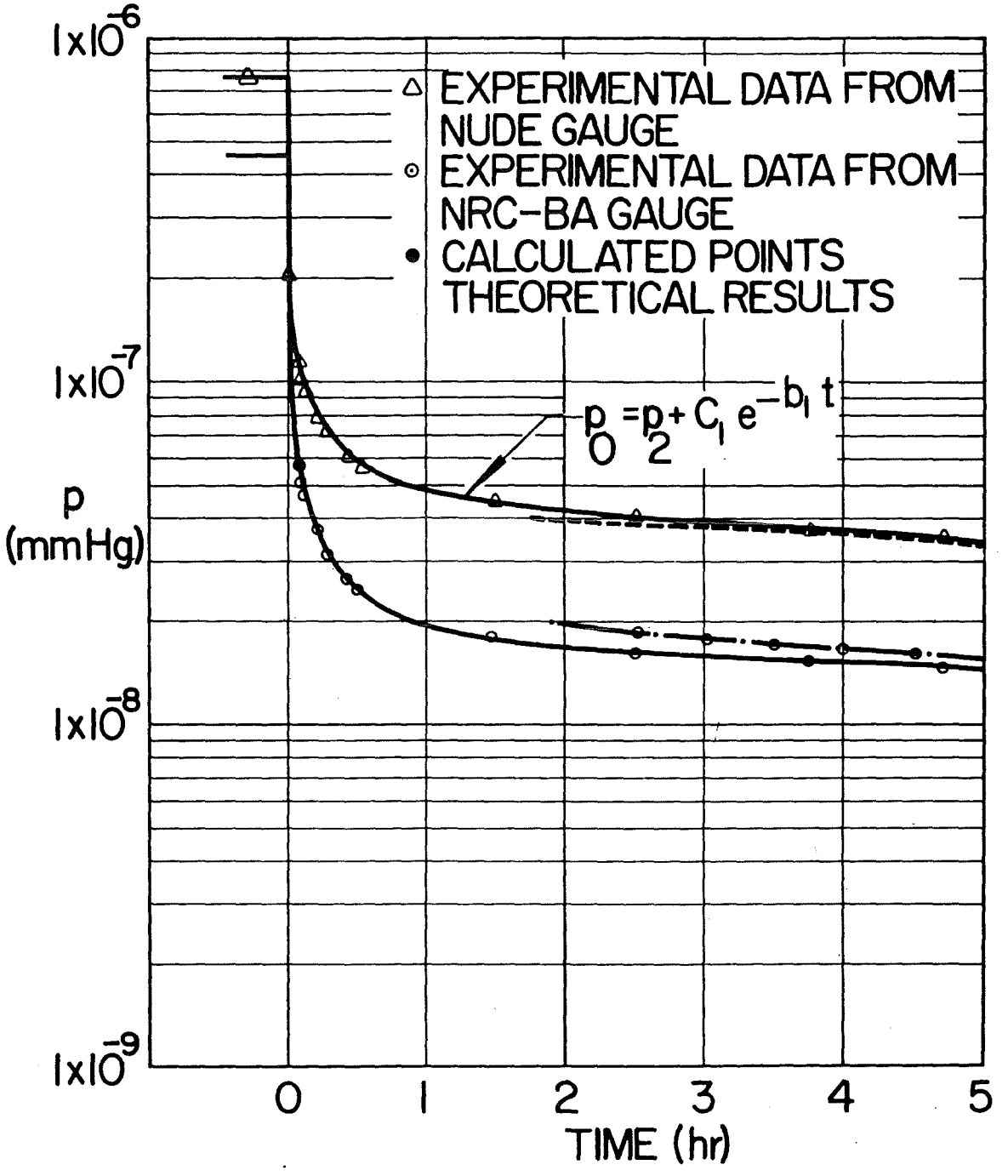

Fig. 5.21 Comparisons of Theoretical and Experimental Data